SYNTHESIS OF

GOLD NANO-PARTICLES IN A MICROFLUIDIC PLATFORM FOR

WATER QUALITY MONITORING APPLICATIONS

A Thesis

by

SAYAK DATTA

Submitted to the Office of Graduate Studies of
Texas A&M University
in partial fulfillment of the requirements for the degree of

MASTER OF SCIENCE

December 2008

Major Subject: Mechanical Engineering

SYNTHESIS OF

GOLD NANO-PARTICLES IN A MICROFLUIDIC PLATFORM FOR

WATER QUALITY MONITORING APPLICATIONS

A Thesis

by

SAYAK DATTA

Submitted to the Office of Graduate Studies of
Texas A&M University
in partial fulfillment of the requirements for the degree of

MASTER OF SCIENCE

Approved by:

Chair of Committee,	Debjyoti Banerjee
Committee Members,	Jerald Caton
	Kamran Entesari
Head of Department,	Dennis O' Neal

December 2008

Major Subject: Mechanical Engineering

ABSTRACT

Synthesis of Gold Nano-Particles in a Microfluidic Platform for Water Quality Monitoring Applications. (December 2008)

Sayak Datta, B.E., R.V. College of Engineering, Bangalore, India

Chair of Advisory Committee: Dr. Debjyoti Banerjee

A microfluidic lab-on-a-chip (LOC) device for in-situ synthesis of gold nano-particles was developed. The long term goal is to develop a portable hand-held diagnostic platform for monitoring water quality (e.g., detecting metal ion pollutants).

The LOC consists of micro-chambers housing different reagents and samples that feed to a common reaction chamber. The reaction products are delivered to several waste chambers in a pre-defined sequence to enable reagents/ samples to flow into and out of the reaction chamber. Passive flow actuation is obtained by capillary driven flow (wicking) and dissolvable microstructures called ‘salt pillars’. The LOC does not require any external power source for actuation and the passive microvalves enable flow actuation at predefined intervals. The LOC and the dissolvable microstructures are fabricated using a combination of photolithography and soft lithography techniques.

Experiments were conducted to demonstrate the variation in the valve actuation time with respect to valve position and geometric parameters. Subsequently, analytical

models were developed using one dimensional linear diffusion theory. The analytical models were in good agreement with the experimental data. The microvalves were developed using various salts: polyethylene glycol, sodium chloride and sodium acetate.

Synthesized in-situ in our experiments, gold nano-particles exhibit specific colorimetric and optical properties due to the surface plasmon resonance effect. These stabilized mono-disperse gold nano-particles can be coated with bio-molecular recognition motifs on their surfaces. A colorimetric peptide assay was thus developed using the intrinsic property of noble metal nano-particles. The LOC device was further developed on a paper microfluidics platform. This platform was tested successfully for synthesis of gold nano-particles using a peptide assay and using passive salt-bridge microvalves.

This study proves the feasibility of a LOC device that utilizes peptide assay for synthesis of gold nano-particles in-situ. It could be highly significant in a simple portable water quality monitoring platform.

DEDICATION

To God for His blessings

To my grandmother, Late Smt. Chitralekha Datta

To my grandfather, Late Sri Surhid Kumar Sinha

To my parents

To my advisor, Dr. Debjyoti Banerjee for his inspiration and support.

ACKNOWLEDGEMENTS

At the outset, I wish to express my heartfelt gratitude towards Dr. Debjyoti Banerjee for identifying my potential and supporting me throughout the research tenure at Texas A&M University. A great mentor for academic and professional pursuits, Dr. Banerjee has been a true source of inspiration for all his students.

I would like to express my gratitude to Dr. Kamran Entesari and Dr. Jerald Caton for being a part of my thesis committee. I would also like to thank Dr. Wilson at the Materials Characterization Facility for allowing me to use their laboratory facilities at Texas A&M University for my research.

I would like to extend my sincere gratitude towards my colleagues and friends in the research group and to the faculty at the Department of Mechanical Engineering, Texas A&M University for providing me with invaluable experience. I want to take this opportunity to extend my gratitude to the Air Force Research Laboratory (AFRL-Materials Division) for providing the funding for my research.

A sincere vote of thanks towards my parents, my friends, Sandeep, Abhi, Sameer, Sidharth, Varun, Vivek, Ankur, Anupriya, Aarti, Zaheen, Sujitha, Arjun, Rohit Gargate, Sharan Sriraman and others for being the best room-mates and being by my side through thick and thin.

NOMENCLATURE

D	-Diffusion Coefficient (m^2/s)
L_0	-Distance between the position of the valve and the reservoir (mm)
l	-Length of the valve (mm)
w	-Width of the valve (mm)
d	-Height of the valve (mm)
ρ	-Density of liquid (Kg/m^3)
Cs	-Saturation Concentration (Kg/m^3)
Ci	-Initial Concentration (Kg/m^3)
t	-Time of valve rupture (minutes or s)
λ	-Dimensionless parameter
v	-Velocity of fluid flow (m/s)
ERF	-Error Function
θ	-Concentration Gradient
Ja	-Jakob Number
Re	-Reynolds Number
μ	-Dynamic Viscosity (Pa.s)
ν	-Kinematic Viscosity (m^2/s)

TABLE OF CONTENTS

Page

Page

LIST OF TABLES

Page

LIST OF FIGURES

Page

Page

Page

Page

Page

Page

Page

Page

Page

Page

Page

Page

1. INTRODUCTION

1.1 Microfluidics and Water Quality Monitoring

Monitoring water quality is important for various situations. Most of the pollutants in water are usually not detectable on visual inspection. Since water sources are diverse (rivers, springs, creeks, swamps, estuaries, wetlands, lakes, bays, municipal supplies, underground, etc.), development of a versatile and portable water quality testing apparatus can be of great significance. A portable apparatus for testing water quality is important for various civilian, domestic, futuristic manned deep space missions and military missions. Efficient monitoring of the quality of surface water will help protect our waterways from growing levels of pollution. Incidentally, there is a famous quotation that states:

> Water and air, the two essential fluids on which all life depends, have become global garbage cans. - Jacques Cousteau (1910-1997)

The local, state and national governments use monitoring information to help control pollution levels. This information is used to understand exactly how human activity influences water resources and supply – which aids conservation strategies.

This thesis follows the style of *IEEE Transactions on Components and Packaging Technologies*.

Conventionally, testing water starts with sample collection which is then typically transported to the laboratory for testing purposes. This is a long drawn process which requires expensive equipments that involve cumbersome tests using corrosive reagents that are detrimental to the environment (with associated handling and disposal issues) and requires highly skilled personnel. Hence, a portable hand-held diagnostic device needs to be developed which could be effectively used to detect the presence of metallic impurities/ pollutants in water samples.

Fig. 1 illustrates the impact of various diseases on human health. A large proportion of these infectious and parasitic diseases are water borne. Metallic impurities, often in the form of arsenic, osmium, mercury etc. have been known to be detrimental to life. Few of the existing technologies adopted for water quality monitoring are reviewed here.

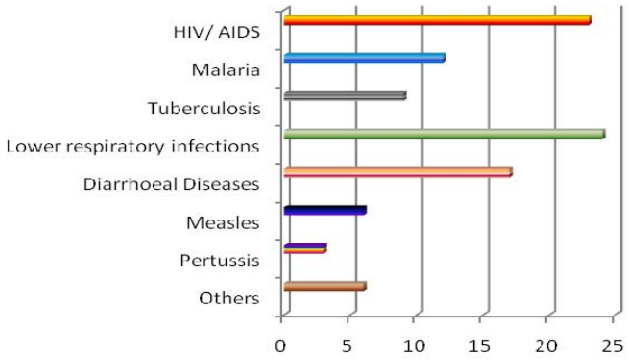

Fig. 1. Disability adjusted life years (DALYs) for infectious and parasitic diseases. †

† The graph is an attempt to reflect the impact of diseases on human health. Many of them are due to infested water consumption (US Centers for Disease Control & Prevention, 2005).

Baghel *et al.* [1] developed a rapid field detection method for arsenic ions in drinking water. Various reagents including magnesium turnings were used as a colorimetric assay for the metal ion detection. This could be used to increase the efficacy of arsenic detection kits. Jia *et al.* [2] demonstrated the use of gold electrodes to detect the presence of arsenic ions. Since minute concentrations of arsenic (~10μg/ml) could be potentially detrimental to human health, it is important to test its presence in samples where sulfur interference could be present. The most effective method for eliminating the interference caused by phosphate is by sequestering the arsenic from the phosphate by reducing the former to arsine gas (AsH_3). The most common technique for the field detection of arsenic is a modified Gutzeit test [3]. In this test, arsenic is reduced in the presence of zinc and hydrochloric acid to form arsine gas (AsH_3), as follows:

$$As_2O_3 + 6\ Zn + 12HCl \rightarrow 2\ AsH_3 + 6\ ZnCl_2 + 3\ H_2O$$

$$H_3AsO_4 + 4\ Zn + 8\ HCl \rightarrow AsH_3 + 4\ ZnCl_2 + 4\ H_2O$$

In the Gutzeit test, the liberated arsine gas (AsH_3) is then allowed to react with a detector paper that has been impregnated with mercuric bromide (HgBr). The arsine reacts with the mercuric bromide to produce mixed arsenic mercury halogenides to create a yellow to brown color change.

In the common photometric method for the detection of arsenic (silver diethyl-dithio-carbamate method), the production of arsine is also used to remove interferences. The silver diethyl-dithio-carbamate is dissolved in a chemical called pyridine. The generated

arsine gas is then bubbled through this solution. Arsine reacts with the silver salt, forming a soluble red complex suitable for photometric measurement, in this process. However, during the generation of arsine gas by reduction in these tests, sulfides are also reduced simultaneously with the arsenic to form hydrogen sulfide (H_2S). Hydrogen sulfide also reacts with the indicators for arsenic (mercuric bromide, silver diethyl-dithio-carbamate, etc.) to form colored complexes that interfere with the detection of arsenic.

Traditional methods of laboratory testing of water include the following:

- Atomic absorption spectrophotometer (hybrid generator) [4]
- Atomic absorption spectrophotometer (electro-thermal)[4]
- Electrochemical methods
- Total reflection X-ray fluorescence [5]
- Instrumental Neutron Activation Analysis (INAA) [6]
- Proton induced X-ray Emission (PIXE) [7]
- Spectrometer [8]

Numerous field kits have been developed by researchers to monitor the quality of water. A brief comparison between the traditional laboratory methods and the field kits is presented in Table 1.

Table 1: Comparison between laboratory methods and field kit method for arsenic detection.

Feature	Laboratory Method	Field Kit Method
Investment cost and maintenance	High	Low
Sample Preparation	Takes a long time	Not required
Skilled Personnel	Needed	Not Needed
False Negative Result	Less	Cross checking is suggested.

The Department of Occupational and Environmental Health (DOEH), at the National Institute of Preventive and Social Medicine (NIPSOM), has developed a low cost 'Field Test Kit' for the detection of arsenic in water. Researchers at the Northwestern University have developed a technology to detect mercury ions using gold nano-particles and DNA based on a simple 'litmus-like test'. In this research, Mirkin *et al.* [9] studied gold nanoparticles held together by complementary strands of DNA. This gold nano-particle solution is typically blue in color owing to the specific distance between the atoms. Upon heating, the DNA ruptures and the particles are no longer in proximity with each other and the solution turns red in color. It was established that mercuric ion binds selectively to the bases of a thymidine- thymidine (T-T) mismatch. The researchers designed each strand of DNA attached to a gold nano-particle, to have a single thymidine- thymidine (T-T) mismatch. If present, the mercury binds tightly to the T-T mismatch site. As per their study, the key to the technology is that the color change from blue to red occurs at 46 °C if the solution has no mercury, while it occurs at higher temperatures in the presence of mercury.

The MicroChem project consortium, headed by Danish water instrumentation specialist Danfoss, aimed to develop a new micro-analysis system for monitoring the levels of various chemical agents in wastewater at the outlets of sewage plants and factories. It also aimed to monitor the quality of drinking water supplies. According to the source of this article, the chemistry and the microchips have been formulated and tested for optical detection of ammonium, phosphorus and aluminium. The response time for ammonium detection, including the time needed for sampling and sample pre-treatment, as achieved in the laboratory was around four minutes. Laboratory optimization of the phosphorus detection method showed that a two-minute response time could be obtained [10].

Microfluidics is a multidisciplinary field encompassing engineering, physics, chemistry, microfabrication technology and biotechnology. Microfluidics deals with the behavior and control of small volumes of fluids (micro-liters to femto-liters). The behavior of fluids at the micro/nano-scale level can differ from macro-fluidic behavior primarily due to the surface effects (e.g., surface tension, wall friction, etc.) dominating the volumetric forces (body forces, pressure, etc.). Surface tension and fluidic resistance are factors that dominate the flow system as the device size is reduced.

The Reynolds number (Re) is extremely low in such cases, ensuring that the flow is laminar. Fluid mixing is very slow due to absence of turbulence. Hence, it is of prime importance to understand the low Re flows where diffusion alone must cause the fluids to mix.

Lab-on-a-chip (LOC) refers to a class of devices that miniaturizes, automates and integrates a number of laboratory functions on a single chip, capable of handling minute volumes of fluids (micro to less than pico liters). It would be apt to classify such platforms as a subset of Micro-Electro-Mechanical-Systems (MEMS) devices. A subset of LOC is the micro Total Analysis Systems (μTAS). A principal advantage of using micro Total Analysis Systems (μTAS) is that only a minute quantity of the chemicals/ reagents or samples are used. This enables fast reactions (diffusion limited reaction processes have a smaller reaction time constants when they are miniaturized due to the small thermo-chemical inertia of the reacting volumes), which are highly sensitive and provide precise results.

1.2 Review of the Existing Techniques to Fabricate Microvalves

Any fluid handling technology requires flow control elements in the form of flow actuators (pumps) and valves. A crucial landmark in the history of microfluidics was the development of efficient microvalves enabling the technology to reach its true potential and exploit the commercial opportunities. However, micro-valve fabrication is expensive and most of the micro-valves are not leak proof. In this section, the evolution of micro-electronics and the growth of micro-fabrication techniques, with an emphasis on micro-valves are presented.

In 1958, Jack St. Clair Kilby invented the first integrated circuit (IC) while working at Texas Instruments [11]. In the latter half of 1970, the concept of micro-fabrication was

extended to the realm of mechanical devices integrated with electronics [12, 13]. Manz *et al.* [14] introduced the term miniaturized total analysis systems (μTAS) which is abundantly used in a range of applications. These micro-fabrication technologies have resulted in reduction in feature sizes leading to the development of microfluidics systems such as the lab-on-chip.

Terry [1979] pioneered the development of microvalve [13]. At present, microvalves can be broadly classified as active and passive. These can be further categorized into valves with mechanical parts and valves with non-mechanical moving parts. Fig. 2 below outlines the various microvalve technologies reported in the literature.

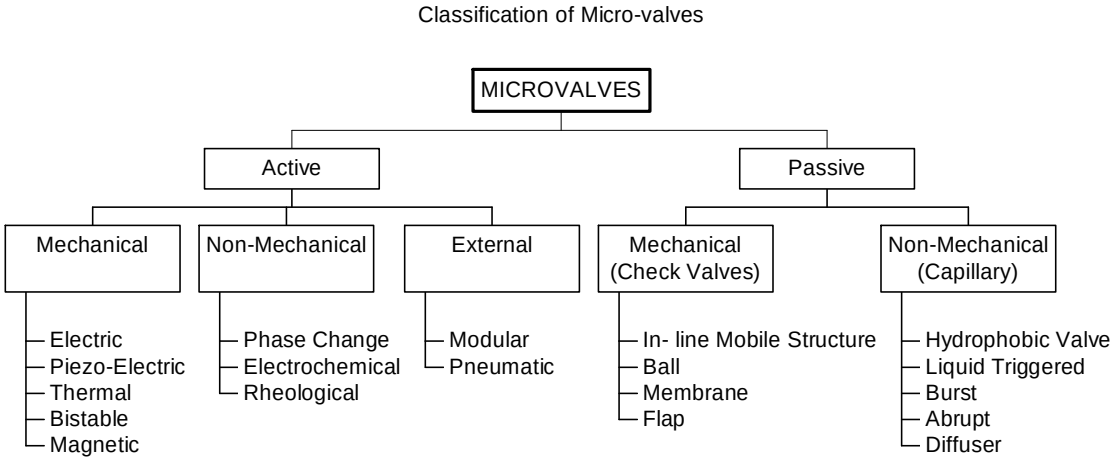

Fig. 2. Classification of microvalves.

1.2.1 Active Microvalves

An active microvalve typically requires an external source of power for its actuation. Kwang *et al.* [15] classified the active microvalves into three categories according to their actuation technique: mechanical, non-mechanical and external.

1.2.1.1 Mechanically Active Valves

These microvalve technologies were developed from MEMS based bulk or surface micro-machining techniques on the surface of the substrate [15]. The actuation modes for these microvalves are diverse: magnetic, bi-stable, thermal, piezo-electric and electrostatic.

Magnetic valves use external magnetic fields (e.g. Terry [13]). Another approach is based on the integrated magnetic inductors [16-19]. Electric valves use the principles of electrostatics (flexible membranes [20-22] or rigid membranes [23, 24]) or electro-kinetics. Other possibilities include piezo-electric valves as demonstrated by Rogge *et al*. [25] and Shao *et al*. [26]. Peirs *et al*. [27] proposed a robotic manipulator using this technique for self-propelling endoscopy application. Thermal valves can again be divided into thermo-pneumatic, bimetallic and shape memory alloy (SMA) types. Jerman [28] fabricated a bi-metallic microvalve with a Silicon layer of 8-micrometer thickness and an Aluminium layer of 5-micron thickness. Rich and Wise [29] developed a microvalve based on the thermo-pneumatic concept. Ruzzu *et al.* [30] developed a catheter tip consisting of a thermo-pneumatic three-microvalve system. PDMS membranes could also be used to fabricate valves based on this concept as demonstrated

by Takeo *et al.* [31]. Microvalves using shape memory alloys (SMA) were demonstrated by Kohl *et al*. [32]. These microvalves consume power only in a transient mode between two stable positions thereby obviating the requirement for continuous power supply. Goll *et al.* [33] proposed a microvalve with a bistable membrane made of polyimide. Ren and Gerhard [34] developed a bistable magnetic actuator making use of current pulse in trip coils to switch from one stable position to another.

Few of these types of microvalves are illustrated in the figures below. Fig. 3 illustrates a typical electromagnetic type of active mechanical microvalve. Fig. 4 shows a microvalve developed using shape memory alloys (SMA's). Fig. 5 shows a typical electrostatic mechanical valve. Piezo-electric transducers can be used to make active valves as shown in Fig. 6. Fig. 7 shows a typical bimetallic active valve. Fig. 8 shows a thermo-pneumatic valve.

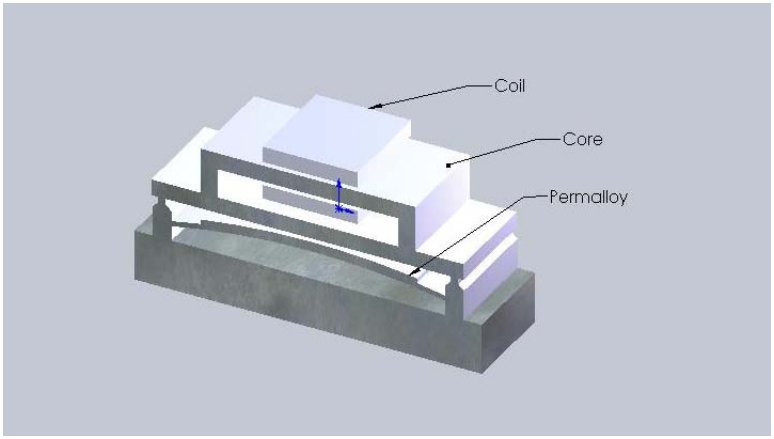

Fig. 3. Electromagnetic type of active mechanical microvalve.

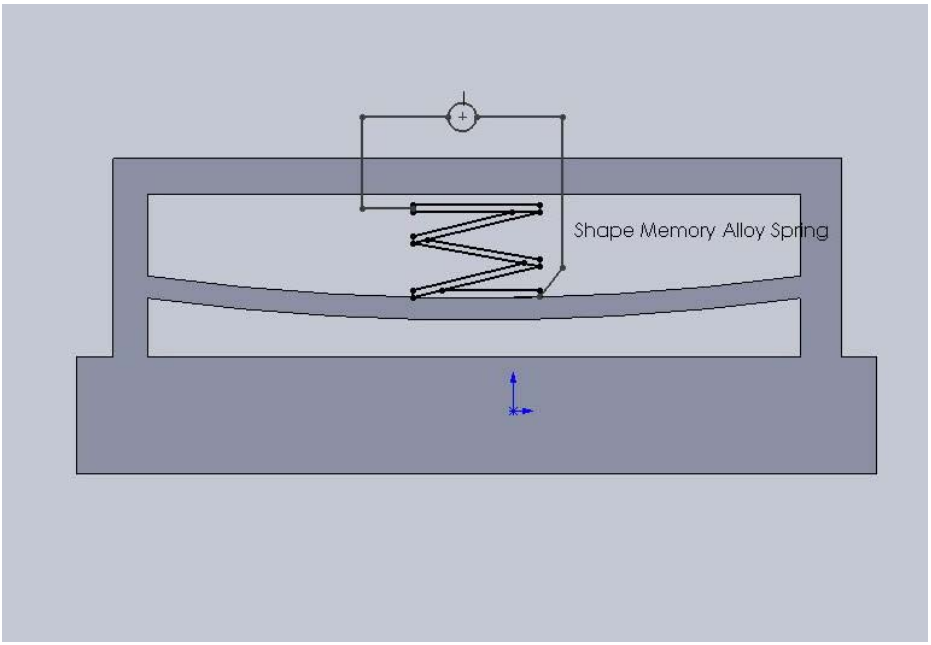

Fig. 4. Shape memory alloy active mechanical microvalve.

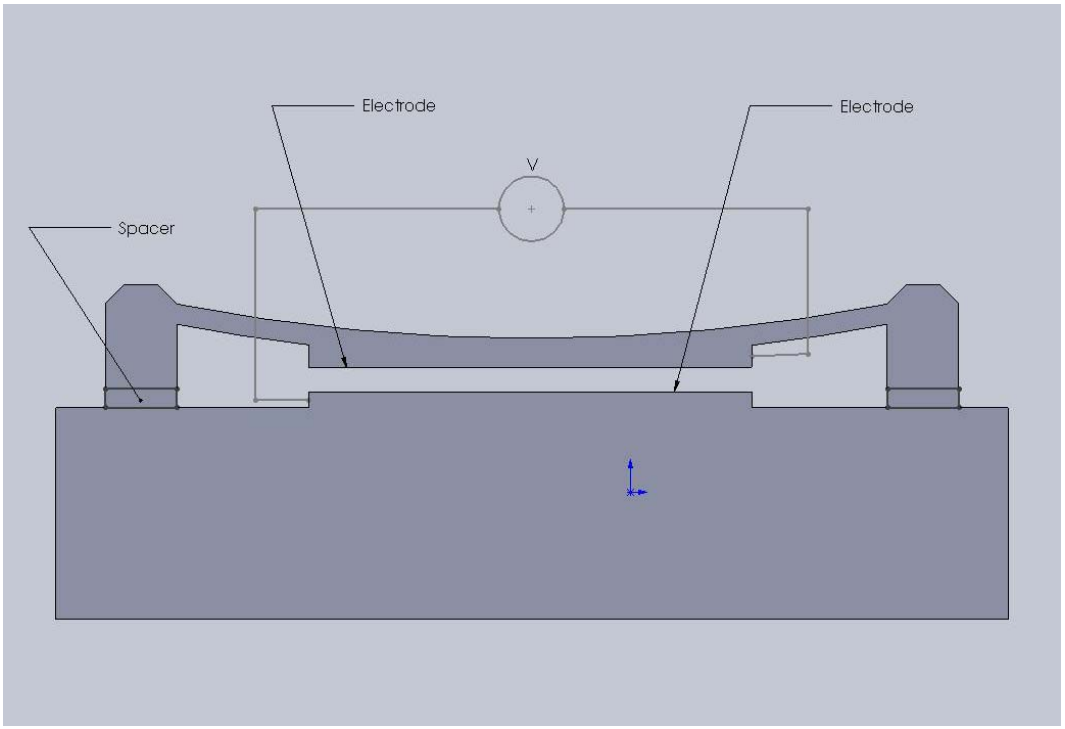

Fig. 5. Electrostatic based active mechanical microvalve.

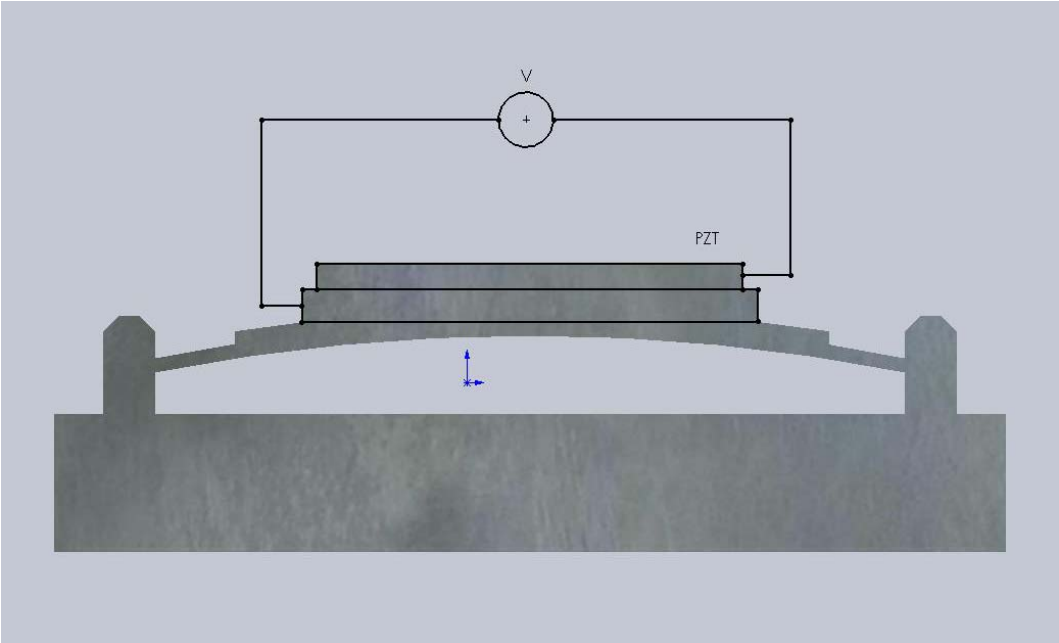

Fig. 6. Piezoelectric active mechanical microvalve.

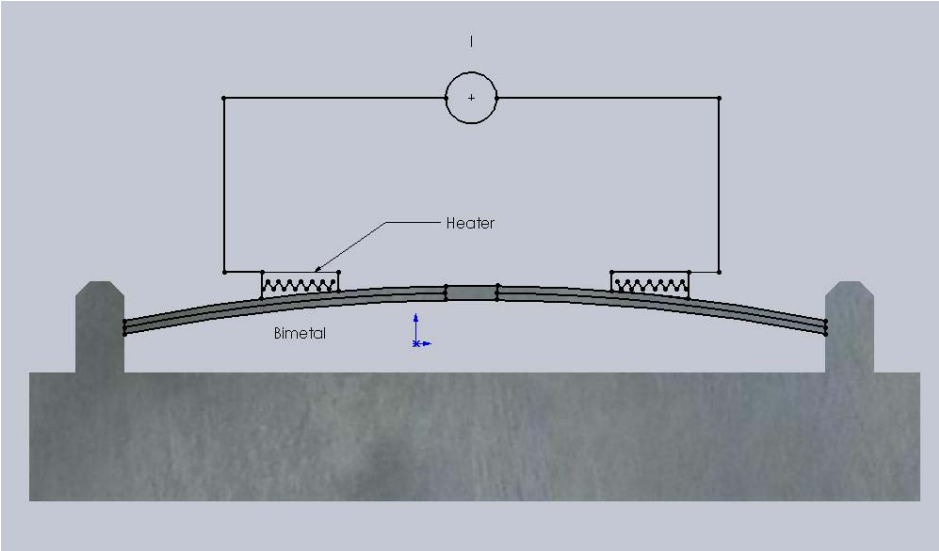

Fig. 7. Bimetallic active mechanical valve.

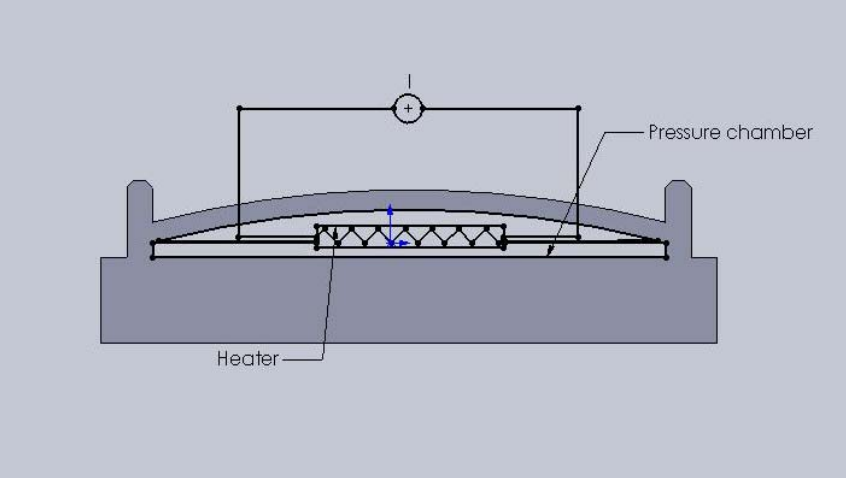

Fig. 8. Thermo-Pneumatic active mechanical valve

1.2.1.2 Non-Mechanical Valves

These active valves are based on various actuation principles: electrochemical, phase change and rheological materials. These valves are typically cheaper as compared to the others and possess a simple structure. Another advantage is conferred by their ease of disposal.

Neagu *et al.* [35] suggested the concept of using a deflectable membrane due to oxygen gas generation by electrolysis. Electrochemically or thermally generated bubbles in a capillary have been used as an actuation force in active check valves. They used a hydrogen bubble (generated electrochemically) to develop an active check valve in their microfluidics system. Microvalves utilizing phase change phenomena were reported by several investigators. Hydrogel microvalves have been developed to achieve autonomous flow control. These are very useful in drug delivery applications because of

the slow response time of hydrogel microvalves. Sol-gel microvalves were developed for micro polymerase chain reaction (PCR) demonstrations. Tashiro *et al.* [36] developed a microfluidic gel valve using reversible sol- gel transition. Paraffin microvalves were developed by Klintberg *et al*. [37]. Yoshida *et al.* [38] demonstrated the working of an Electro-Rheological (ER) microvalve using an electric field of strength of 50 KV/mm. He obtained a response time of 0.2 seconds. Hartshorne *et al*. [39] illustrated the working of a ferrofluid valve. The transition time for valve actuation was 15 -30 seconds.

Active microvalves can also be actuated from external sources. Modular in-built valves and rotational valves are two possibilities. Oh *et al.* [40] designed a modular in-built microvalve. Yang and Maeda [41] devised a similar valve specifically for electrophoretic applications. Hasegawa *et al.* [42] developed a rotary ten-way switching microvalve with auto-positioning of outlets. Cepheid's GeneXpert® system uses a microvalve with the same technique. Various types of pneumatic valves (membrane, in-line) are also reported in the literature.

1.2.1 Passive Microvalves

Passive microvalves do not require any external power sources for actuation and therefore enable autonomous operation resulting in cheaper fabrication costs. These valves can be divided into two broad classes: Mechanical and Non- Mechanical.

1.2.2.1 Mechanical Valves

Valves of this type consist of flaps, membranes, spherical balls and in-line mobile structures. Cantilever type flaps made of Silicon were demonstrated by Zengerle *et al.* [43, 44]. Oosterbroek *et al.* [45] developed a novel method to fabricate duckbill like flap valves on silicon wafers. Li *et al.* [46] developed a bridge-type membrane valve integrated with a piezo-electric micro-pump. Membrane check valves were made of a variety of polymers like Parylene, SU-8, Kapton, Mylar or Silicone. Carrozza *et al.* [47, 48] used a ball-type check valve for a piezo-electric micro-pump. Hasselbrink *et al.* [49] developed an in-line microvalve using a movable polymer structure. Reichmuth *et al*. [50] used similar valves for HPLC applications.

1.2.2.2 Non- Mechanical

Passive valves using diffusers or nozzles rely on direction dependent behavior of tapered flow channels. Tsai and Lin [51] developed a net flow from an inlet to an outlet by a thermally actuated bubble micro-pump. Capillary forces can be controlled actively or passively using electro-capillary, thermo-capillary or passive capillary effects. Ahn *et al.* [52] used passive microvalves on a smart lab-on-chip for point-of-care medical applications. A microfluidics multiplexer with an integrated dispenser could be used to illustrate the principle of structurally programmable microfluidics systems (sPROMS). A major drawback of most passive micro-valves (mechanical or non-mechanical types) is that the majority of these types of micro-valves, used in microfluidics, are not leak proof.

2. OBJECTIVE AND APPROACH

2.1 Scope and Definition of the Problem

In this work we report the design, analysis, development, manufacture and testing of various autonomous microfluidic devices that use passive micro-valves for flow control of micro-capillary flow actuation to achieve a set of pre-designed fluid handling steps. The passive micro-valves developed in this study are leak proof. The fluid handling steps involve flow actuation, mixing, bio-chemical reactions and separation of reaction products. The feasibility of using this device to achieve an autonomous micro-TAS platform is demonstrated by the synthesis of gold nano-particles using a peptide assay. The resulting gold nano-particles can be used for plasmonic detection of various analytes.

A plasmon is a theoretical construct which is defined as a quasi-particle resulting from the quantization of plasma oscillations. It is analogous to photons and phonons being quantization of light and sound waves, respectively. Hence, collective oscillations of the free electron gas density may be called plasmons. The excitation of these plasmons on the surface by light is denoted as a surface plasmon resonance (SPR).

This surface phenomenon forms the backbone of various instruments for measuring adsorption of a material onto a planar metal surface such as noble metal nano-particle

surface. It is the underlying principle in many colorimetric biosensor applications and different lab-on-a-chip sensors. Surface plasmon polaritons are electromagnetic waves that propagate parallel to the surface along a metal/dielectric interface. Such oscillations are very sensitive to any change of this boundary, such as the adsorption of molecules to the metal surface.

Numerous models (quantum theory, Drude-model, etc.) have been developed to describe the physics of surface plasmons. To simplify the problem, each material is treated as a homogeneous continuum, characterized by a dielectric constant. In order for these electronic surface plasmons to exist, the real part of the dielectric constant of the metal must be negative and its magnitude must be greater than that of the dielectric. This criterion is satisfied in the Infra Red-visible wavelength region for air/metal and water/metal interfaces (where the real dielectric constant of a metal is negative and that of air or water is positive).

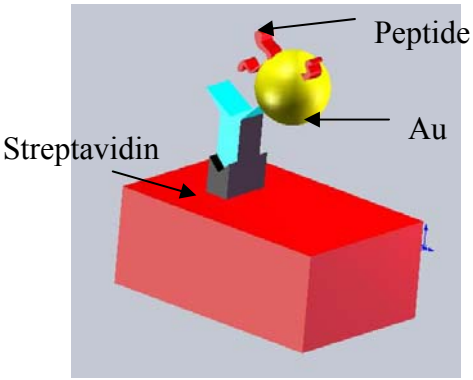

Fig. 9. Diagram showing the affinity interactions of gold nano-particle and peptides on a Streptavidin surface.

A number of methods could be used to obtain gold nano-particles of various sizes and shapes. Although classical methods like the *Citrate Reduction* [53], *Brust & Sonolysis* [54] have been used for a long time; we have used the method proposed by Slocik *et al.* using multi-functional peptides [55]. The primary reason for choosing this method of gold nano-particle synthesis is the uniform size distribution obtained in this method. Fig. 9 shows the schematic of an anti Flg coated glass slide. The biotinylated anti Flg antibodies attach to the Streptavidin. The peptides get attached to the gold nano-particles which in turn have an affinity towards the biotinylated anti Flg antibodies as illustrated.

The following reagents are used in this study for the synthesis of gold nano-particles:

1. Chloroauric acid (concentration 0.1M)
2. HEPES Buffer (concentration 0.1M)
3. Poly-tyrosine (concentration 10mg/ ml)

It is imperative to control the reaction by allowing different reagents to enter the reaction chamber in a specific order at definite time intervals.

Passive micro-valves can be used to control the sequence of flow actuation desired for this synthesis platform. Autonomous flow actuation using capillary wicking in properly designed microchannels and reservoirs obviate the need for external power sources. Valves composed of dissolvable materials (e.g., ionic and organic salts), control the sequence of reaction. A variety of salts could be used for this purpose. *Polyethylene*

glycol (PEG) is a suitable microvalve material, which was expected to meet the requirements for the microfluidic device. It was determined in the experiments that PEG interferes and competes with the peptide activity and therefore suitable substitutes were also investigated. *Sodium chloride* was explored as a viable alternative for the microvalve material. Alternate materials for microvalves explored in this study are *potassium chloride* (KCl) and s*odium acetate* (CH_3COONa). Various types of characterization experiments were performed to test the efficacy of the valves for obtaining gold nano-particles using the peptides. Analytical models for valve actuation were developed and calibrated using data from the characterization experiments. Valve actuation time was defined as the time required for opening a specific microchannel for flow actuation, after dissolution of the salt plug of a particular length placed at a specific distance from the reservoir housing the liquid reagent.

The following pictures will illustrate the reactions. First, the HEPES flows into the reaction chamber followed by Poly-tyrosine. After this, Chloroauric acid ($HAuCl_4$) [2] enters the reaction chamber. Gold nano-particles are obtained in the reaction chamber. We conducted experiments on a micro-fluidic platform made of a polymer, Poly di-methyl siloxane (PDMS), which has been used for various microfluidics applications in the past. Two separate designs were used in the experiments. The first design is a single layer microfluidic device while the second layout involves a bi-layer device. Fig. 10 illustrates the simple apparatus used to fabricate the salt bridge microvalves. A micro-

[2] Chloroauric Acid (Hydrogen Tetra-Chloro Aurate III Hydrate from Sigma Aldrich Co. CAS -27988-77-

needle tip is used to manipulate the molten PEG (melting point ~30 °C for PEG of molecular weight of 30,000 Daltons used in this study). The molten PEG is introduced into the microchannels fabricated in PDMS using the micro-tip needle as shown in Fig. 10. Typically the PDMS substrate is heated on a hot-plate during this operation. This ensures that the molten PEG flows easily into microchannel such that the shape of the plug is conformal to the shape of the microchannel and flush to the surface.

2.2 Design of the Microfluidic Substrate

Considerable effort was expended in the development of the microvalves in order to decide the final design for the microfluidic substrate. The basic objective of this device was to create gold nano-particles in-situ using a bio-chemical assay. There are various ways to manufacture gold nano particles. The method used in this study is based on using multifunctional peptides as proposed by Slocik *et al.* [55].

In this process, gold acid is reduced by multifunctional peptides to obtain gold atoms in the form of mono-disperse nano-particles. A 0.1M solution of Chloro-auric acid (gold acid- 2.5 µl) was reduced using a 10mg/ ml solution of poly-tyrosine peptide (10 µl) to obtain the noble metal nano-particles. The presence of a buffer solution (0.1M HEPES-500 µl) was necessary to ensure appropriate conditions for the reaction. Thus, three reagents were necessary for the assay apart from the water sample. In order to detect metal ions in this sample of water, the HEPES buffer needed to be introduced at two separate intervals into the reaction. Thus, in all, five micro-chambers were fabricated on

the microfluidic platform. Each of these chambers house a particular reagent (two of them filled with HEPES) which flow into the central reaction chamber at pre-defined intervals. Hence, all the five chambers were connected to the reaction chamber by means of micro-channels. To aid the flow of the fluid from one reservoir to another, the micro-channels were constricted in the direction of flow. This design eliminated any flow reversal.

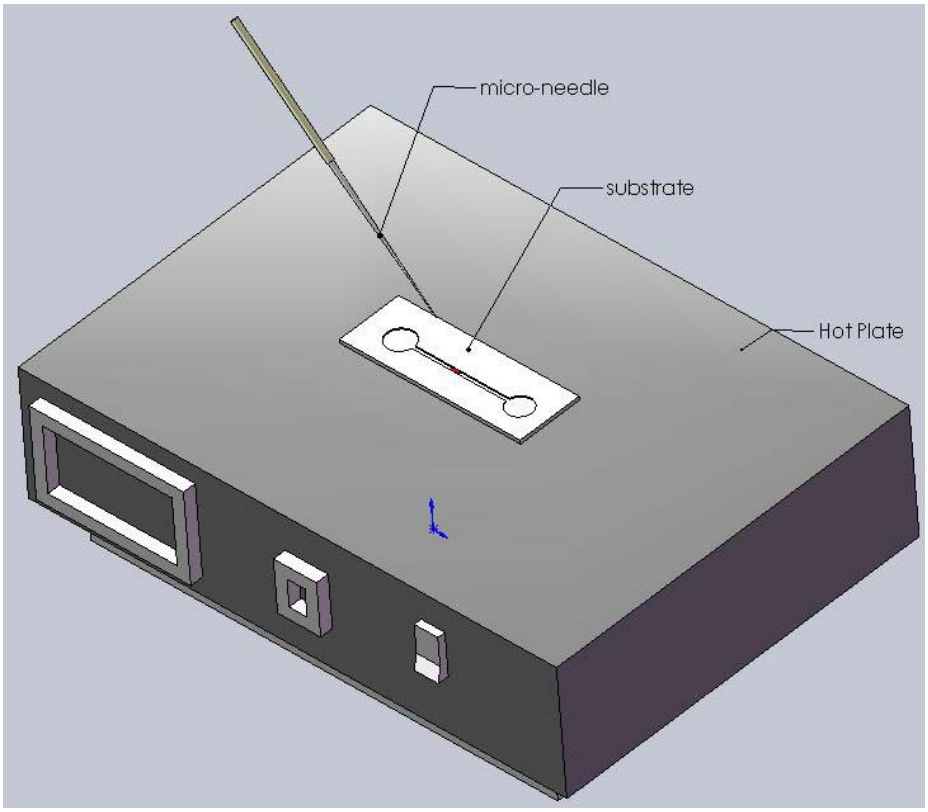

Fig. 10. Experimental set-up to fabricate microvalves in a lab-on-a-chip device. A micro-needle can be used to manipulate the chemical salt and placed inside a microchannel at a desired location.

The flow actuation was designed to enable continuous flow of the liquids downstream of the reservoirs without any flow reversal. Two separate sets of waste chambers were

fabricated on the microfluidic substrate to ensure continuous removal of the reaction products from the reaction chamber. Each of these flow paths was designed to contain a set of dissolvable microstructures that ensured that the capillary pressure gradient was always in the forward direction and therefore the fluid motion was always directed away from the reaction chamber into the waste chamber.

To ensure the formation of mono-dispersed gold nano-particles, the ratio of gold acid and HEPES buffer needs to be 1:200 by volume. The micro-channels were designed to have a depth of 150 microns. Thus, a microfluidic substrate of size 5 cm x 2.5 cm (2 inch x 1 inch) was designed as shown in Fig. 11.

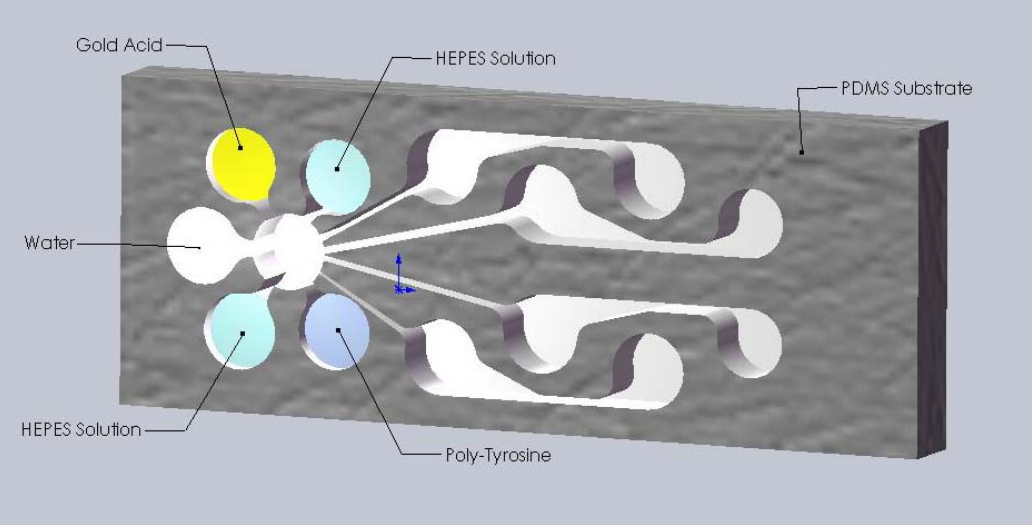

Fig. 11. Solid model showing the design of the single layer microfluidic substrate

This concept of a single layer microfluidic substrate could be extended onto a bi-layer device, which is explained in the later sections. The obvious advantage would be that

this device would be closed to the environment and be less susceptible to evaporation of water from the reagents.

The microfluidic assay was first fabricated on a polymer platform. A commercially available silicone called Poly- dimethyl siloxane (PDMS) was used for this purpose. Later, the same assay was reproduced on a microfluidic platform fabricated on a paper substrate. High quality chromatography paper was used for this purpose as discussed in the later sections [56].

3. ANALYTICAL MODELS

3.1 Introduction

One of our major objectives was to determine which experimental parameters would significantly affect the actuation time for the salt bridge valves. The geometric parameters used in the analytical models are length of the valve (l), width of the valve (w), depth of the valve (d) and distance between the valve and the reservoir (L_0). Fig. 12 shows the solid model diagram of the microfluidic device used for experimental characterization. It consists of two micro-chambers connected by a micro-channel. The valve is placed inside this channel and a drop of liquid is inserted into one of the chambers. This fluid flows into the channel, dissolves the valve and eventually flows into the other reservoir. The dependence of valve actuation on the size of the valve and its position in the micro-channel from the mouth of the reservoir is determined in this analysis.

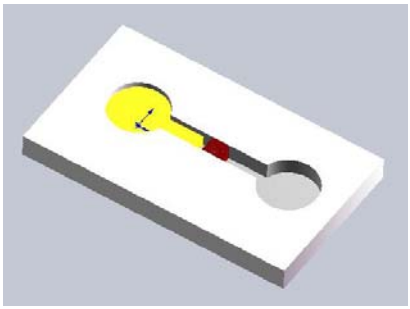

Fig. 12. Diagram showing the basic model used for valve characterization.

The material properties used in these models are – saturation concentration (C_s) of the salt that typically occurs at the water-valve interface and the diffusivity (*D)* of the dissolved salt material in water. In this analysis, a linear diffusion model is employed, where the diffusion of the mass is linearly proportional to the concentration gradient. The diffusivity is independent of the position and salt concentration (low concentration assumption). The sequence of flow is illustrated in Fig 13.

3.2 Model 1: Linear Profile

The first analytical model was developed by assuming a one dimensional (1-D) mass-diffusion model with a linear concentration profile for the dissolved salt. The concentration of the salt was highest at the interface of the valve with the water. The lowest concentration for the dissolved salt was expected at the entrance to the reservoir.

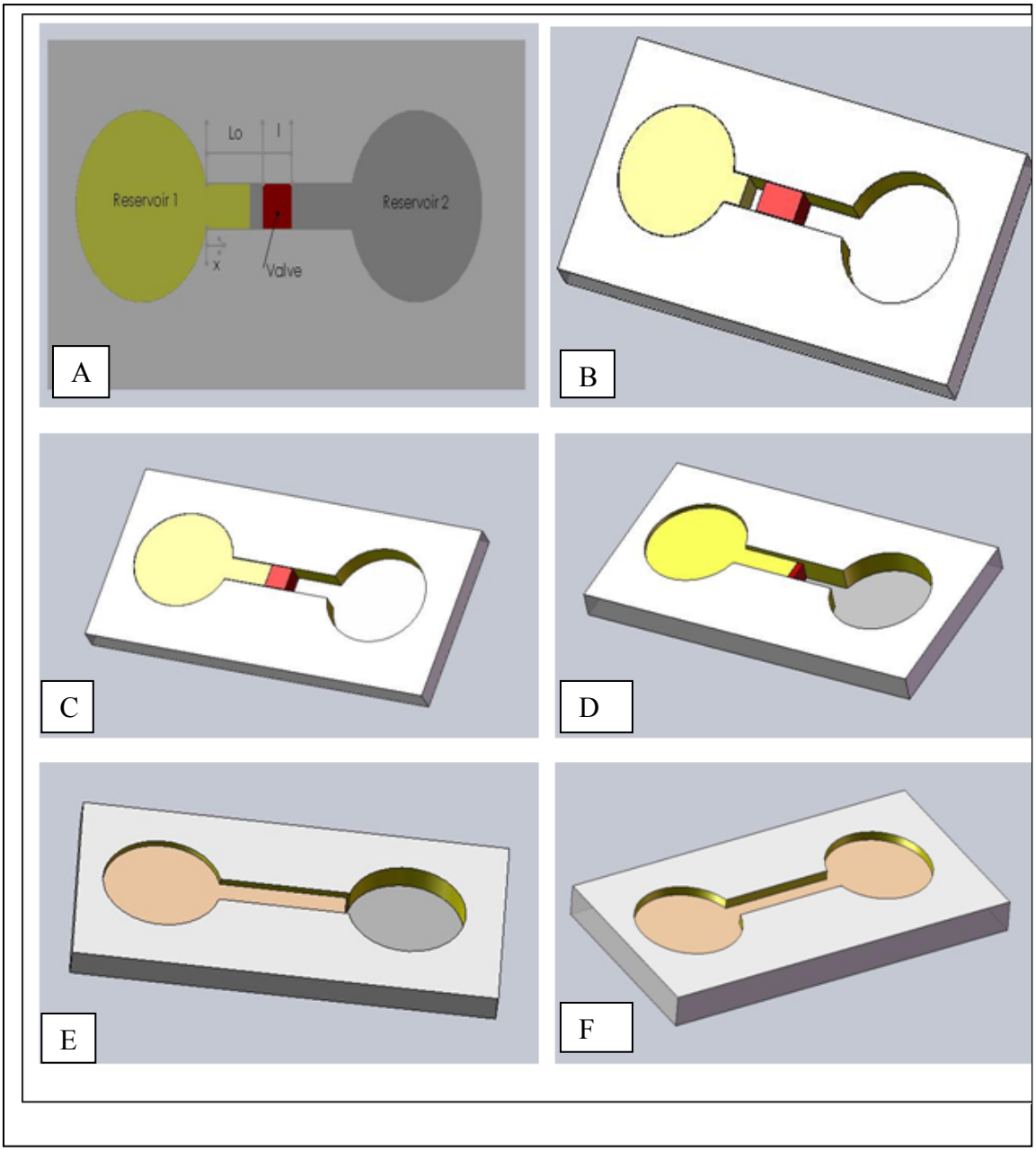

Fig. 13. Schematics for microvalve actuation. Fig. A. Mask used for valve characterization (showing coordinate system and parameters). Fig. B. Fluid flowing from reservoir 1 to 2 by capillary action. Fig C. Fluid meniscus in contact with the salt bridge valve. Fig. D. Valve in partially dissolved state. Fig. E. The valve has completely dissolved and the fluid flowing towards reservoir 2. Fig. F. Fluid filling up reservoir 2. It can be noticed that the level of fluid in the microfluidic device reduces in Fig. D, E and F.

The parameters L_0 and l are illustrated in Fig. 13A. Since the mass is conserved, the governing differential equation for this model is given by Equation 1. Here, x is the distance along the microchannel measured from the origin (base of the reservoir as shown in Figure 13A). The time for valve actuation is determined by integrating Equation 1, given by Equation 2. Alternately, to calculate the length of the valve required for a specific valve actuation time, Equation 3 can be used.

$$\frac{dx}{dt}.A.\rho. = (C_s - C_i).D.A / x \tag{1}$$

$$t = (L_o + l)^2.\rho / 2D(C_s - C_i) \tag{2}$$

$$(Lo + l)^2 = \frac{2D(C_s - C_i)t}{\rho} \tag{3}$$

Using the appropriate values of D, C_s, C_i andρ, for each salt solution in water the predicted values for valve actuation time can be plotted. The results were obtained by varying the values of Lo and l, to determine the dependence of the valve actuation time on these two independent parameters. By fixing the position of the valve, we can predict the size and geometry of the valve plug needed in order to obtain a particular valve actuation time. On the other hand, by assuming a value of l (fix the length of the valve), we can predict the precise position of the valve that would be necessary to facilitate the necessary time of actuation.

3.2 Model 2: Moving Boundary Profile

Moving boundaries are infinitesimally thin surfaces that separate adjacent phases; therefore, the coefficients of the underlying PDE and its derivatives may suffer discontinuities across interfaces. A typical example of a moving boundary problem would be the solidification from a melt. Fig. 14 shows a cross-sectional view of the valve characterization assay.

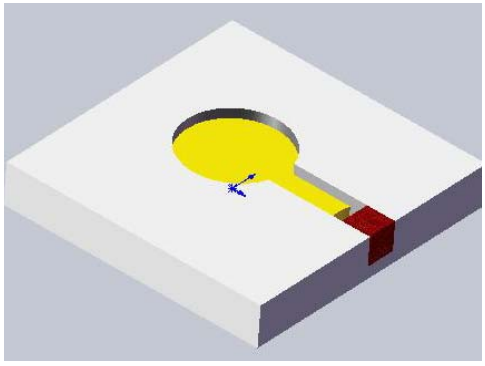

Fig. 14. Cross-sectional view of the microfluidic assay used for valve characterization.

The governing differential equation is given by Equation 6. Equation 7 can be used to determine the value of the dimensionless parameter λ. The value of Jakob number *(Ja)* is given by Equation 8. The velocity is a function of Jakob number (*Ja*), diffusivity (*D*) and time (*t*), which could be determined by using Equation 9. In the moving boundary approach, the concentration gradient, $\theta = (C - C_i) / (C_s - C_i)$ is given by Equation 10.

$$(Cs - Ci).D.\frac{\partial \theta}{\partial z} = \rho V = -m^{*"} \qquad (4)$$

$$\theta = A.erf\left(\frac{z}{\sqrt{4Dt}}\right) \tag{5}$$

$$(Cs - Ci).D.(1/erf\,\lambda).e^{-\lambda^2}.(1/\sqrt{4Dt}).(2/\sqrt{\pi}) = \rho\lambda\sqrt{\frac{D}{t}} \tag{6}$$

$$\lambda = \sqrt{\frac{C_s - C_i}{2\rho}} \tag{7}$$

$$Ja = 2\lambda^2 \tag{8}$$

$$v = \sqrt{\frac{Ja.D}{2t}} \tag{9}$$

$$\theta = \frac{erf\left(z * 10^4 / \sqrt{t}\right)}{erf\,0.363} \tag{10}$$

$$z = 3.77 * 10^{-5}\sqrt{t} \tag{11}$$

4. EXPERIMENTAL PROCEDURE

4.1 Introduction

Experiments were performed to study the dependence of valve actuation time on the geometric parameters. The parameters include the length of the salt bridge (or plug), width, height and the distance of the plug boundary from the reservoir, as explained earlier. Other parameters include the solubility of the salt in the working liquid and its diffusivity. Valve actuation is defined as the time taken by the solvent (or any other working liquid) to dissolve the salt plug to enable the liquid to flow into the remaining part of the channel.

To simplify the problem, it is expected that the total time (t) for valve actuation is a function of the distance from the reservoir (L_o) and length of the valve (l) only (assuming a 1-D diffusion model). Various lengths of salt plugs were implanted into the micro-channel at various distances from the reservoir. A fixed volume of water droplet was introduced into the reservoir, which in turn resulted in micro-capillary wicking of water into the micro-channel until it came in contact the salt plug. The water in contact with the salt plug gradually dissolved the salt until the salt plug was completely dissolved. Once this happened, micro-capillary wicking of water continued into the remaining portion of the micro-channel.

Experiments were performed using a variety of salts: sodium chloride (NaCl), Polyethylene glycol (PEG), potassium chloride (KCl) and sodium acetate (CH_3COONa) as the valve material. From the graphs shown below, the experimental data was used to validate and calibrate the predictions by the numerical models for valve actuation as a function of the length of valve (l) and position (L_o).

4.2 Sodium Chloride

Sodium chloride is commonly available, easy to handle and provides consistent experimental results with good repeatability. There is some amount of variability in valve actuation time as a function of geometric dimensions of the plug. Valve plugs of length (l) = 0.5mm, 0.7mm, 1mm and 1.3mm were implanted at distances (L_o) of 0mm, 3.5mm, 5mm and 7 mm from the micro-well.

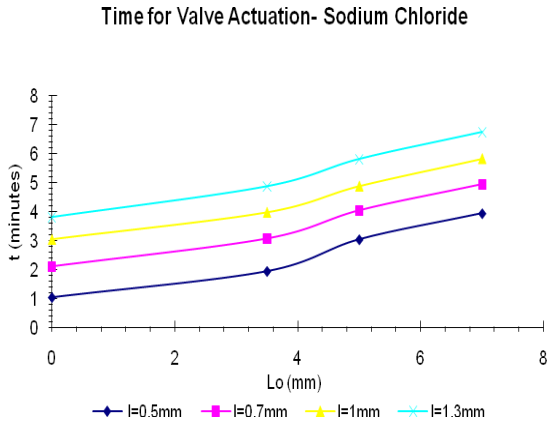

Fig. 15. Graph showing the variation of valve actuation time with distance L_o for particular values of *l*.

The graphs for valve actuation time as function of distance from the reservoir for various lengths of salt plug are shown in Fig. 15. The graph shows that for a given length of the salt plug the valve actuation time increases monotonically with distance from the reservoir. Also for a given distance from the reservoir, the valve actuation time increases with the length of the salt plug as shown in Fig. 16. It can be seen that this graph follows a linear profile, with some amount of distortions.

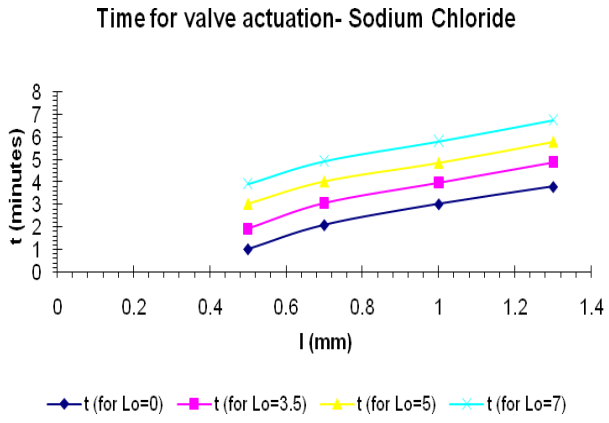

Fig. 16. Graph showing the variation of valve actuation time with length of the valve (*l*) for different values of L_o.

Another approach to characterize the valve actuation time could be in terms of the volume of salt to be dissolved. A simple formula to calculate the volume of salt would be:

Volume= length (*l)* x width (*w)* x Height (*d)* of the valve (mm^3)

The height of the valve is assumed to be equal to the depth of the channel, which is about 80 microns in this case. A plot of the time required for valve actuation against the volume of salt valve is shown in Fig. 17.

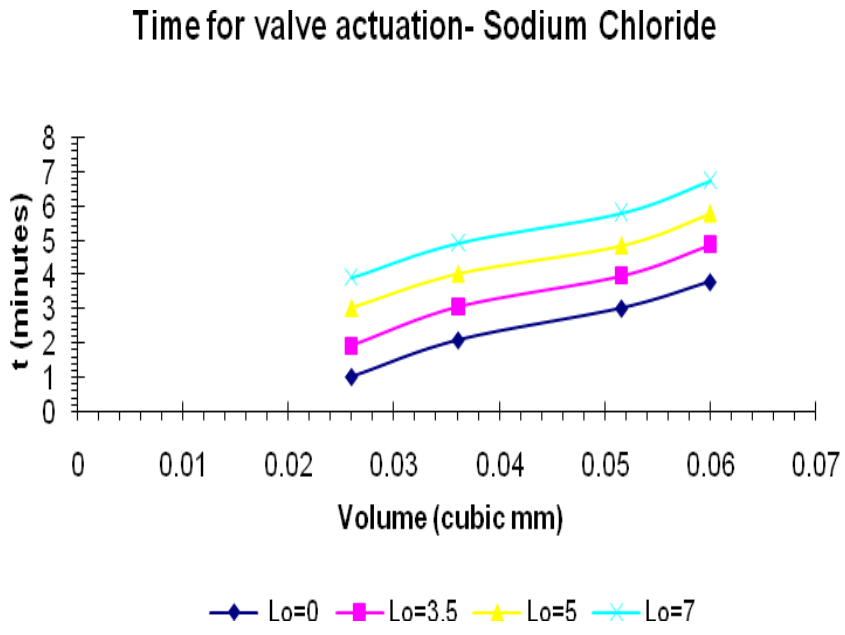

Fig. 17. Graph showing the variation of valve actuation time (*t*) with the volume of the salt bridge valve for different values of L_o.

4.3 Sodium Acetate

This salt provides a very high repeatability in the experiments and is easy to handle, which are desirable characteristics. Fig. 18 shows the increase in the time of valve actuation with an increase in the value of L_o i.e. the value of time (*t*) increases as the distance of the valve location from the reservoir is increased. Fig. 18 shows the result, for a valve of length l= 0.5mm. Fig. 19 shows the variation of time of valve actuation with respect to Lo for a value of l = 0.7mm while Fig. 20 demonstrates the same for a

value of l = 1mm. The standard deviation amongst the three trials is the least in case of sodium acetate showing a higher repeatability of the experiments using this salt.

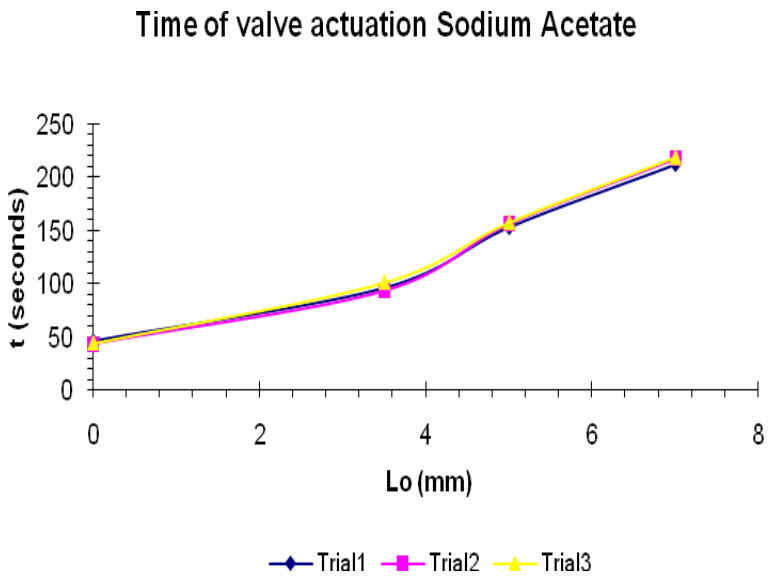

Fig. 18. Graph showing the variation of valve actuation time (*t*) with the distance L_o (*l* = 0.5 mm) for three experiments. The results indicate a high degree of repeatability.

The time of valve actuation increases with distance Lo for each of the three trials, as illustrated in Fig. 18.

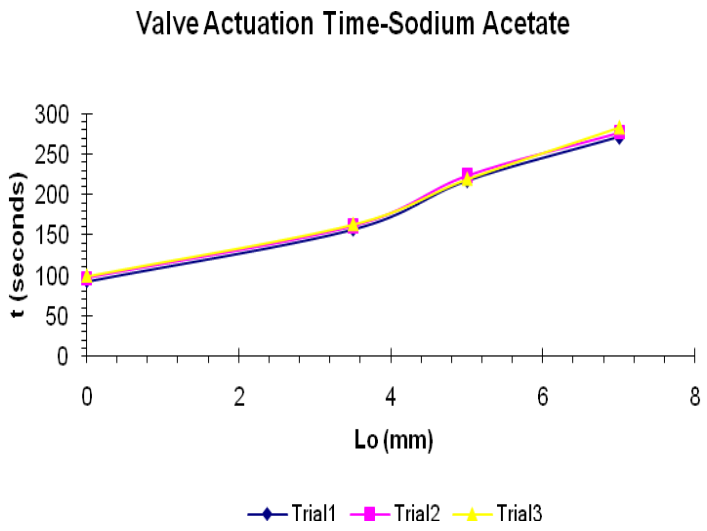

Fig. 19. Graph showing the variation of valve actuation time (*t*) with the distance L_o (0.7 mm) for three experiment trials. The results, once again, indicate a high degree of repeatability.

The graphs show a similar trend for valve lengths of 0.7 mm and 1 mm as illustrated in Fig. 19 and 20.

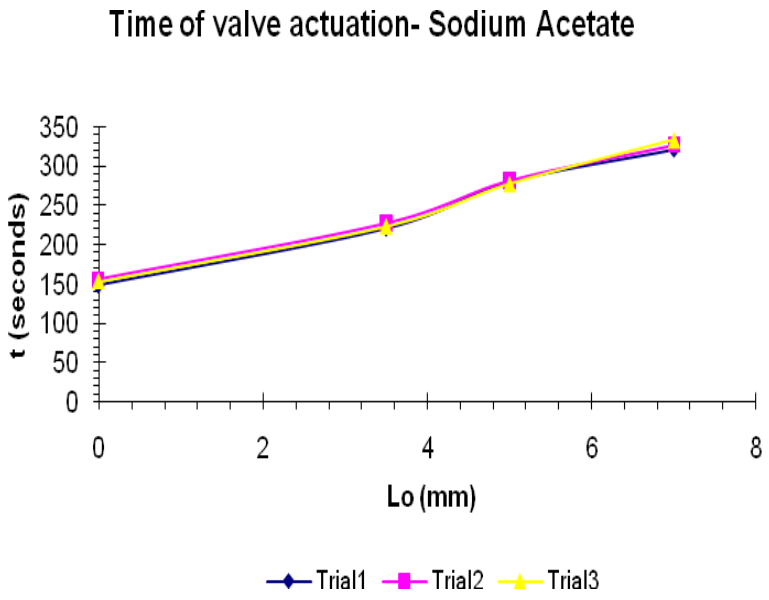

Fig. 20. Graph showing the variation of valve actuation time (*t*) with the distance L_o (*l* = 1mm) for three experiment trials. The results, in this case too, indicate a high degree of repeatability.

4.4 Polyethylene Glycol

Polyethylene Glycol (PEG) is another choice for fabricating the passive actuation valves for obtaining the microfluidic device**.** Fig. 21 shows the variation of time for valve actuation with Lo for various lengths of valve (*l)*. With an increase in L_o the value of time (*t)* gradually increases.

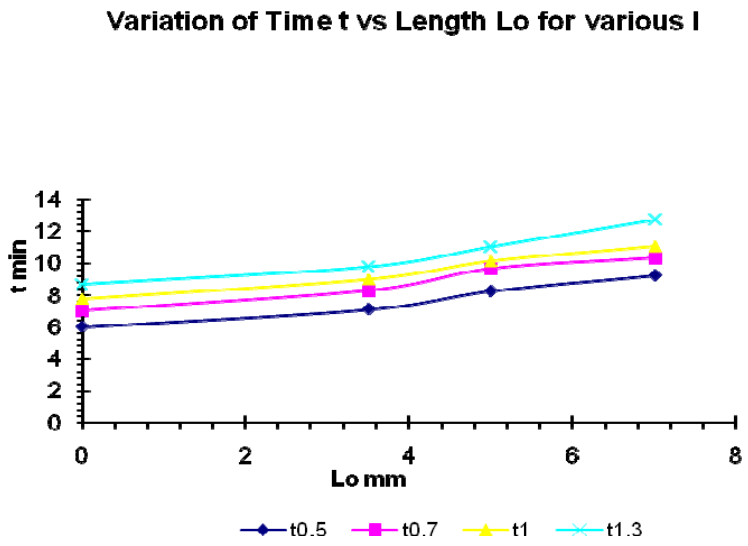

Fig. 21. Graph showing the variation of valve actuation time with distance L_o for various values of *l*.

A definite pattern can be observed from the change in the valve actuation time as compared with valve size (l) for various values of L_o, as illustrated in Fig. 22.

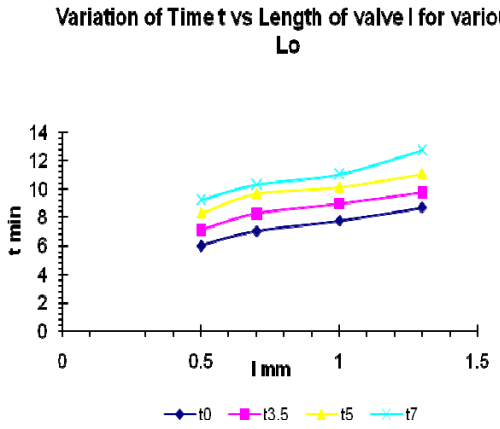

Fig. 22. Graph showing the variation of valve actuation time with length of the valve (l) for various values of L_o.

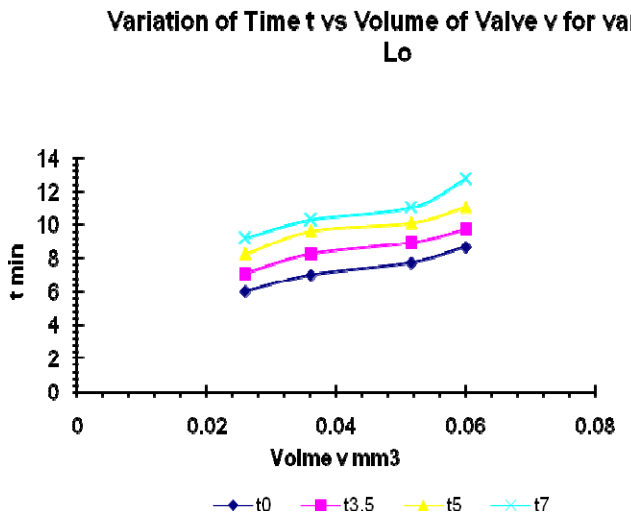

Fig. 23. Graph showing the variation of valve actuation time with volume of the salt used to fabricate the valve. The results are plotted for various values of L_o.

Fig. 23 illustrates the change in valve actuation time with respect to the volume of salt used to fabricate the valve. The reason for large variation in the valve actuation time for PEG as the valve material is due to the thermo-physical properties of PEG, which is known to dissolve water in all concentrations and vice versa. In other words, there is no finite value for saturation concentration of PEG to dissolve in water (theoretically, the saturation concentration is infinite). Hence, the valve performance is inconsistent for the different experimental runs. The variations occur from experiment to experiment, potentially due to different concentrations of PEG at the water-valve interface for each experimental run. Due to the material property of PEG, this cannot be controlled in-situ during the experiments and hence the large variation of valve actuation time is observed in the experimental data.

5. DISCUSSION- VALIDATION OF MODELS

5.1 Introduction

The results obtained from the linear and non-linear models were compared with that obtained from the valve characterization experiment.

5.2 Comparison of the Linear Model with Experimental Data

The graphs below show the comparison of the predictions from the linear model (in blue) with the obtained experimental data (red data points). This particular analysis has been performed with a sodium chloride- water combination. Fig. 24 shows the comparison of the linear model profile and the experimental data. Fig. 24 shows the variation of valve actuation time (t) against the length L_o for a value of l = 0.7 mm. Fig. 25 shows the variation of time of valve actuation (t) against the length L_o for l = 1 mm. Fig. 26 shows the variation of time of valve actuation (t) against the length L_o for l = 1.3 mm.

These graphs show that the predictions from the linear model, for the time for valve actuation for various values of L_o and l, are in good agreement with the experimental data for specific values of the experimental parameters. It should be noted that these predictions are more accurate for small values of L_o, i.e., the linear model is accurate as long as the valve is placed close to the micro-well or reservoir. The accuracy of the model decreases with an increase in the distance L_o.

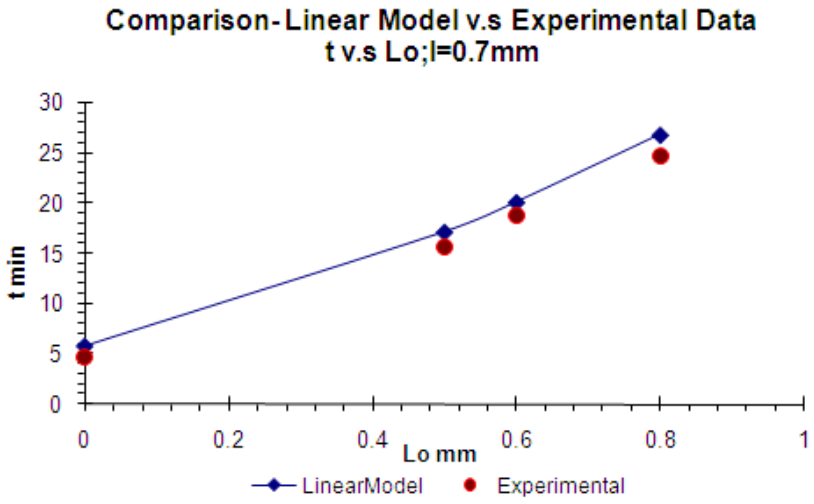

Fig. 24. Comparison between the linear model (in blue) with the experimental data (in red) for valve actuation time as a function of the position of the salt plug (L_o) where l = 0.7 mm. The salt used is sodium chloride in water.

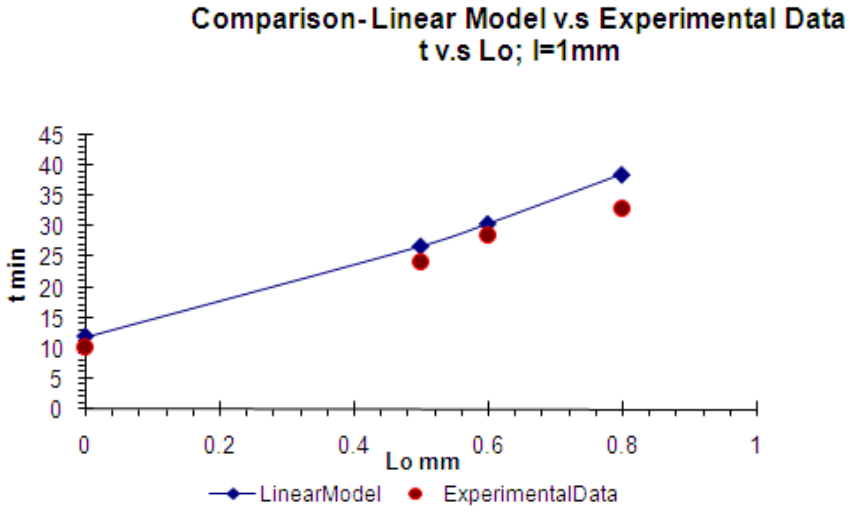

Fig. 25. Comparison between the linear model (in blue) with the experimental data (in red) for valve actuation time as a function of the position of the salt plug (L_o) where l = 1 mm. The salt used is sodium chloride in water.

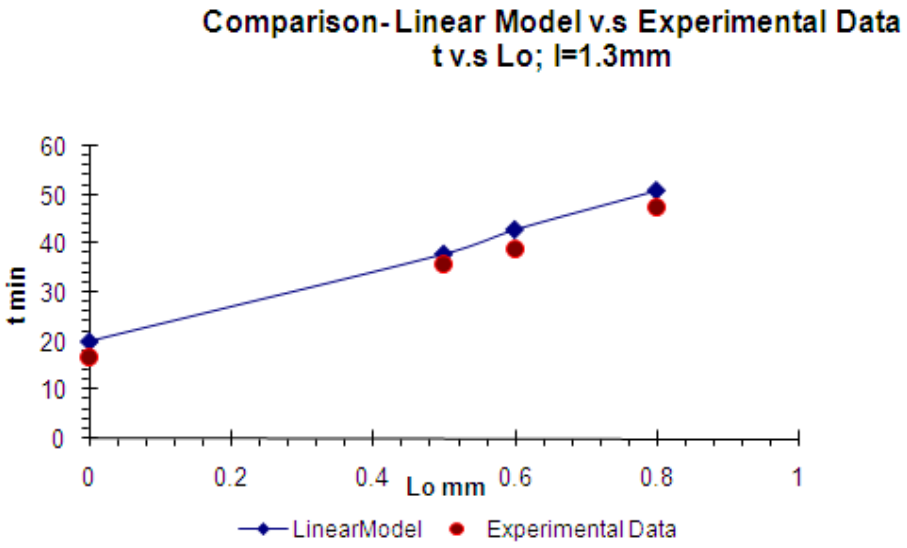

Fig. 26. Comparison between the linear model (in blue) with the experimental data (in red) for valve actuation time as a function of the position of the salt plug (L_o) where l = 1.3 mm. The salt used is sodium chloride in water.

5.3 Comparison of the Moving Boundary Model with Experimental Data

This section is dedicated to the comparison of the data obtained from the non-linear profile (moving boundary model – also designated as "Model2") and the experimental results for valve actuation time. The non-linear model assumes a moving boundary approach, as discussed in the previous sections.

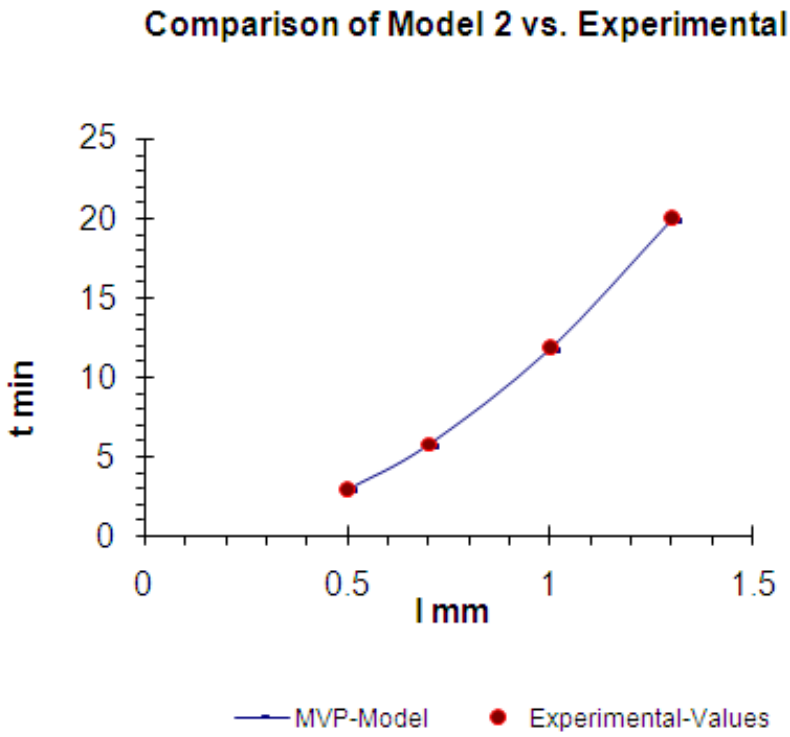

Fig. 27. Graph showing the variation of valve actuation time with length of the valve (*l*). This plot compares the moving boundary profile with the experimental data for sodium chloride.

The graph shows that the valve actuation time obtained from the non-linear model is in close agreement with the experimental data. It would thus be fair to say that, in order to predict the size of the valve required for any specific application, the non-linear model would provide more accurate results. Fig. 27 shows that the profile is almost linear in the initial stages. Thus, it can also be inferred that the moving boundary profile is in agreement with the linear model for small values of *l* and where the valve actuation time is smaller. This profile was generated using a sodium chloride salt bridge valve.

Fig. 28 shows the concentration profile at a particular point. At this point, the value of z is fixed and the concentration gradient is plotted against time, as obtained from the moving boundary solution.

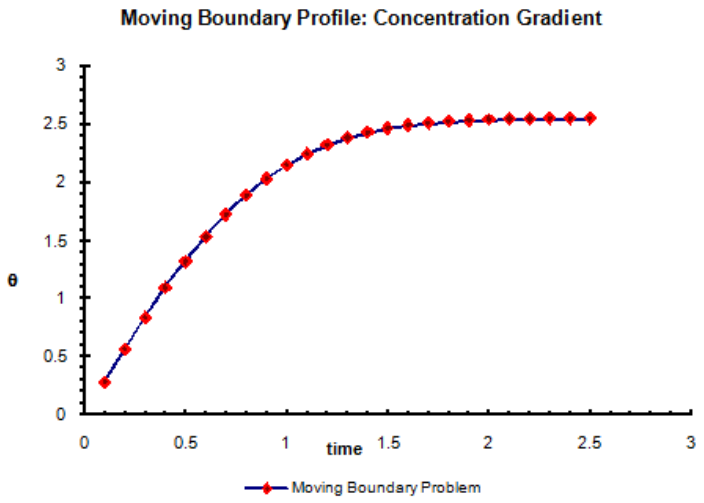

Fig. 28. The concentration profile predicted using the moving boundary model: variation of concentration gradient with time for an assumed value of z.

Using a profilometer, the salt profile within the microchannel was obtained as shown below. The depth of salt valve (*d*) typically matched the depth of the microchannel. Using three profiles of the valve at different cross-sections, a three dimensional profile for the same could be created as shown below. Fig. 29 illustrates the three dimensional model for the PEG valve while Fig. 30 shows the same for a sodium chloride valve.

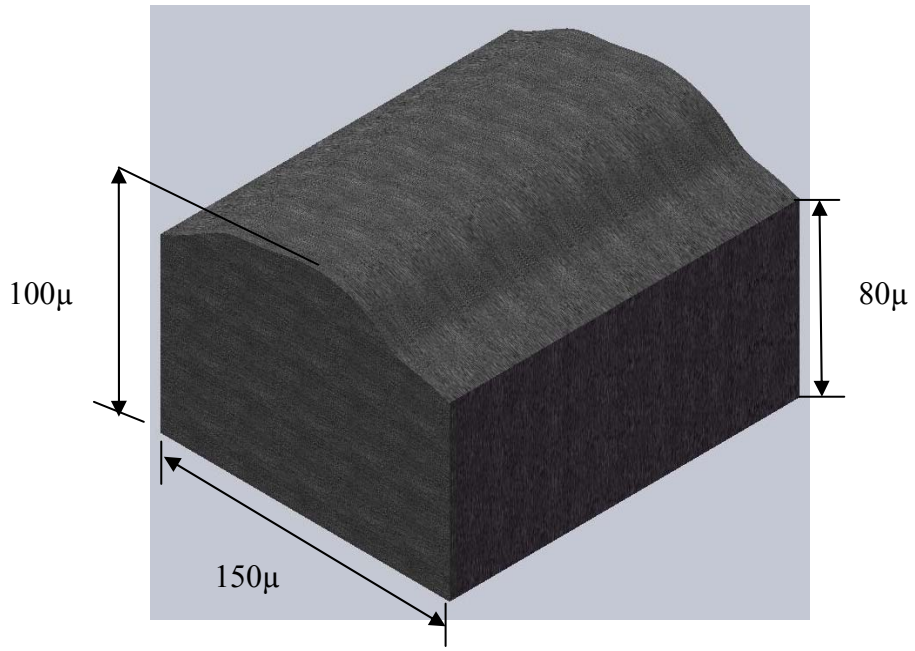

Fig. 29. Solid model showing the three dimensional profile of the PEG salt valve obtained from experimental measurements, once it solidified in the microchannel.

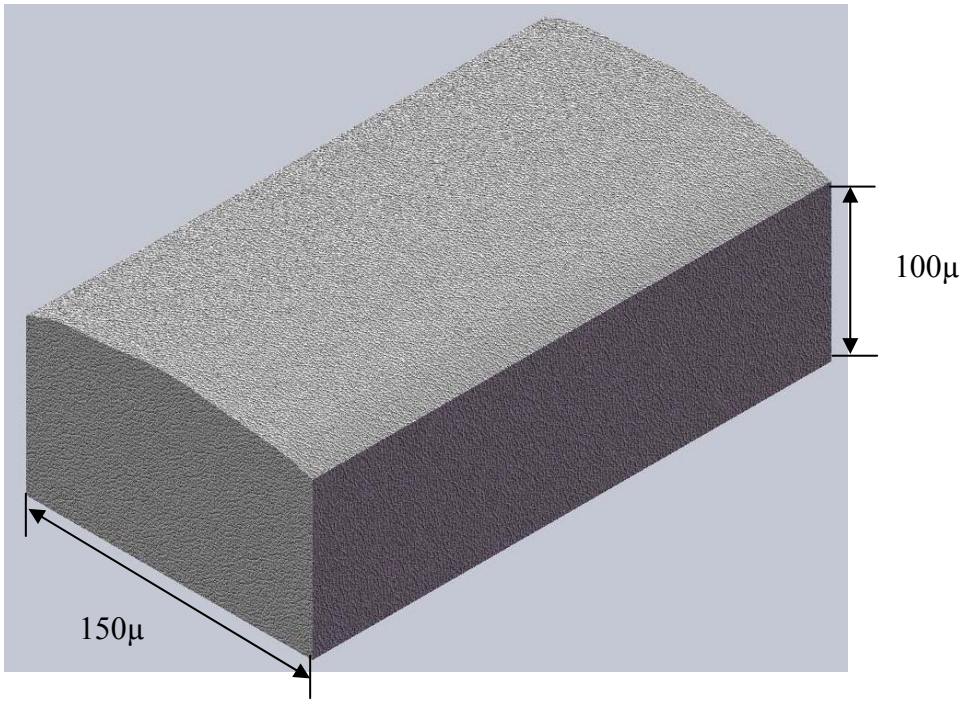

Fig. 30. Solid model showing the structure of a sodium chloride salt bridge valve inside a microchannel.

6. RESULTS

6.1 Introduction

This section is divided into four major sections. The microfluidic assay was developed on PDMS as well as on high quality chromatography paper. Two different forms of PDMS substrates were developed for this purpose: a single layer and a double layer device. Initially, we demonstrated that the single layer microfluidic device fabricated on PDMS substrate can be used to produce gold nano-particles from Chloro-auric acid. Next, we implemented the peptide assay in the LOC. In this assay all the reagents are introduced into the substrate at the same time and the complete assay is performed independently in the microfluidic device.

6.2 Single Layer Assay on PDMS

This assay has been previously described in section 2.2.

6.2.1 Production of Gold Nano-Particles on the PDMS Substrate

The following figures describe each step in the reaction. Fig. 31 shows the image of the micro-fluidic substrate prepared by soft lithographic processes using a negative photo-resist (SU-8). A solid plug of sodium chloride can be seen inside the micro-channel strategically placed to serve as a passive microvalve.

Fig. 32 shows the reaction chamber in the microfluidic device. Five reservoirs are connected to this central chamber by micro-channels. Each of these chambers typically

carries a reagent, which is transported to the central reaction chamber. To make the valves out of sodium chloride, the concentrated salt-water solution is heated to a temperature of about 160 ˚C. With the help of the tip of the needle of a micro-syringe, the salt can be manipulated and placed inside the microchannel at the desired location.

The experiment starts with the delivery of a 0.1 M solution of HEPES buffer into one of the reservoirs as shown in Fig. 33. A micro-syringe was used for this purpose. HEPES (ethane-sulfonic acid) acts as a buffering reagent in the chemical assay. Fig. 34 demonstrates the capillary flow of the fluid into the reaction chamber. The whole volume of fluid flows into the reaction chamber as illustrated in Fig. 35 and Fig. 36. There is no need for any external source of power to achieve this flow. A key step in this process was to make the surface of the polymer (PDMS substrate) hydrophilic by an oxygen plasma treatment.

The next step in this assay involves the introduction of a peptide called Poly-tyrosine. A 10mg/ ml solution is delivered into another reservoir on the microfluidic substrate. This fluid dissolves the sodium chloride valve and enters the reaction chamber as shown in Fig. 37. After the valve actuation, the two fluids (HEPES Buffer and Poly-tyrosine) mix with each other in the reaction chamber.

Chloro-auric acid (gold acid or $HAuCl_4$) is now introduced into the third reservoir as shown in Fig. 38. The acid solution dissolves the valve and, as anticipated, dissolves it to

flow into the reaction chamber. Once this is accomplished, the gold ions in the acid are reduced to gold atoms as shown in Fig. 39.

$$Au^{3+} \longrightarrow Au^{0}$$

The gold ions are reduced by the peptide and form a dark brown precipitate. This dark colored liquid flows into the drainage chambers as shown in Fig. 40 and Fig. 41. The dark colored precipitate is caused by the formation of gold nano-particles. This forms the basic fluid handling sequence of the entire assay.

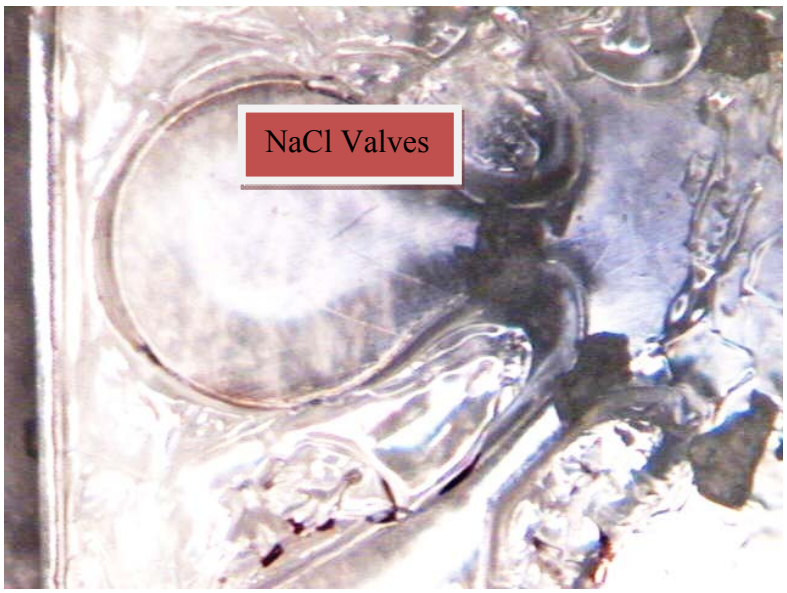

Fig. 31. Image showing a salt-bridge valve placed inside a micro-channel at the junction between the reservoir and the central reaction chamber. The size and position of this valve influences the valve actuation time.

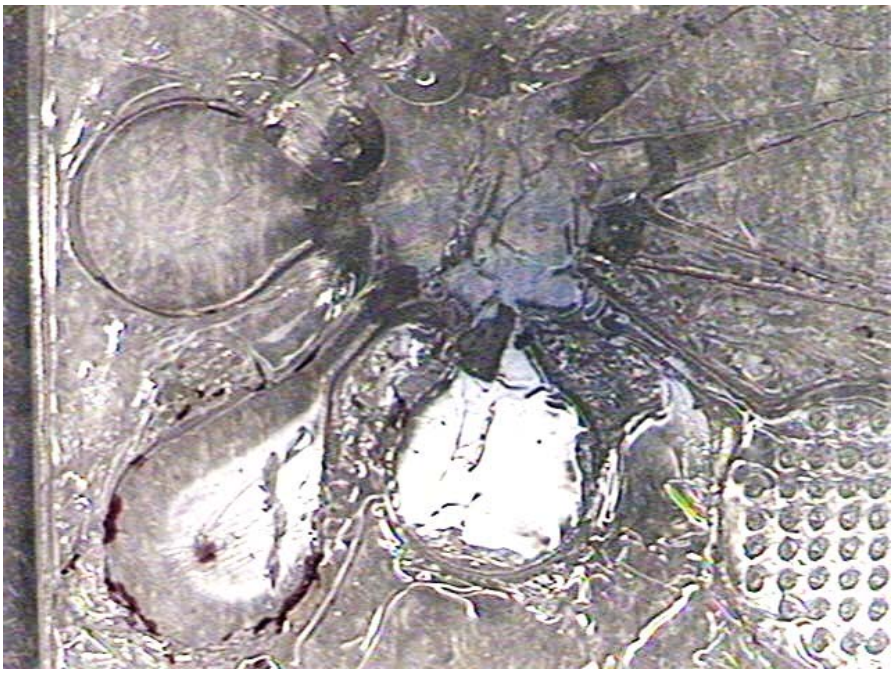

Fig. 32. Image showing the reaction chamber of the microfluidic device. Each of the reservoirs is connected to this central chamber by micro-channels with passive actuation valves placed inside them.

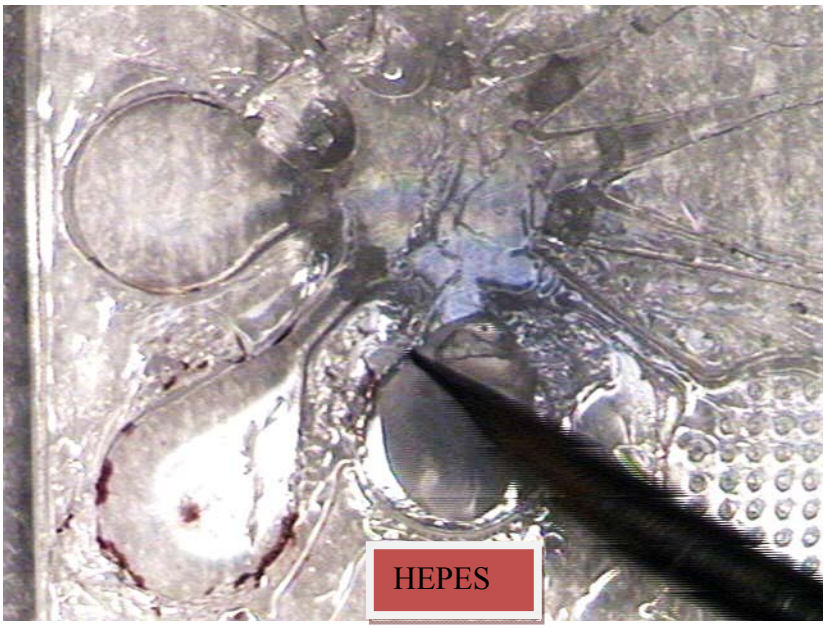

Fig. 33. Image showing the introduction of HEPES buffer solution using a micro-syringe into the reservoir.

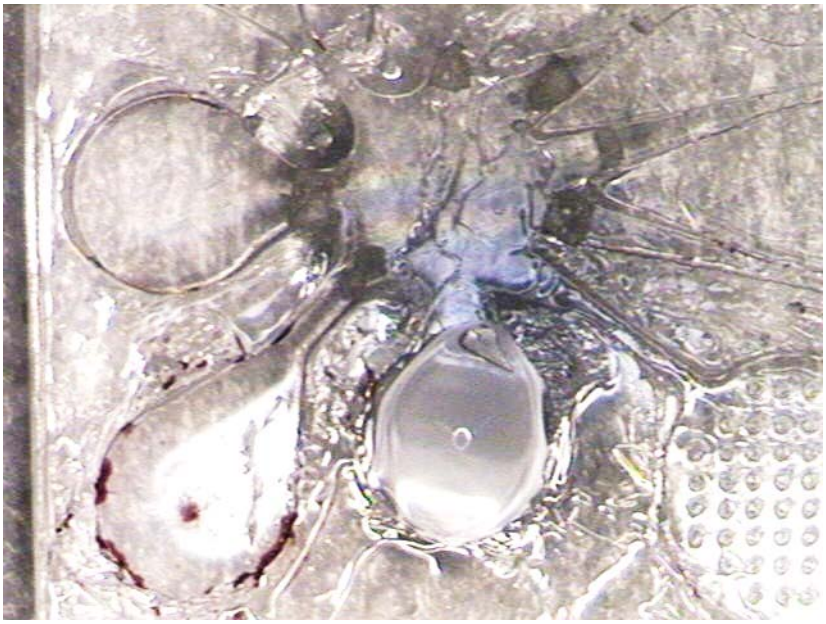

Fig. 34. HEPES starts flowing into the reaction chamber. The flow is due to capillary action and no external source of power is necessary for this action.

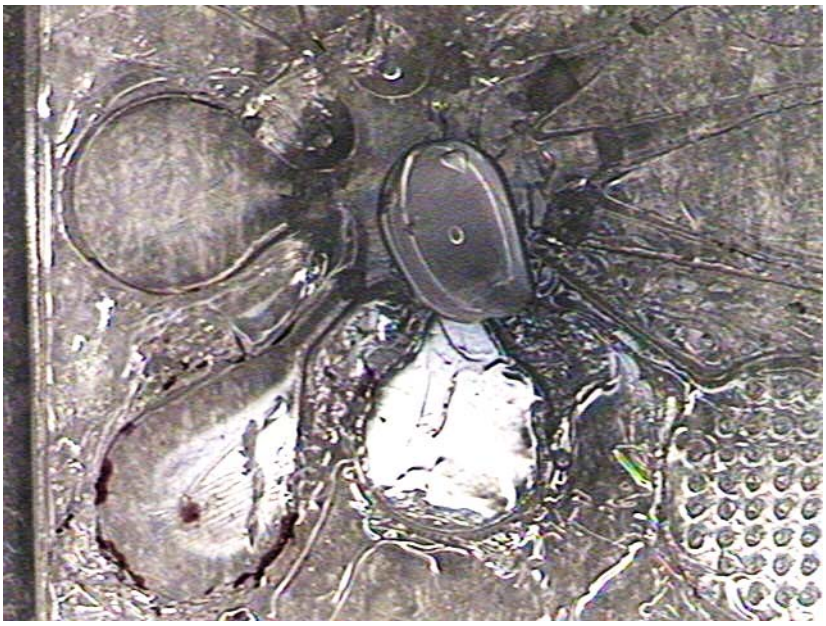

Fig. 35. The HEPES solution gradually flows into the reaction chamber and fills it up.

Fig. 36. HEPES fills the reaction chamber of the microfluidic substrate. The surface is made hydrophilic by oxygen plasma treatment prior to the experiment.

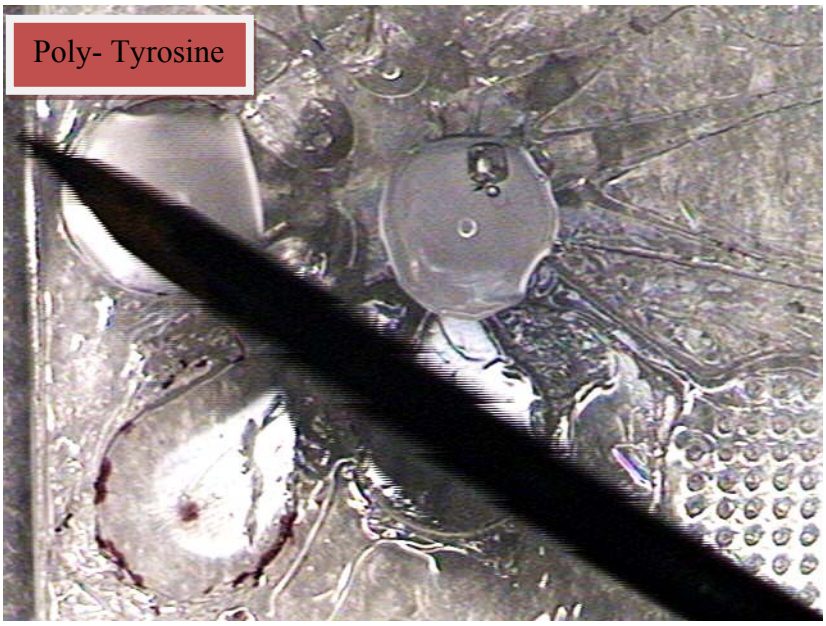

Fig. 37. Poly-tyrosine is introduced into the substrate. This reagent is a peptide and is instrumental in reducing the gold ions.

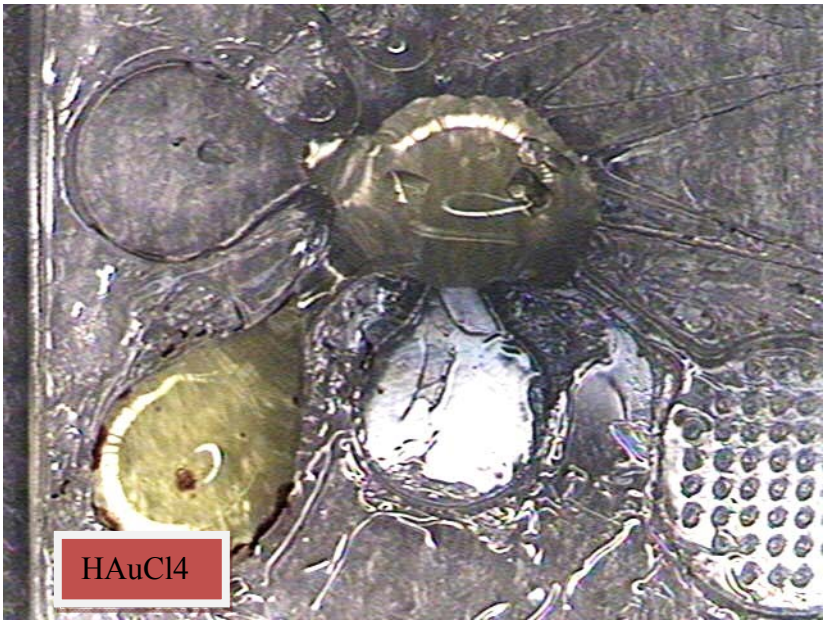

Fig. 38. Chloroauric acid is introduced while HEPES and Poly-tyrosine react in the chamber.

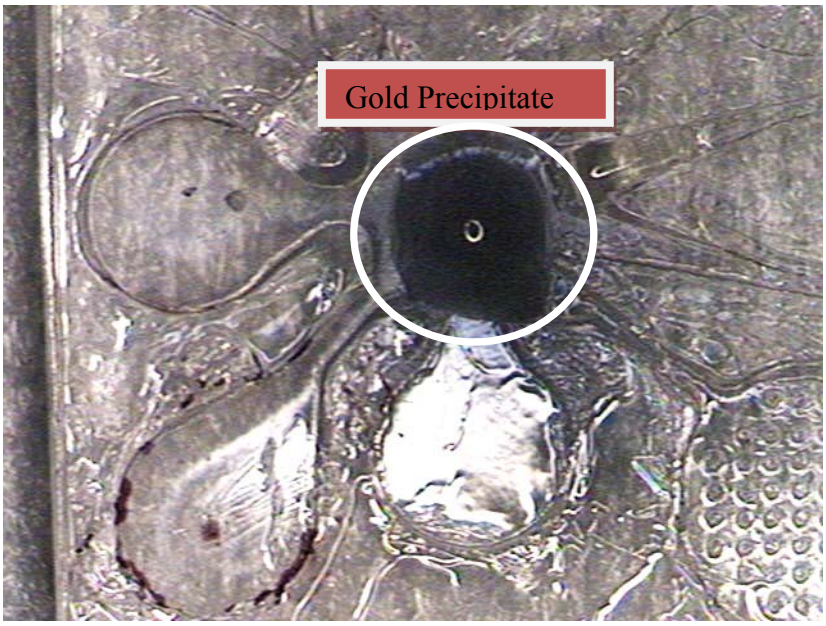

Fig. 39. Image showing gold precipitate obtained in the reaction chamber. This is a consequence of the formation of gold nano-particles.

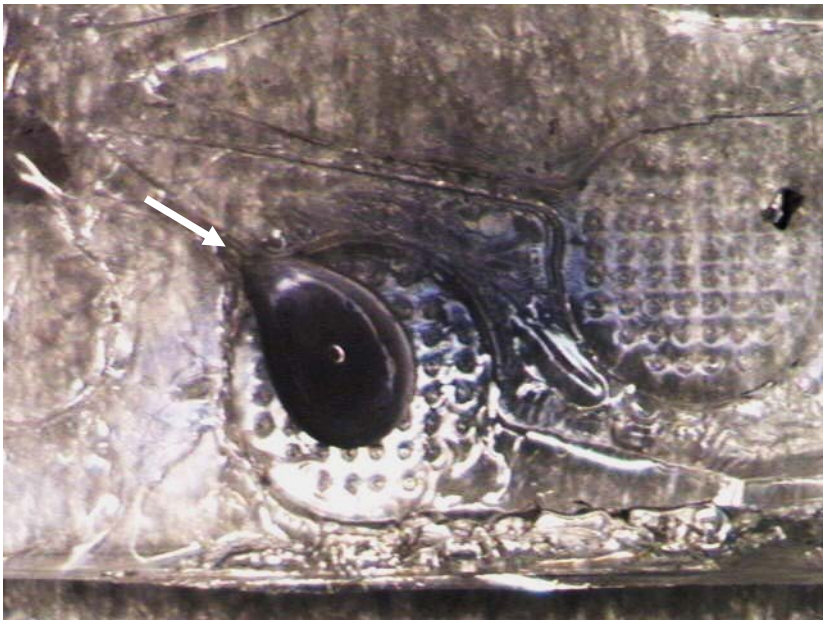

Fig. 40. The darkish liquid (gold precipitate) flows out of the reaction chamber into the drainage chambers.

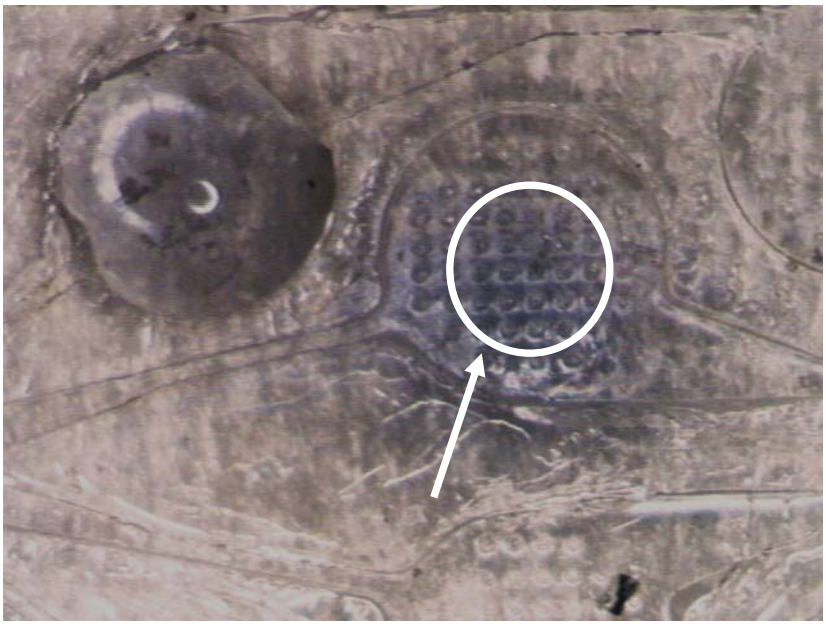

Fig. 41. The flow of the dark colored fluid is a result of capillary action. Micro-capillary flow is induced by the converging shape of the micro-channel and minute micro-structures in the chambers as shown in the image by the arrow.

6.2.2 Synthesis of Gold Nano-Particles on PDMS Microfluidic Platform

This section provides the details of the development of the complete autonomous micro-fluidic assay to produce gold nano-particles from multi-functional peptides. All the reagents participating in the reaction are introduced at the same time into the assay. The chemical reactions occur autonomously and gold nano-particles are formed in the reaction chamber. As previously mentioned, the sequence of reaction is controlled by proper placement of salt bridge valves in the micro-channels based on the design calculations and calibrations described earlier. The valve actuation time is a function of salt plug length (or volume) and its location from the mouth of the reservoir (L_0). In this set of experiments, we had placed same size of the salt plugs (salt-bridge microvalves) at various locations within the respective microchannels. The values of the exact position

of the valves were obtained from the valve characterization experiments. Valves of length 0.7 mm are placed at appropriate distances to obtain the desired assay.

Sodium chloride was used to fabricate the salt bridge valves. A previously weighed quantity of the salt was taken and dissolved in a fixed volume of water (~10 μl). The salt solution was then heated to a temperature of 160 °C. The salt solution was easier to handle after the heating procedure. The required volume of salt was aspirated using a micro-syringe and placed in the microchannel at the desired location. Equal volumes of salt were used to fabricate each of the valves. This was ensured by weighing the substrate before and after the addition of each salt plug to form the salt bridge microvalve. The difference in weight could be correlated to the volume of salt used to form the salt plug.

The chemicals and reagents were added into their respective chambers (or reservoirs) with the help of a micro-syringe. HEPES buffer, poly-tyrosine peptide and gold acid were the three reagents used. Appropriate concentration solutions, for each of the mentioned reagents were freshly prepared. Using the results from the valve characterization experiments (and models), the locations of each of the equal volume plugs was predicted. The valve actuation time for HEPES solution was designed to be the least followed by that of the peptide solution. The valve actuation time for the gold acid was designed to be the largest so that this became the last reagent to participate in the reaction, thus completing the assay.

Fig. 42 shows the basic layout of the microfluidic device with the various salt bridge valves in their respective microchannels. Fig. 43 is a magnified image of the reaction chamber where all the reagents mix and react in the pre-defined sequence. Fig. 44 and Fig. 45 shows the HEPES buffer solution introduced into one of the chambers in the microfluidic device. The buffer solution gradually fills up the entire chamber. Fig. 46 and Fig. 47 show the introduction of the peptide inside another chamber of the polymer device. Fig. 48 and Fig. 49 show an overview of the microfluidic device in the reaction chamber region with all the reagents involved in the assay in their respective chambers.

Fig. 50 and Fig. 51 show the flow of the buffer solution into the reaction chamber. Fig. 52 shows the buffer solution flown into the reaction chamber. The flow actuation occurs by capillary wicking in the microchannels. Fig. 53 shows the peptide solution on the verge of microvalve actuation prior to flowing into the reaction chamber. Fig. 54 shows the mixing of the peptide solution with the buffer solution in the reaction chamber. Fig. 55 shows the flow of the Chloro-auric acid into the reaction chamber to complete the assay. Fig. 56 shows the formation of the dark precipitate in the reaction chamber confirming the presence of gold nano-particles. Fig. 57 shows the gradual flow of the fluid towards the waste chambers. Fig. 58, Fig. 59 and Fig. 60 show the gradual flow of this dark colored fluid into the first set of waste chambers after dissolving the salt bridge valves in the respective micro-channels. Fig. 61, Fig. 62 and Fig. 63 show the dark fluid (containing the precipitated gold nano-particles) gradually filling the drainage chamber. Fig. 64 shows the dark fluid filling up the second set of drainage chambers.

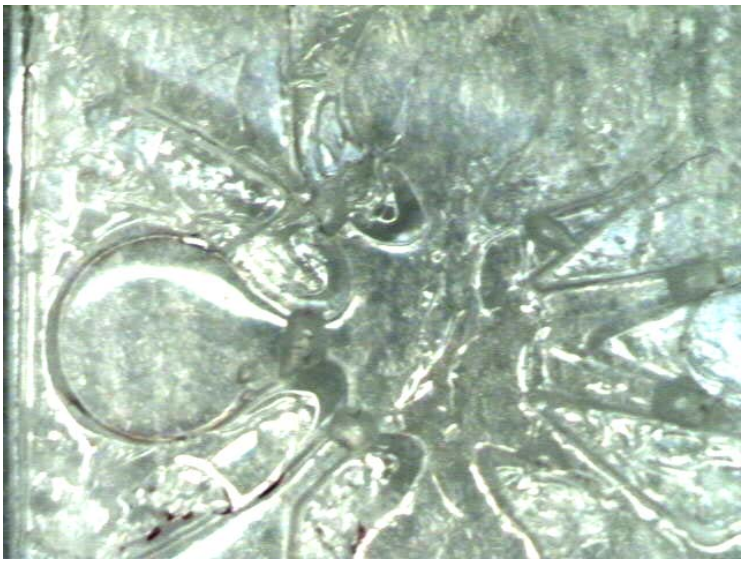

Fig. 42. Image showing a magnified view of the PDMS substrate with salt bridge valves of equal length placed at various positions (different Lo) inside the micro-channels.

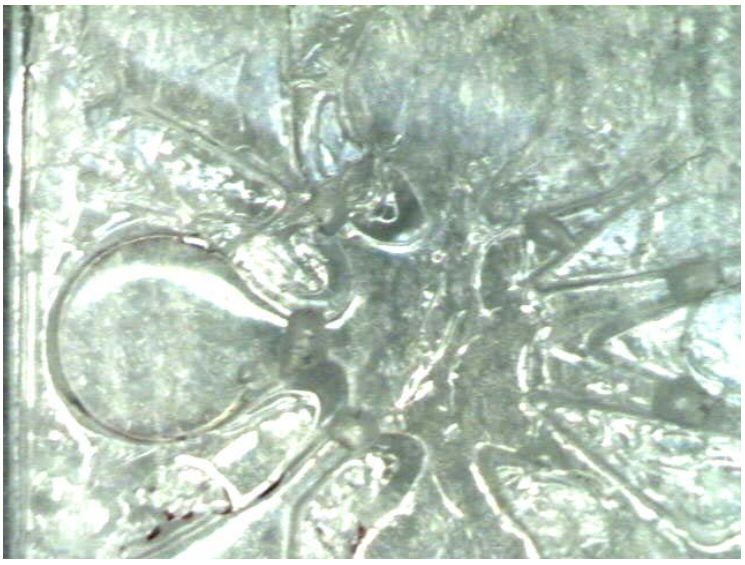

Fig. 43. Image showing a magnified view of the reaction chamber in the microfluidic substrate.

Fig. 44. Image showing the introduction of a drop of HEPES solution with the help of a micro-syringe into one of the chambers.

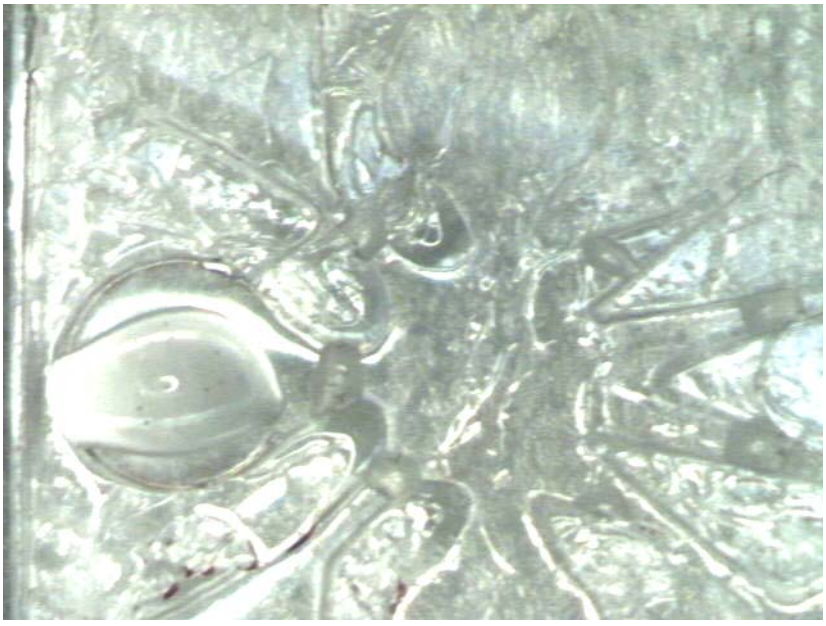

Fig. 45. Image showing the HEPES solution gradually filling up the entire chamber in the microfluidic device.

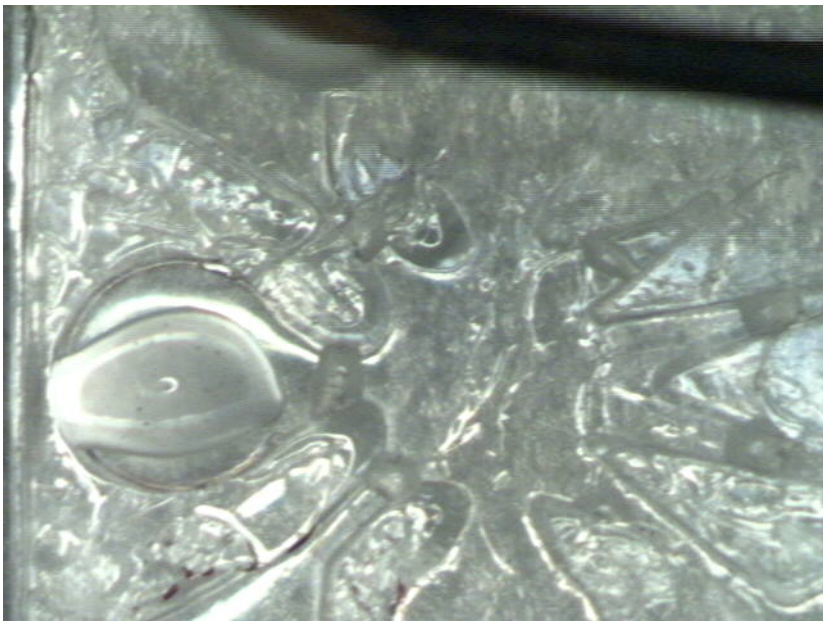

Fig. 46. Image showing the introduction of a droplet of poly-tyrosine (peptide) in another chamber of the device.

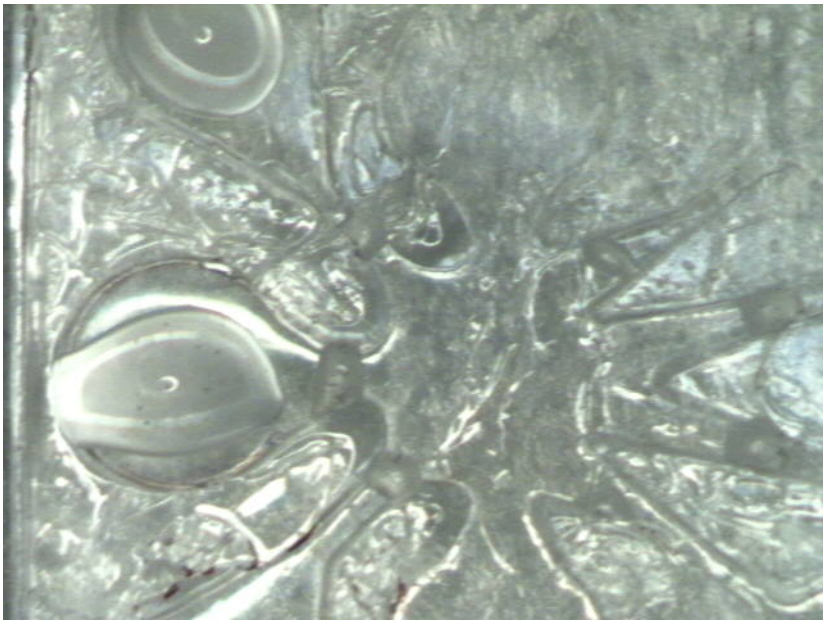

Fig. 47. Image showing the two reagents (HEPES and peptide) in their respective chambers.

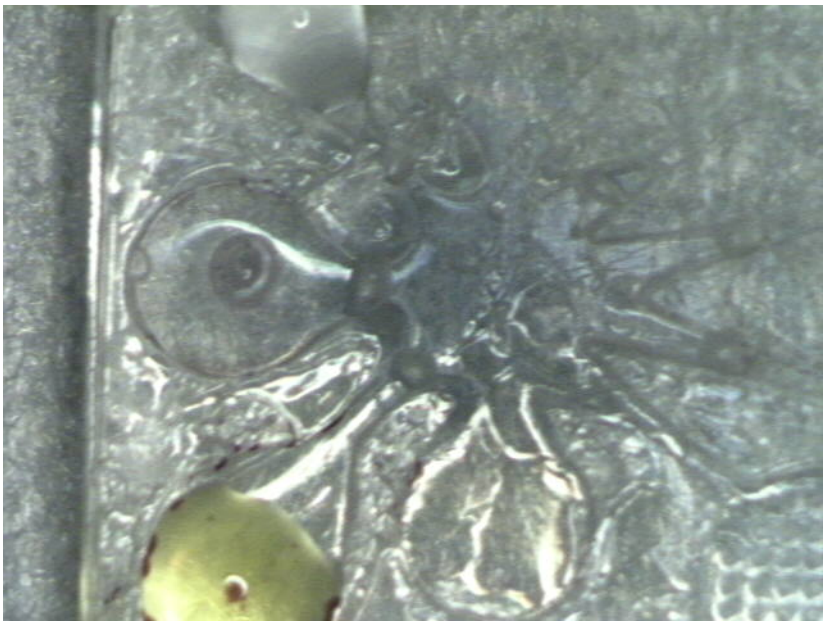

Fig. 48. Image showing the gold acid (third reagent in the chemical reaction) filling up its chamber in the microfluidic device.

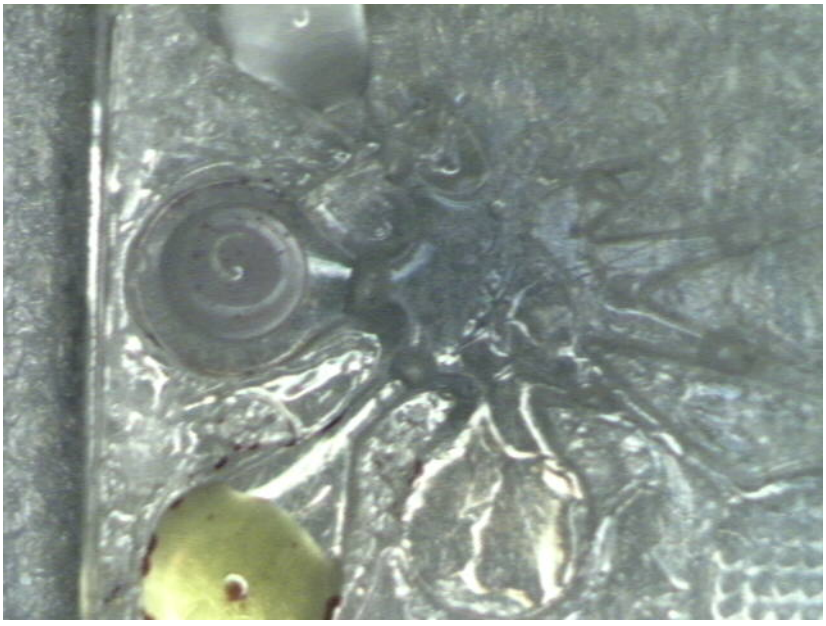

Fig. 49. Image showing all the three reagents placed in their respective chambers in the microfluidic device at the same time.

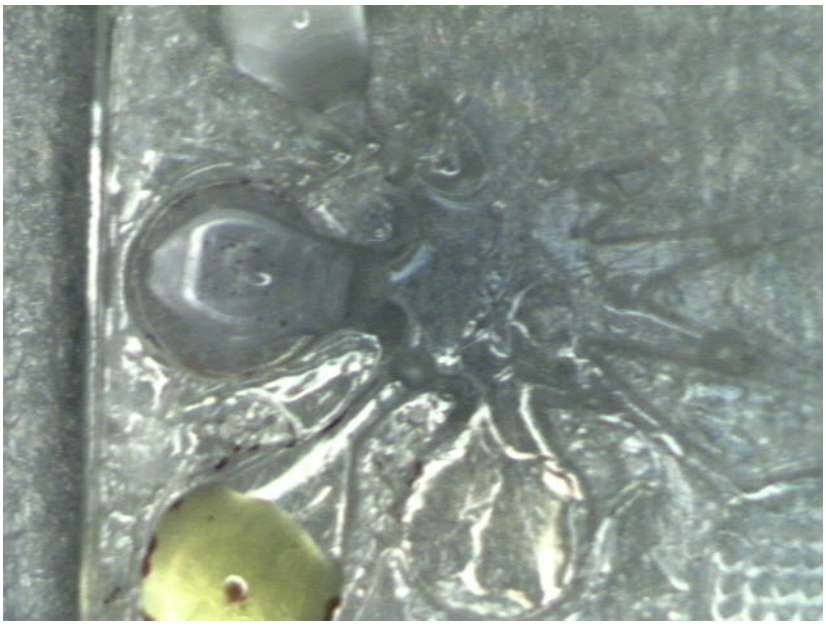

Fig. 50. Image showing the HEPES solution gradually dissolving the valve and flowing into the reaction chamber.

Fig. 51. Image showing the HEPES solution entering the reaction chamber.

Fig. 52. Image showing the magnified view of the reaction chamber showing the HEPES solution inside the reaction chamber.

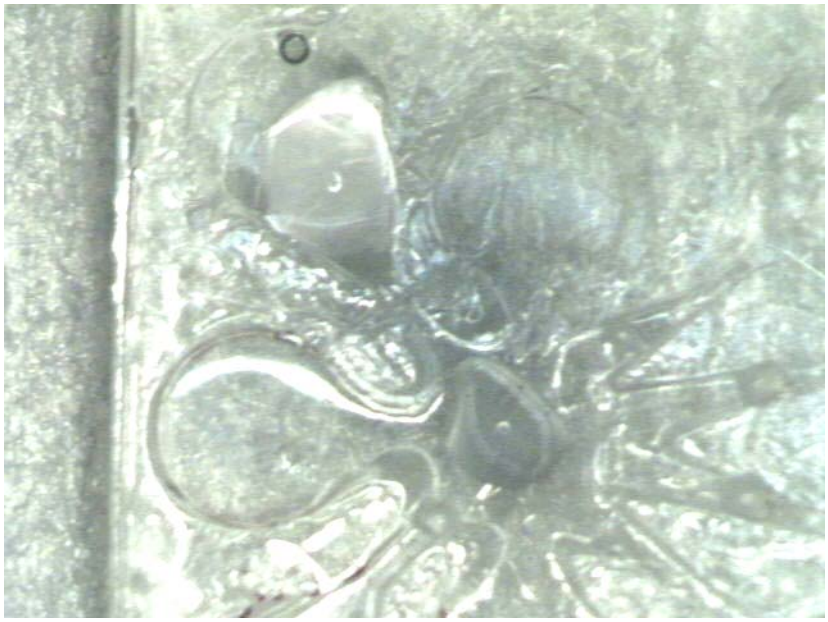

Fig. 53. Image showing the peptide solution about to flow into the reaction chamber and mix with the HEPES solution.

Fig. 54. Image showing the HEPES solution and peptide inside the reaction chamber of the microfluidic device.

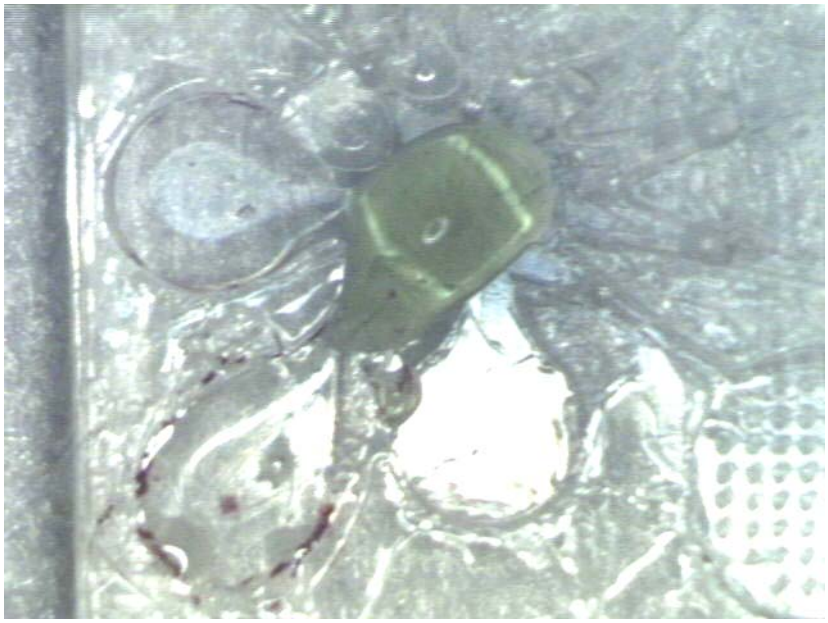

Fig. 55. Image showing the rupture of the valve allowing the Chloroauric acid to flow into the reaction chamber.

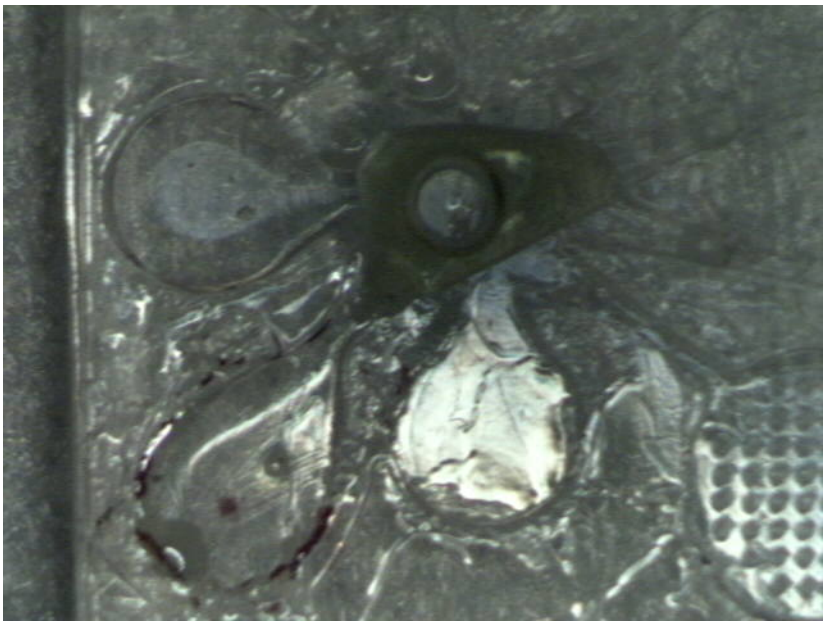

Fig. 56. Image showing the formation of the dark precipitate in the reaction chamber.

.

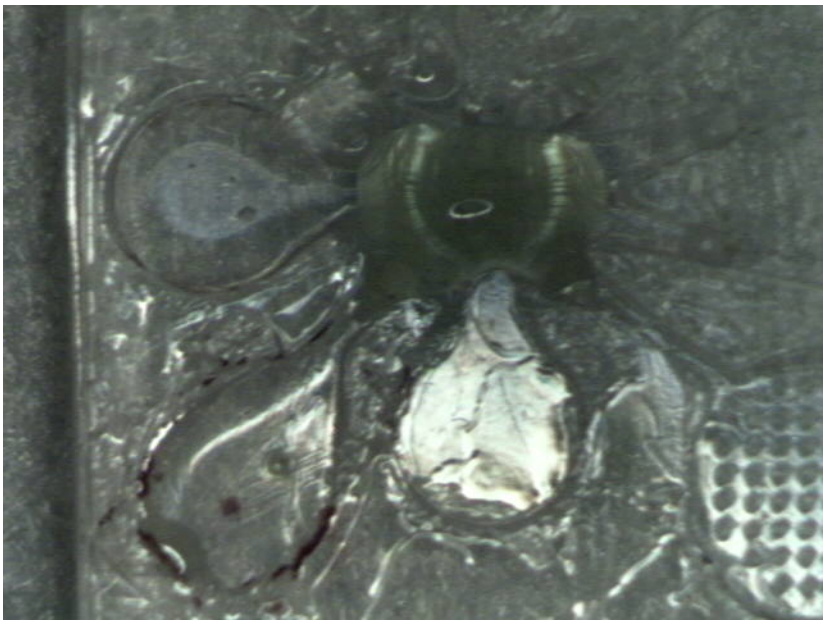

Fig. 57. Image showing the darkish precipitate moving into the drainage chambers.

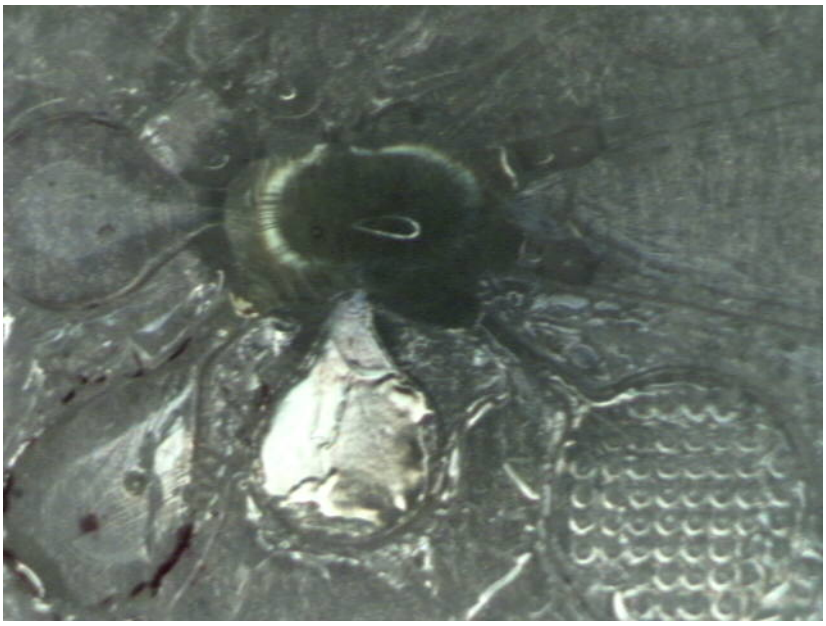

Fig. 58. Image showing the darkish precipitate moving towards the valves inside the micro-channels connecting to the drainage chamber.

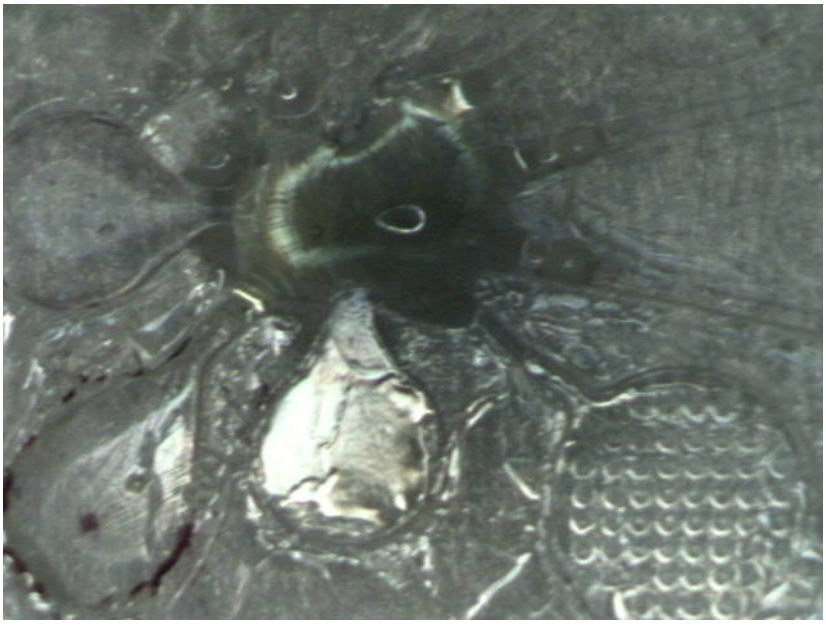

Fig. 59. Image showing the darkish liquid flows inside the micro-channels and about to dissolve the salt bridge valves.

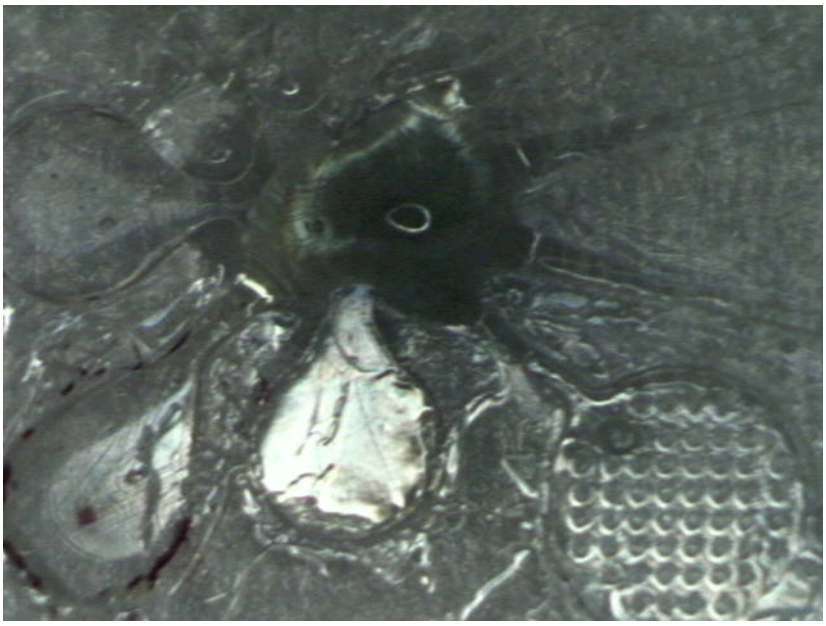

Fig. 60. Image showing the dissolution of the salt bridge valves inside the micro-channels and gradual flow of the fluid towards the first set of drainage chambers.

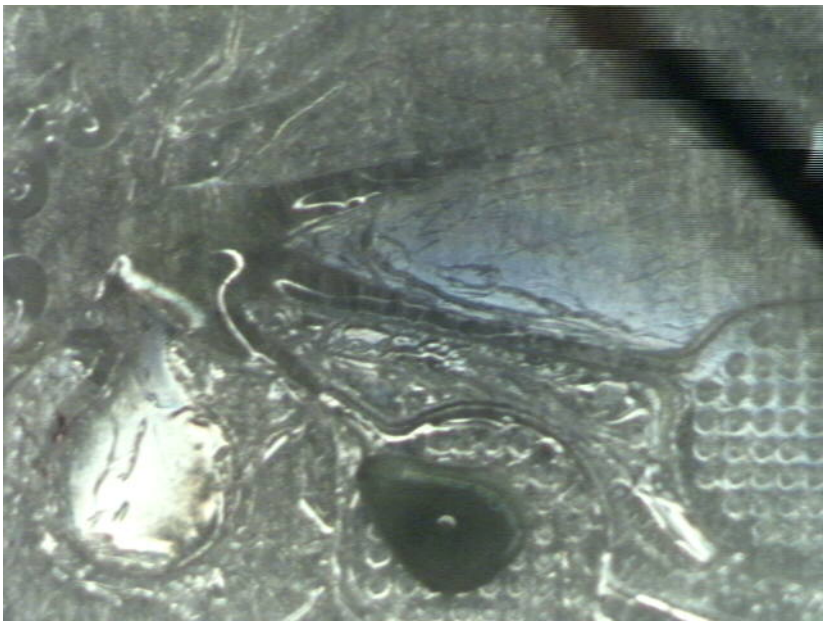

Fig. 61. Image showing the darkish liquid having reached the first set of drainage chambers.

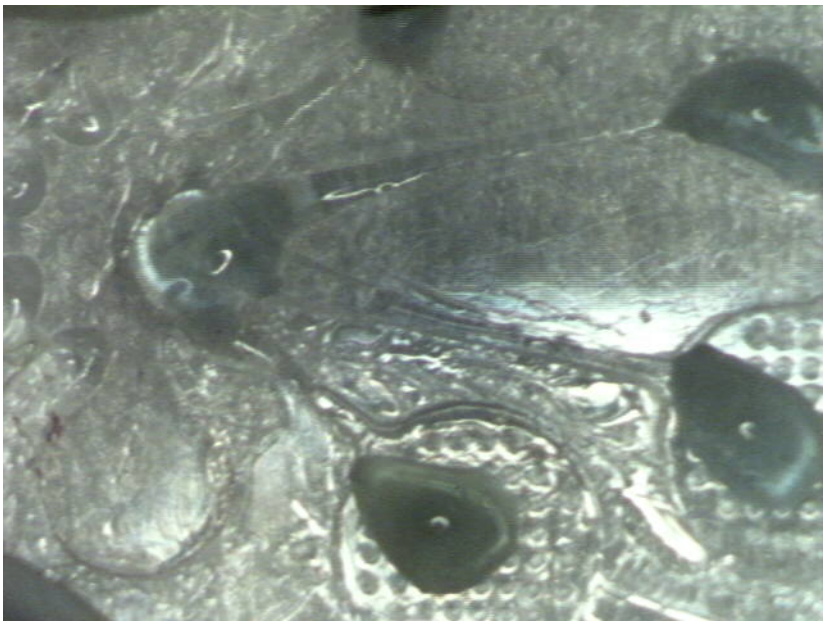

Fig. 62. Image showing the fluid gradually filling the drainage chambers purely by capillary flow.

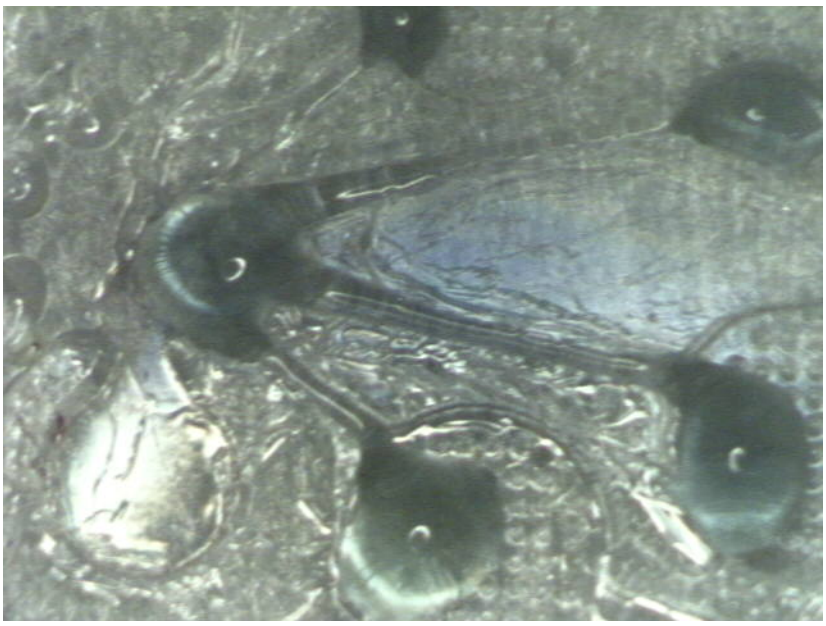

Fig. 63. Image showing an overview of the microfluidic substrate depicting the gradual flow of the fluid from the reaction chamber towards the drainage chambers.

Fig. 64. Image showing a drop of liquid in the second set of drainage chambers in the microfluidic device.

6.3 Bi-Layer PDMS Device

As the name suggests, the bi-layer assay consists of two separate PDMS layers- one housing the valves and the other the reservoirs and micro-wells as shown in Fig. 65. They are constructed in such a fashion that they overlap when placed on top of each other as shown in Fig. 66 and Fig. 67. These two layers are treated in plasma chamber and pressure loaded to bond with each other. A closed microfluidic platform is thus obtained.

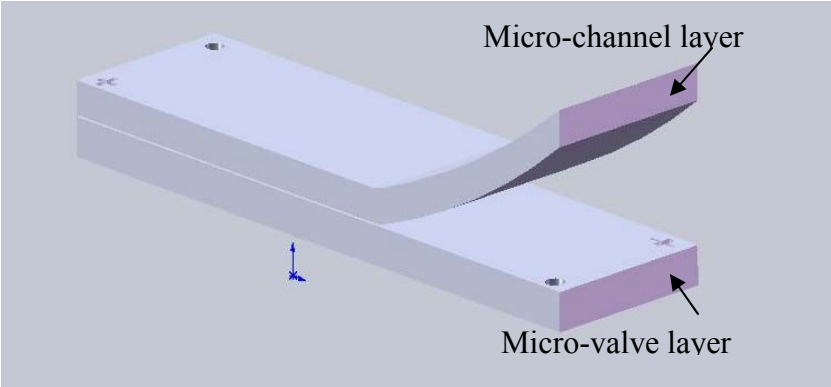

Fig. 65. Diagram showing the basic model of the bi-layer device. The bottom layer houses the valves while the top layer houses the micro-channels and chambers (reservoirs) for the reagents.

The fluid inserted into one of the reservoirs flows into the valve into the bottom layer, dissolves it and then returns to the top layer to flow into the reaction chamber. The PDMS layer with valves are placed on the bottom layer and the microchannels are placed in the top layer. A drop of Chloro-auric acid is introduced into one of the reservoirs on the upper layer as shown in Fig. 68. The droplet gradually flows into the lower layer and starts dissolving the valve as shown in the Fig. 69 and Fig. 70. The flow actuation occurs by capillary wicking. In order to remove air bubbles trapped inside, in between the two layers, holes are punched into the upper substrate with a pin to allow the air to escape, thus ensuring smooth flow of the fluid into the reaction chamber. Fig. 71 shows the droplet inside the reaction chamber. To complete the assay, a droplet of a mixture of HEPES buffer and poly-tyrosine peptide is introduced using a micro-syringe into another reservoir on the upper layer. This mixture is allowed to dissolve the valve in the second layer and flow into the reaction chamber as shown in Fig. 72. After sometime, a black precipitate is seen in the reaction chamber. This is due to the

formation of gold nano-particles as shown in Fig. 73 and Fig. 74. The dark colored liquid moves out of the reaction chamber into the drainage chambers.

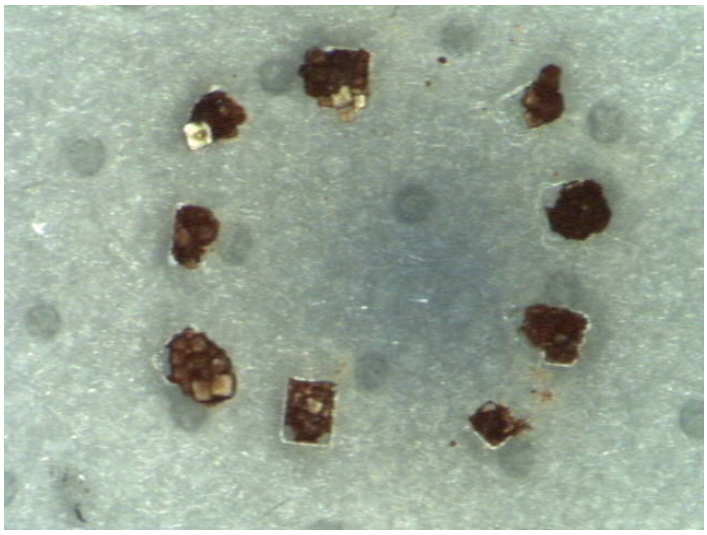

Fig. 66. Image showing one of the layers (housing the salt plugs which serve as the salt-bridge passive microvalves) of the bilayer microfluidic device.

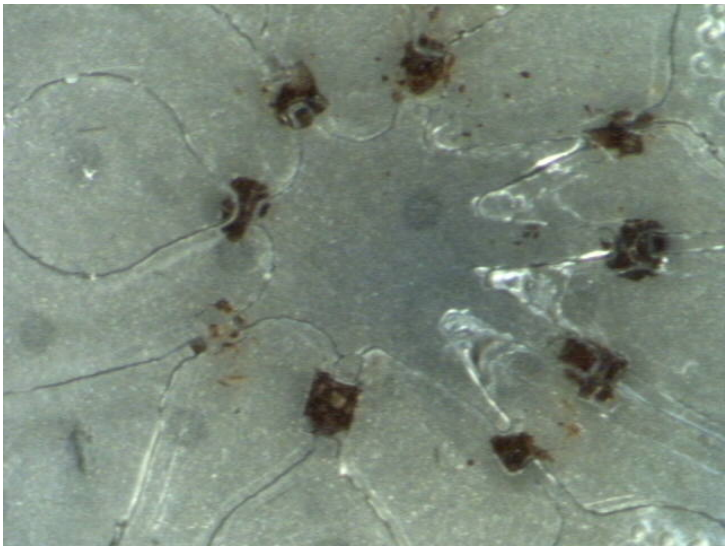

Fig. 67. Image showing how the two layers superimpose on top of each other to yield the bilayer assay. The layer with the valves is placed at the bottom. A closed microfluidic device is thus obtained.

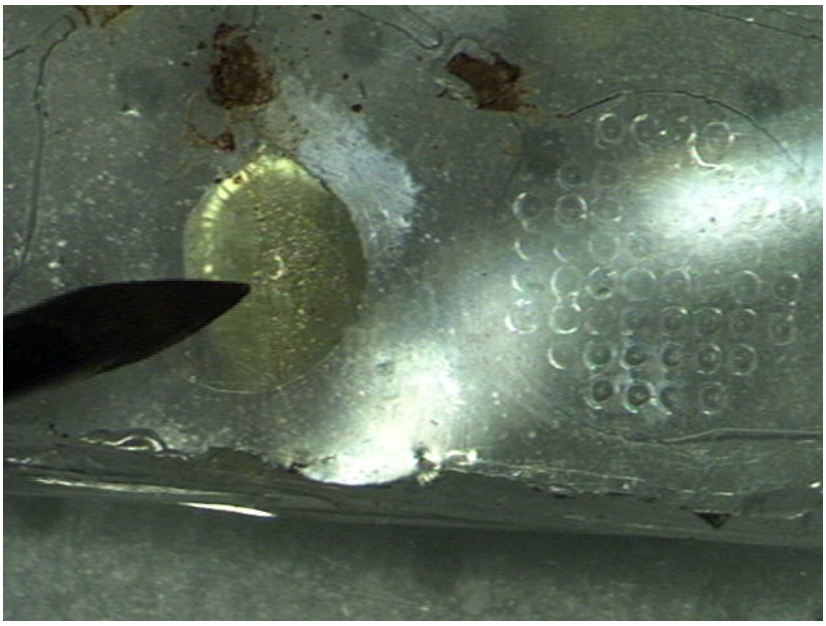

Fig. 68. Image showing the introduction of a droplet of Chloro-auric acid into one of the reservoirs on the top layer.

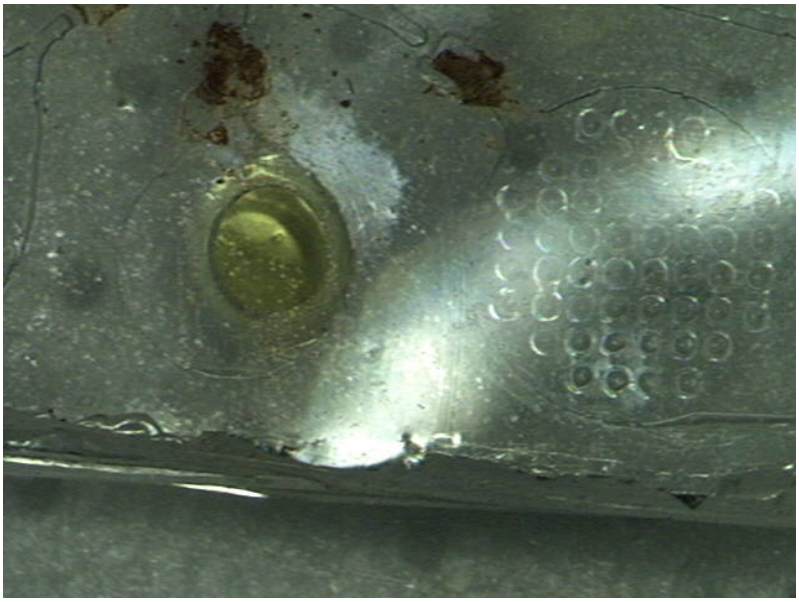

Fig. 69. Image showing a droplet of Chloro-auric acid inside the microfluidic device.

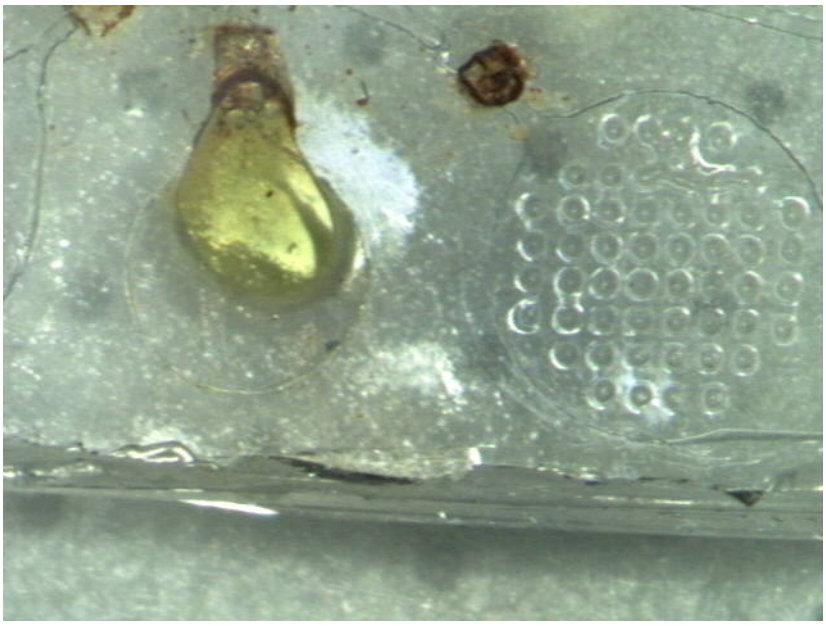

Fig. 70. Image showing the flow of the drop of liquid into the lower layer and the initiation of the dissolution of the valve.

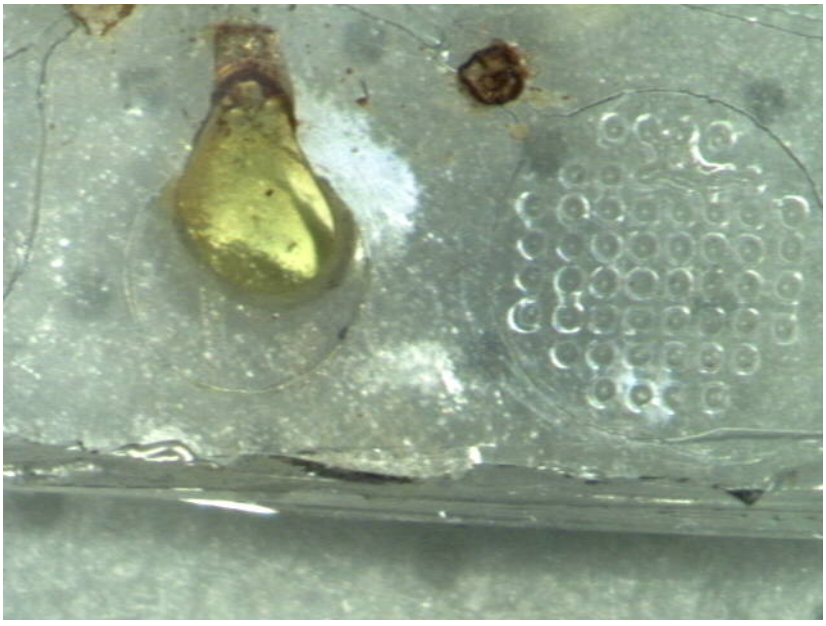

Fig. 71. Image showing the partial dissolution of the valve by the droplet of fluid.

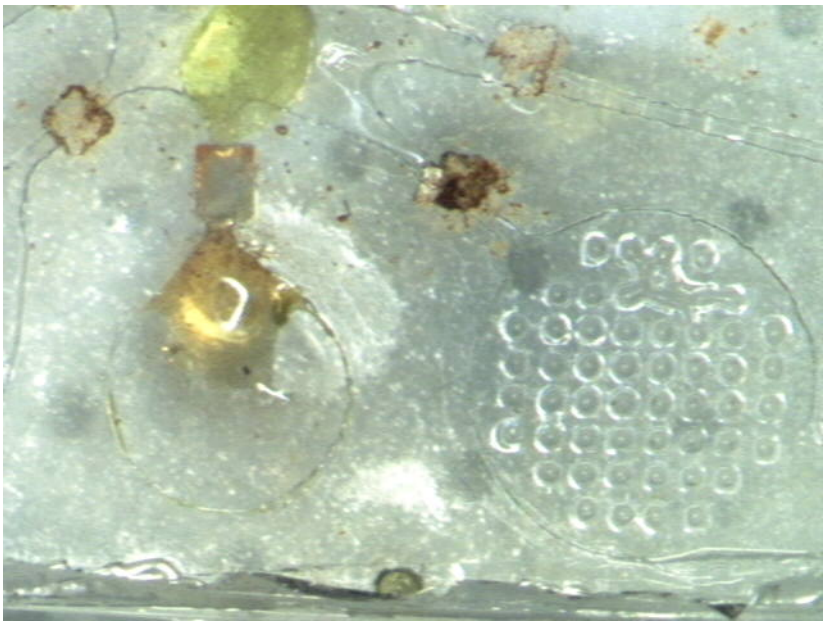

Fig. 72. Image showing the drop of gold acid inside the reaction chamber. The valve has dissolved out completely.

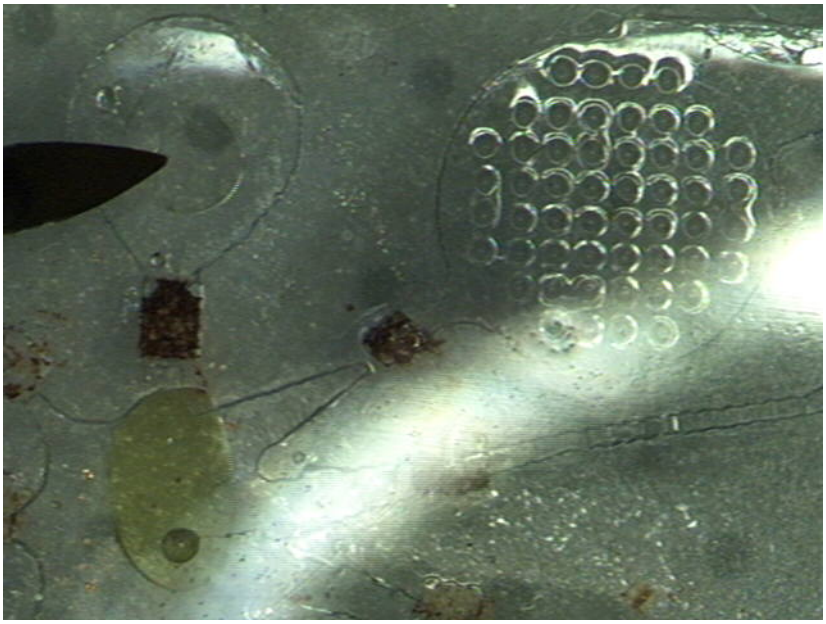

Fig. 73. Image showing the introduction of a mixture of HEPES buffer solution and poly-tyrosine peptide into another reservoir in the upper layer.

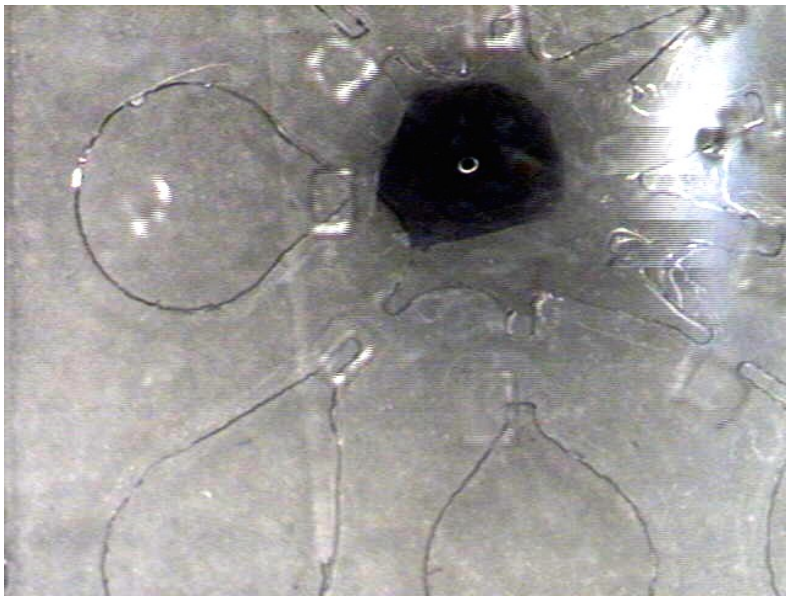

Fig. 74. Image showing the formation of gold precipitate in the reaction chamber of the microfluidic substrate.

6.4 Microfluidics on Paper

A very innovative technique to obtain microfluidic devices was developed by the Whitesides group at Harvard University [56] where microfluidics devices were microfabricated on paper. This technology has the potential to supersede the existing usage of polymers as microfluidic substrates. While the Whitesides' group demonstrated this technique by creating an assay for the detection of glucose in a sample of urine, we present an assay, which could be used to synthesize gold nano-particles in situ. Such a capability is crucial for water quality monitoring applications. The assay to synthesize the gold nano-particles can actually be synthesized on paper just like on the PDMS platform, with minor modifications.

The procedure involved is quite similar to the usual photolithographic technique. A negative photo-resist (SU 8- 2075) has been used in our study. After spin coating a high quality chromatography paper at 2000 rpm for 30 seconds, we obtained a 100-micron thick coat of the photo-resist on the paper. The general procedures like pre-exposure baking, exposure for 30 seconds, post-exposure baking (PEB) are carried out. Finally, the substrate is developed in a solution (MF-319) and washed clean using ethanol.

6.4.1 Development of Gold Nano-Particles on Paper

This assay sequence is similar to that on PDMS described earlier. We began the experiment with the introduction of a droplet of HEPES solution into one of the reservoirs of the microfluidic substrate on paper as shown in Fig. 75. The drop of liquid gradually flows into the reaction chamber by capillary flow as shown in Fig. 76 and Fig. 77. The subsequent step in the assay is the introduction of a droplet of poly-tyrosine into another reservoir as shown in Fig. 78. These two reagents mix inside the reaction chamber as shown in Fig. 79. The last step of the assay involves the introduction of a drop of gold acid into the microfluidic substrate as shown in Fig. 80.

The gold ions in the acid solution precipitate out in the form of dark brown/ black gold nano-particles as seen in Fig. 81. The dark liquid (the gold precipitate) flows into the first and second set of waste chambers as shown in Fig. 82 and Fig. 83. Small microstructures placed in the waste chambers aid the capillary actuation by modifying the capillary pressure in the waste chamber.

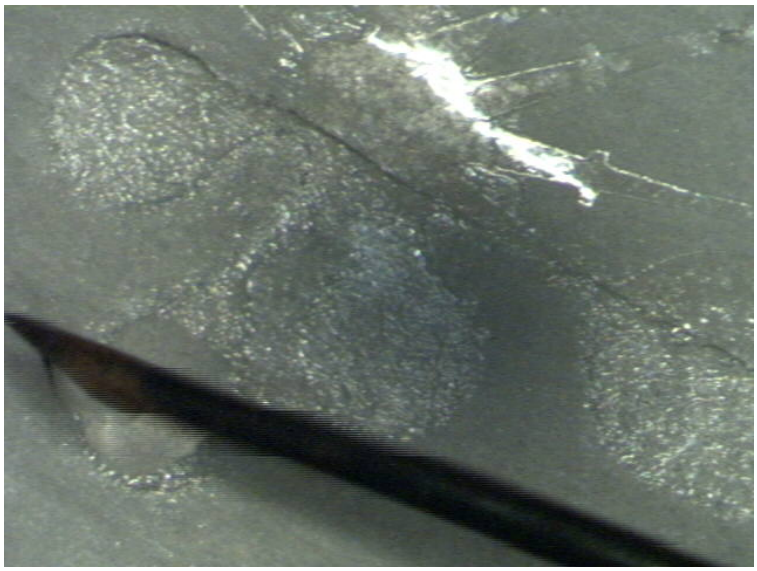

Fig. 75. Image showing a droplet of HEPES solution into one of the reservoirs in the paper microfluidic substrate.

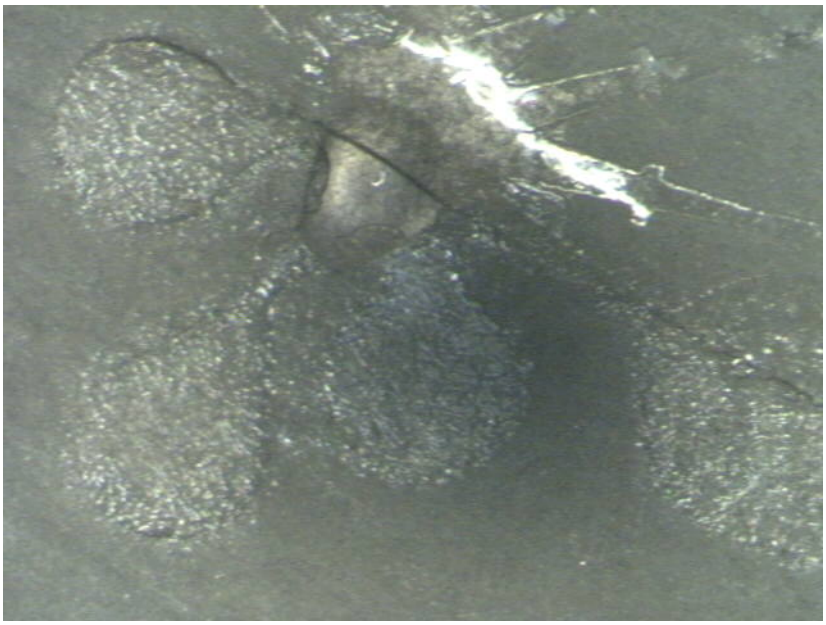

Fig. 76. Image showing the flow of the HEPES solution into the reaction chamber by capillary action.

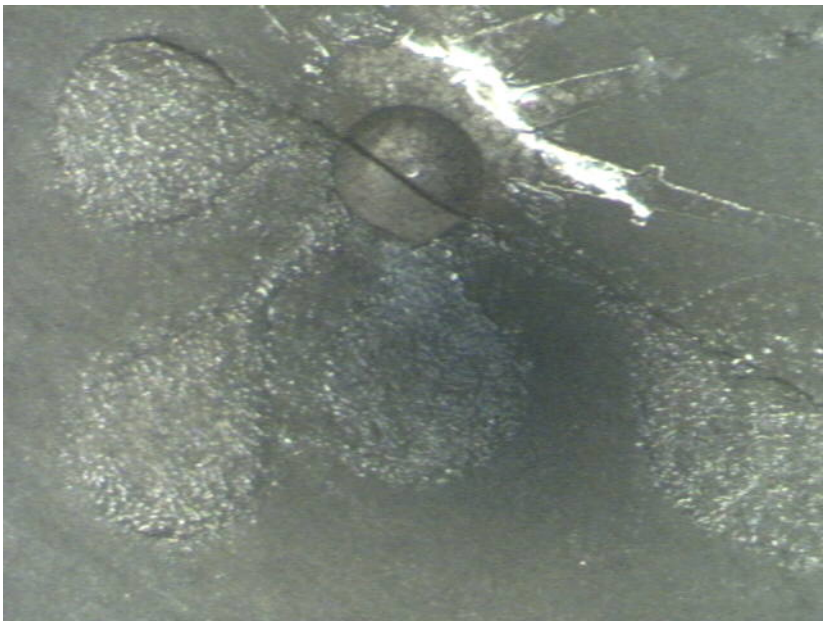

Fig. 77. Image showing the droplet inside the reaction chamber of the microfluidic substrate.

Fig. 78. Image showing the introduction of a droplet of poly-tyrosine inside another reservoir of the paper microfluidic substrate.

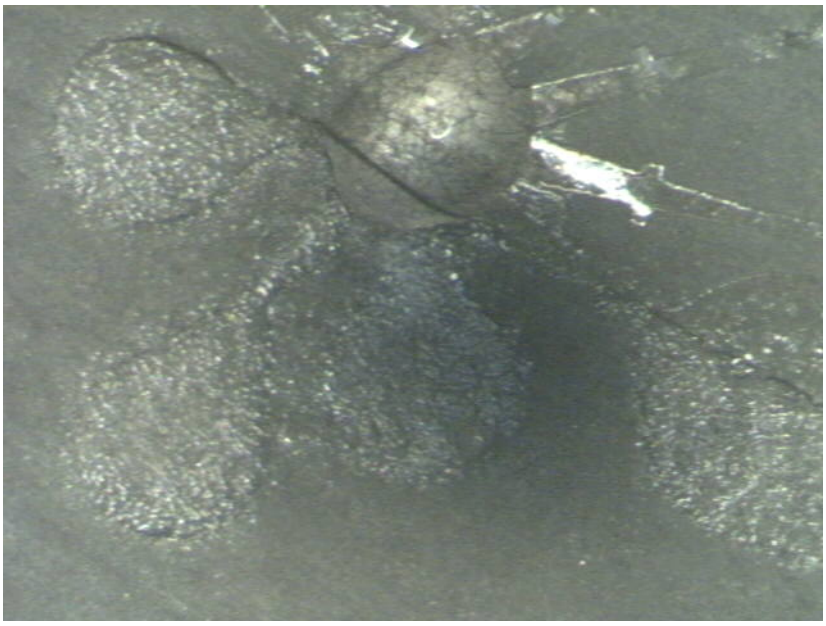

Fig. 79. Image showing the mixture of HEPES solution and poly-tyrosine inside the reaction chamber.

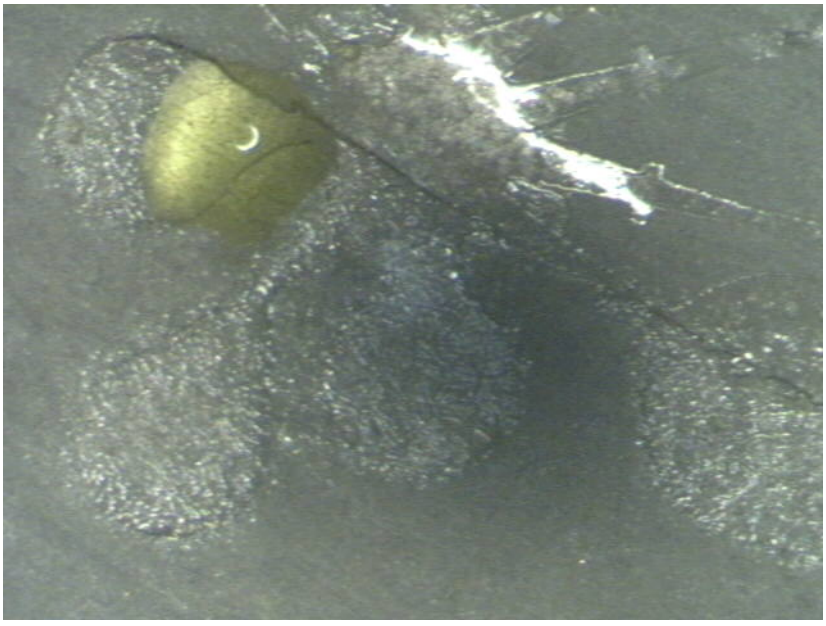

Fig. 80. Image showing a drop of Chloroauric acid inside a reservoir. The drop of fluid moves towards the reaction chamber which is partially filled with the mixture of HEPES and poly-tyrosine solution.

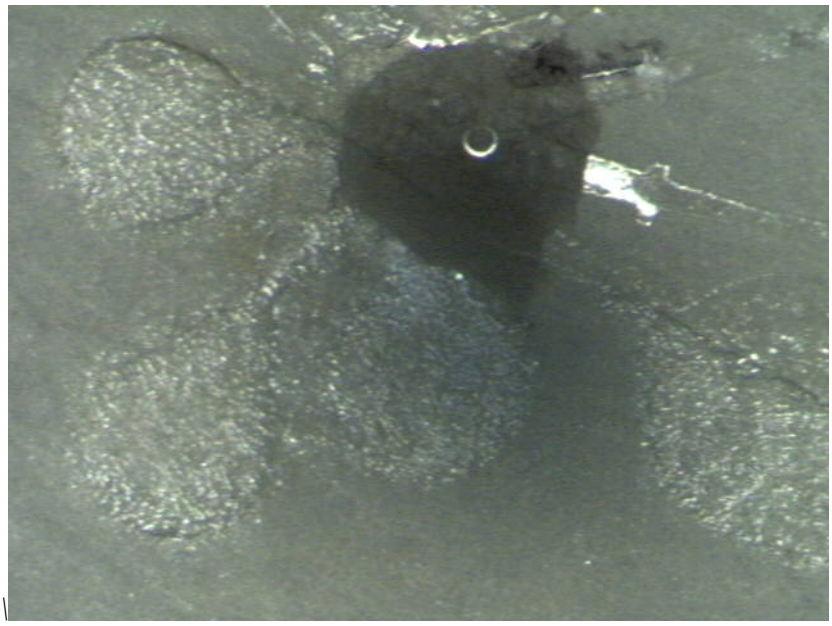

Fig. 81. Image showing the formation of gold precipitate inside the reaction chamber of the microfluidic substrate.

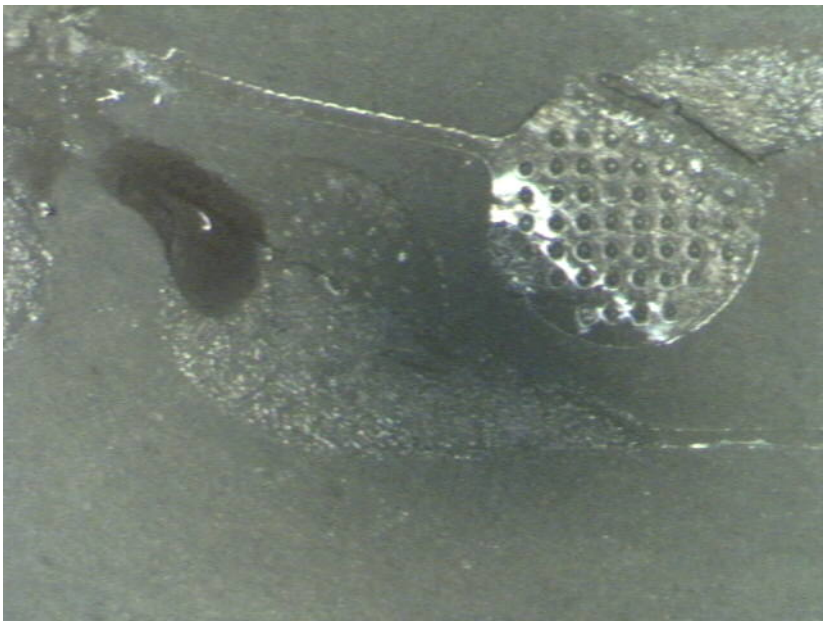

Fig. 82. Image showing the flow of the dark liquid (gold precipitate) into the waste chambers.

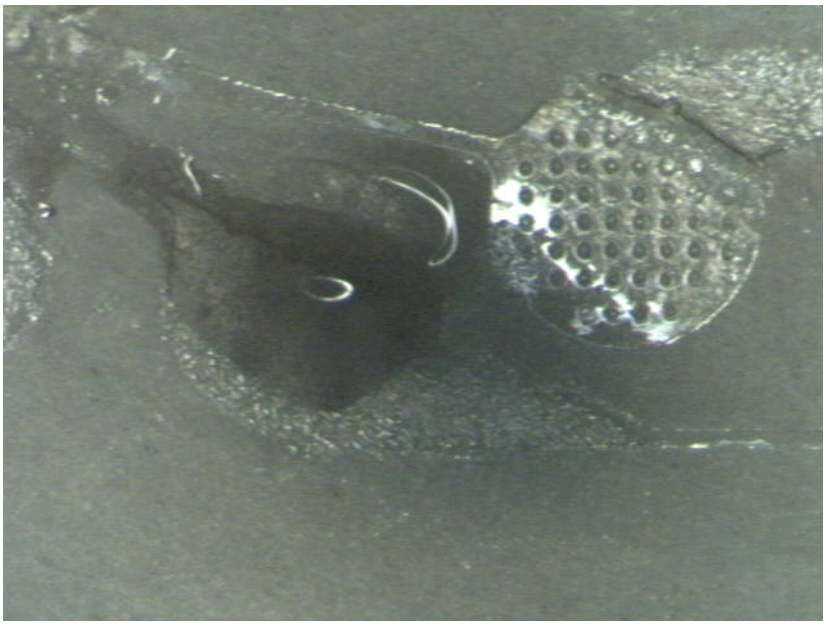

Fig. 83. Image showing the flow of the liquid into the second set of waste chambers. Small micro-structures (to induce the flow) can be seen in the image.

In the next step, we developed the assay on paper with valves impregnated into it to control the reaction and the flow sequence. Fig. 84 shows an overview of the microfluidic substrate with salt valves inside the micro-channels connecting the reservoirs into the central reaction chamber. Fig. 85 and Fig. 86 illustrate the introduction of a droplet of HEPES solution, followed by the dissolution of the salt valve and subsequent flow of the reagent into the reaction chamber. Fig. 87 shows the droplet inside the reaction chamber. At this time, poly-tyrosine is introduced into another reservoir. The peptide dissolves the valve present in the micro-channel connecting its reservoir to the reaction chamber as shown in Fig. 88. Fig. 89 demonstrates the final step

in the assay with the introduction of the Chloro-auric acid. Gold nano-particles precipitate out in the form of dark brown particles as shown in Fig. 90.

We have thus successfully demonstrated the development of a paper- based microfluidic substrate with a mechanism of passive valve actuation to obtain gold nano-particles using multi functional peptides.

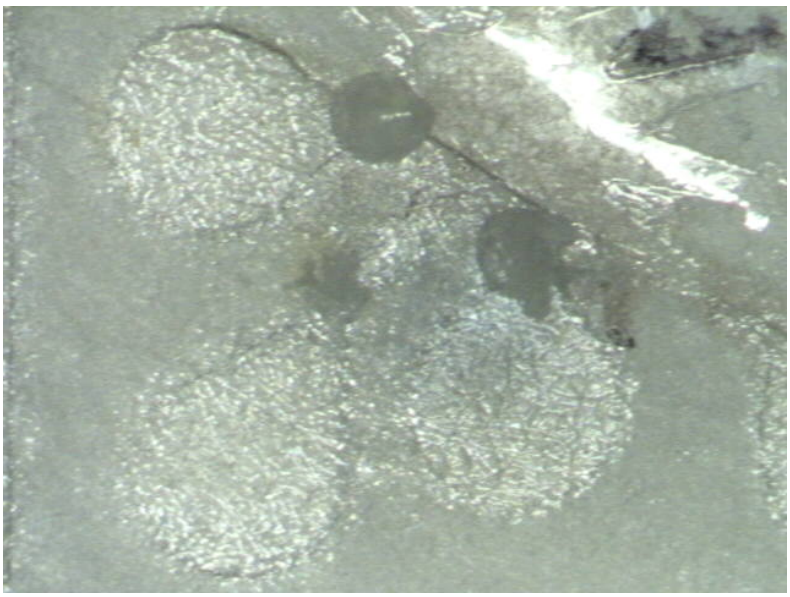

Fig. 84. Image showing the microfluidic substrate developed on a high quality chromatography paper. Microvalves composed of salt plugs are seen inside the micro-channels to control the flow.

Fig. 85. Image showing the introduction of HEPES solution into one of the reservoirs.

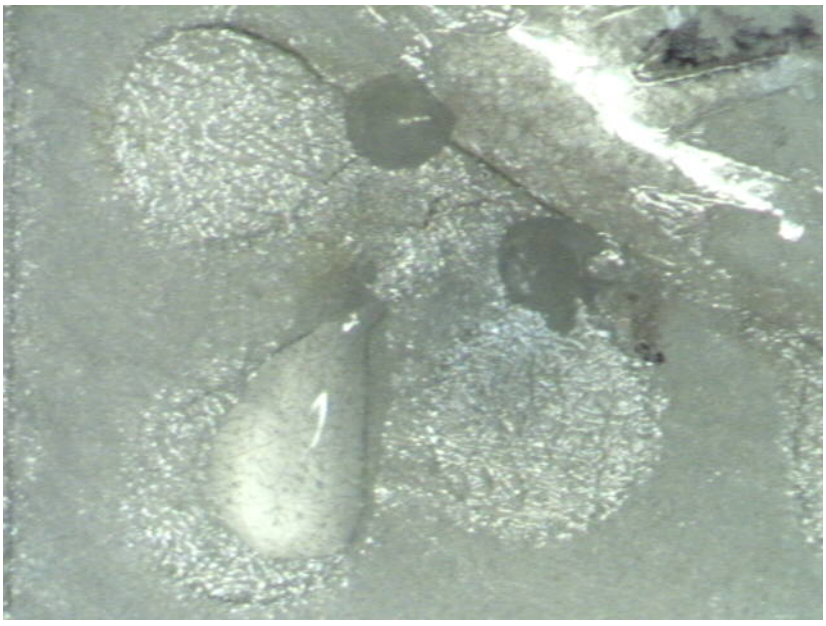

Fig. 86. Image showing the flow of the HEPES solution into the reaction chamber by gradually dissolving into the salt bridge valve.

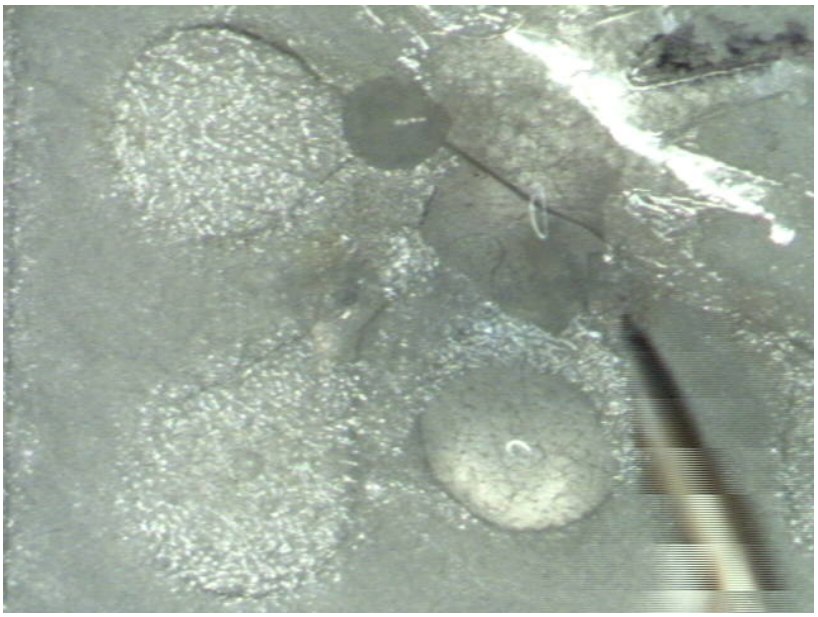

Fig. 87. Image showing the introduction of a drop of poly-tyrosine into another reservoir of the paper microfluidic substrate.

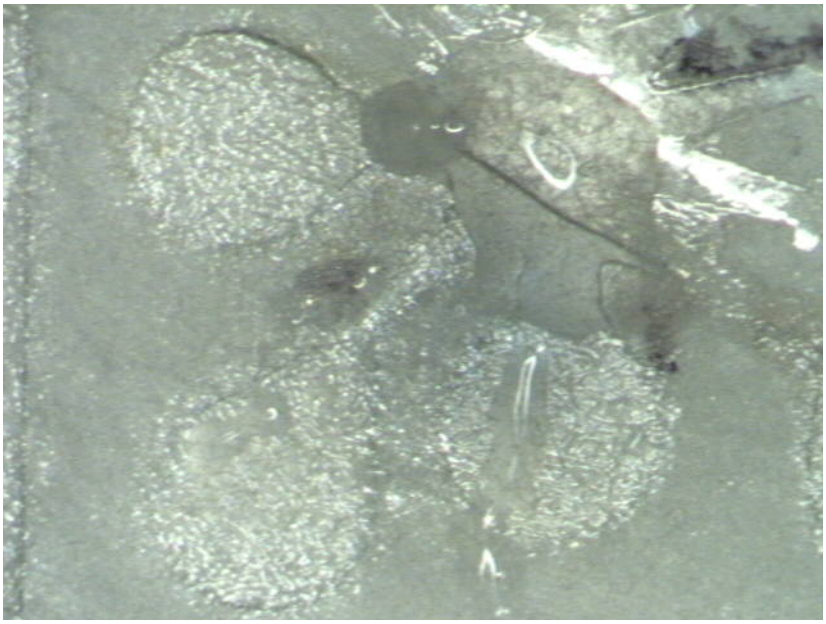

Fig. 88. Image showing the mixture of poly-tyrosine and HEPES solution inside the reaction chamber.

Fig. 89. Image showing the Chloro-auric acid droplet dissolving the salt bridge valve to enter into the reaction chamber.

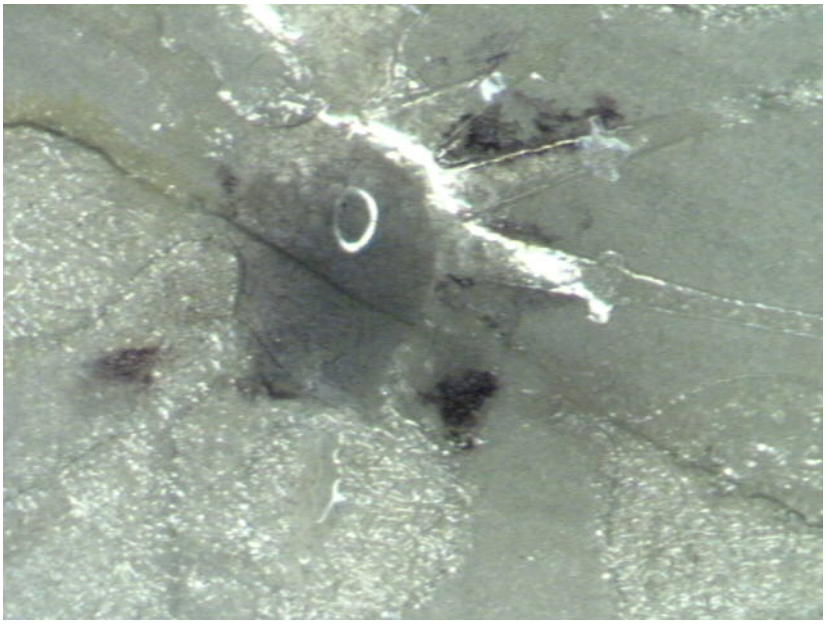

Fig. 90. Image showing the formation of gold nano-particles inside the reaction chamber of the microfluidic substrate on paper.

6.4.2 Development of the Complete Microfluidic Assay on Paper Substrate

We had previously demonstrated the successful implementation of the microfluidic assay on PDMS. In this section, we aim to demonstrate that the same autonomous assay can be developed on high quality chromatography paper. As in the previous case, the sequence of reactions is controlled by the salt bridge microvalves. The time of valve actuation is a function of the length of the salt plug (or the volume) and the position of the valve in the micro-channel (distance L_0).

By placing different lengths of salt plugs inside the micro-channel (keeping L_0 constant), the required valve actuation times were obtained. The salts used in this study comprise sodium chloride, sodium acetate and potassium chloride.

6.4.2.1 Sodium Acetate

As mentioned in the previous sections, sodium acetate was the most easy to handle and resulted in experiments with the best repeatability. Fig. 91 shows the layout of the microfluidic substrate on paper. The central reaction chamber can be seen in this magnified image. Fig. 92 and Fig. 93 show the waste chambers in the microfluidic substrate. The valves made of sodium acetate are placed inside the microchannels as shown in Fig. 94. Fig. 95 shows the introduction of a drop of HEPES solution into one of the micro-chambers while Fig. 96 shows poly-tyrosine solution inserted into another micro-chamber using a micro-syringe. Fig. 97 shows the two solutions in their respective chambers, while Fig. 98 shows the introduction of gold acid into a third micro-chamber.

Fig. 99 shows the HEPES filling up the reaction chamber and coming in contact with the gold acid. Fig. 100 shows the peptide gradually flowing into the reaction chamber to react with the mixture of gold acid and HEPES buffer solution. Fig. 101 shows the dark black precipitate obtained in the reaction chamber confirming the formation of gold nano-particles.

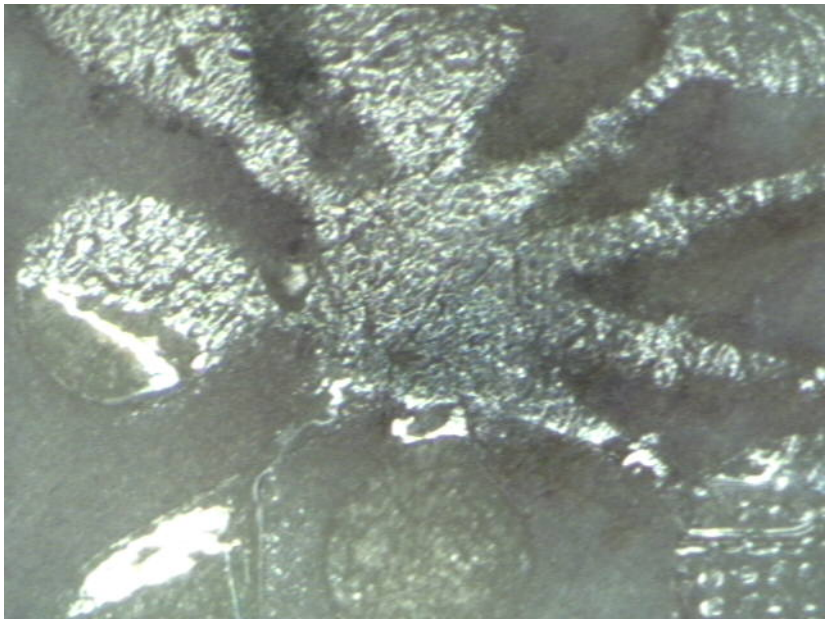

Fig. 91. Image showing a magnified view of the reaction chamber on the paper microfluidic substrate.

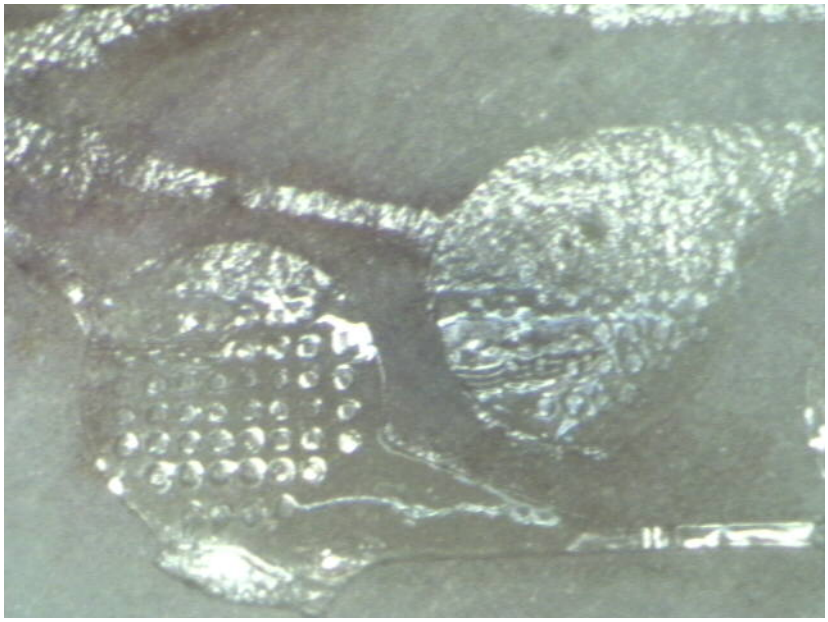

Fig. 92. Image showing the first set of drainage chambers on the microfluidic assay. The minute dissolvable microstructures can be seen in the magnified view.

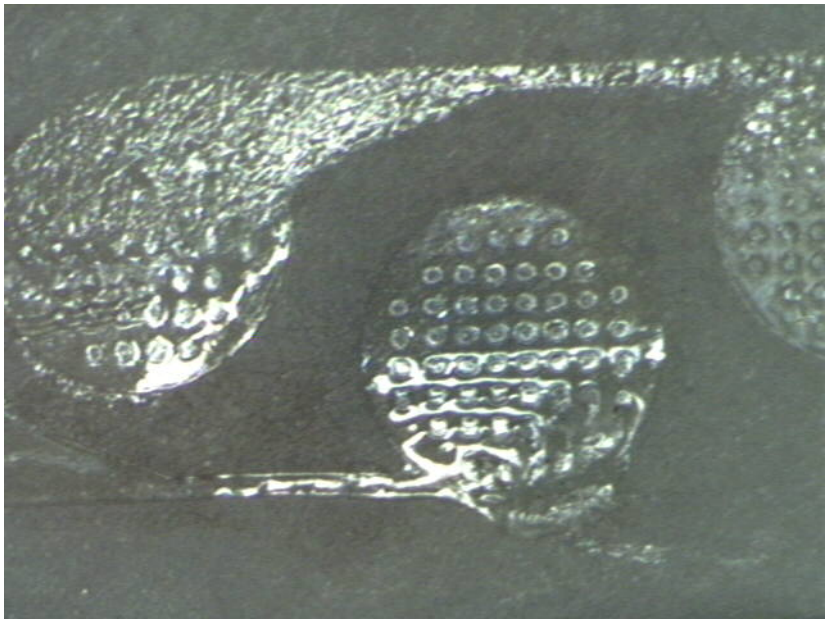

Fig. 93. Image showing the magnified view of the second set of drainage chambers on the microfluidic substrate.

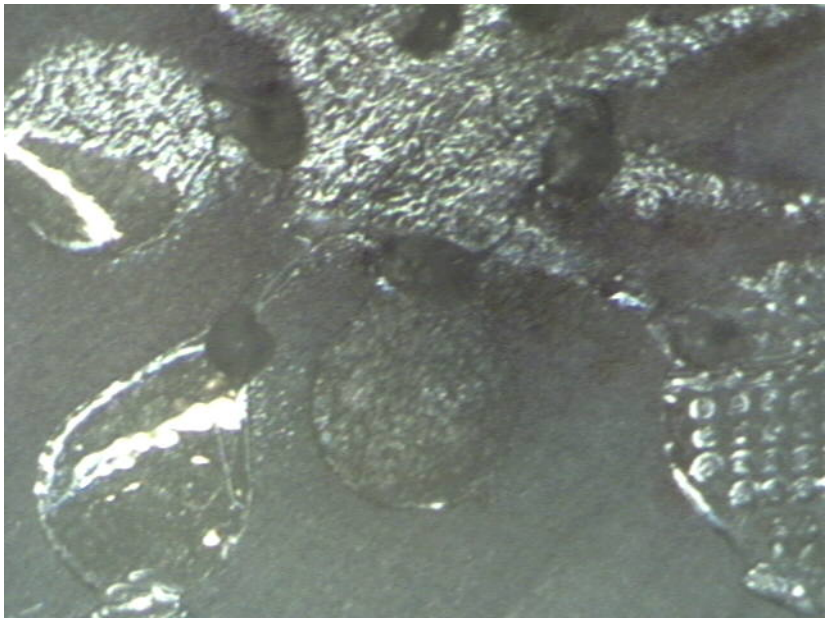

Fig. 94. Image showing an overview of the micro-channels leading to the reaction chamber. Salt bridge valves can be seen impregnated inside these capillaries on the paper substrate.

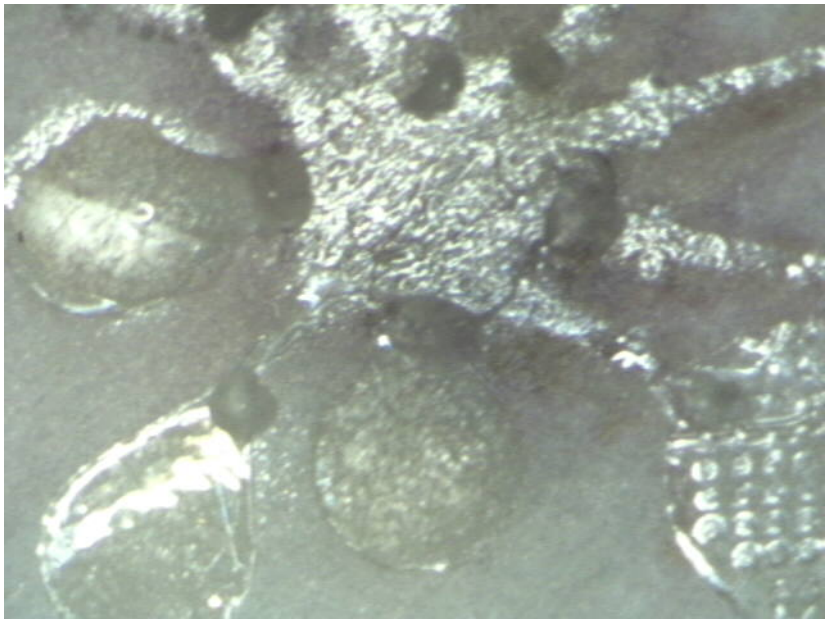

Fig. 95. Image showing HEPES solution introduced into one of the micro-chambers.

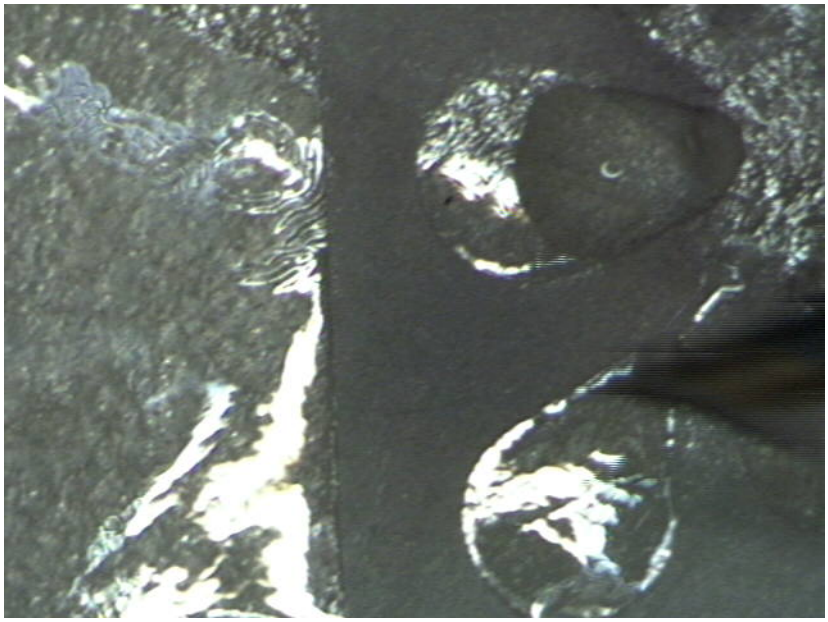

Fig. 96. Image showing the introduction of a drop of peptide solution (poly-tyrosine) into another micro-chamber.

Fig. 97. Image showing the peptide and buffer solutions in their respective micro-chambers at the same time.

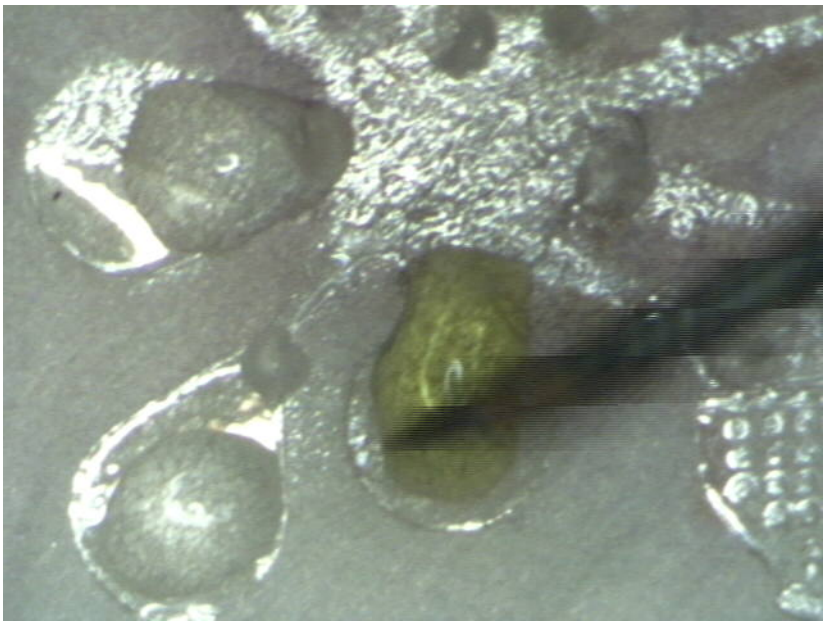

Fig. 98. Image showing the introduction of a droplet of gold acid into another micro-chamber. The HEPES solution meanwhile has dissolved the valve in its micro-channel and is flowing into the reaction chamber.

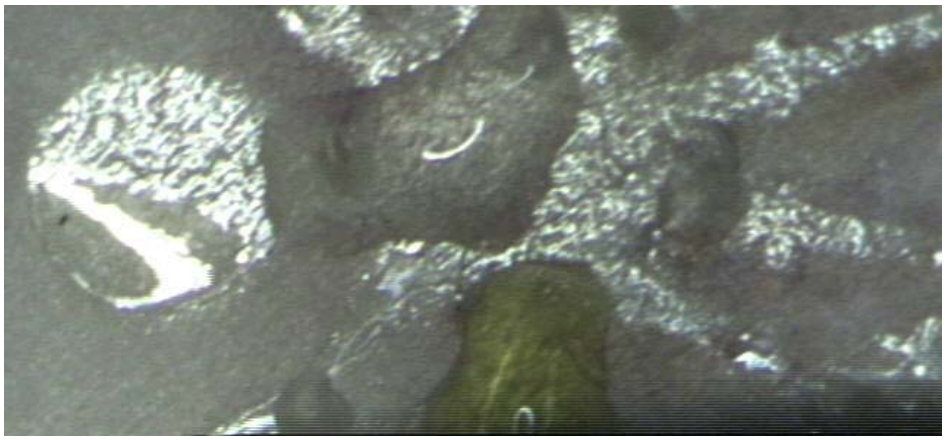

Fig. 99. Image showing the HEPES solution flown into the reaction chamber. The gold acid is also about to enter the reaction chamber.

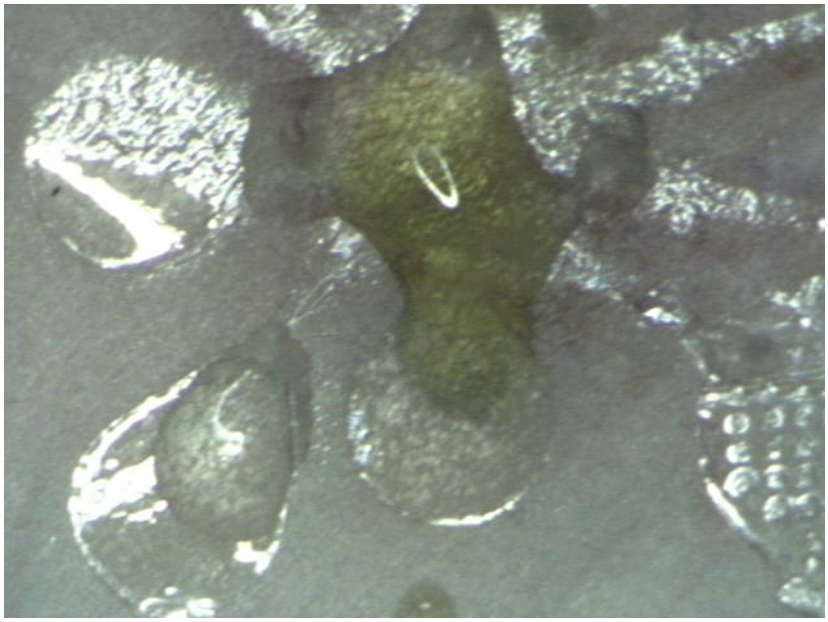

Fig. 100. Image showing the third reagent in the assay (peptide) flowing into the reaction chamber in order to reduce the gold ions to form dark colored precipitate.

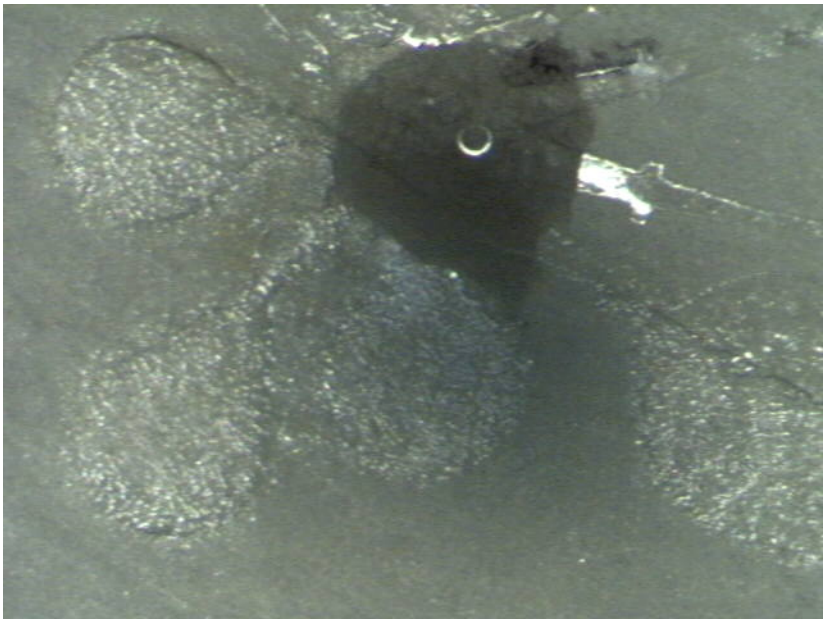

Fig. 101. Image showing the formation of a dark precipitate in the reaction chamber confirming the presence of gold nano-particles.

6.4.2.2 Sodium Chloride

Sodium chloride is another option for manufacturing the passive microvalves. Fig. 102 shows a magnified view of sodium chloride microvalves inserted into the micro-channels leading to the reaction chamber. Fig. 103 is basically a magnified image of the reaction chamber. Fig. 104 shows the introduction of a drop of HEPES solution into one of the reservoirs in the microfluidic substrate. Fig. 105 shows the introduction of poly-tyrosine into another micro-chamber. The two reagents are seen in their respective micro-chambers, flowing towards the reaction chamber as seen in Fig. 106. Gold acid is introduced into a third micro-chamber as shown in Fig. 107. Fig. 108 shows the flow of HEPES solution into the reaction chamber. Fig. 109 shows the gold acid flowing into the reaction chamber to react with the peptide and buffer solutions. Fig. 110 shows the formation of the dark precipitate confirming the formation of gold nano-particles.

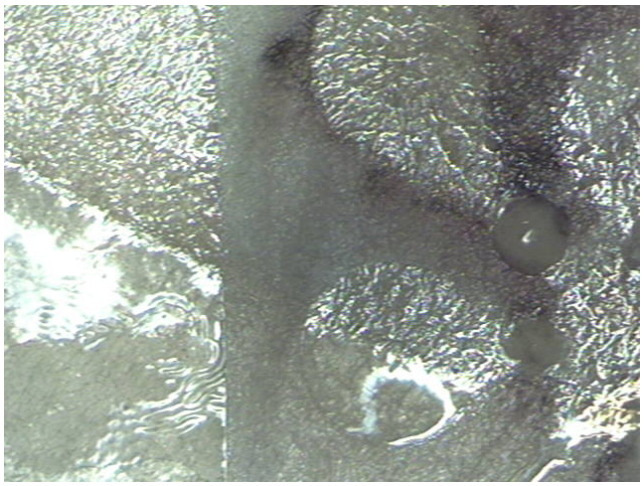

Fig. 102. Image showing a magnified view of a salt bridge valve made of sodium chloride inserted into one of the micro-channel.

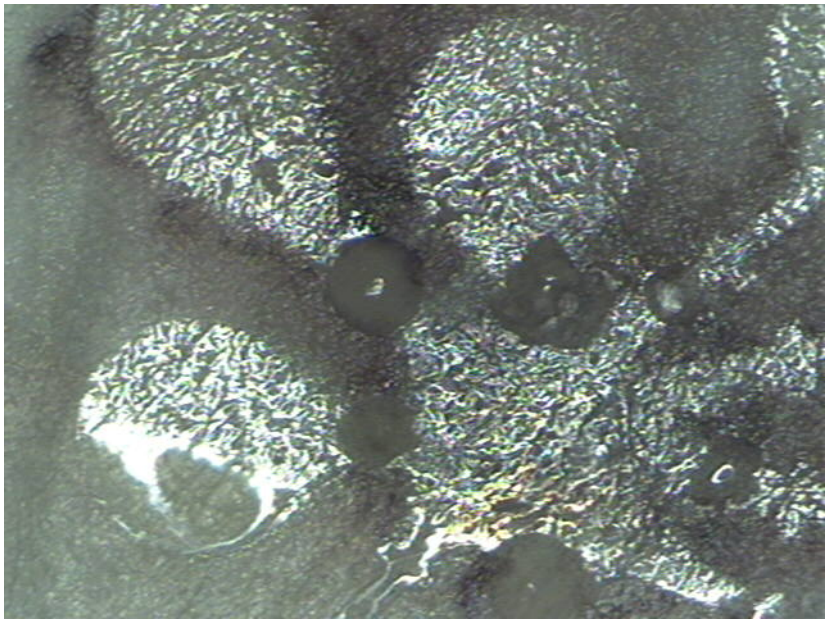

Fig. 103. Image showing the overview of the paper microfluidic substrate with sodium chloride microvalves placed inside the channels as shown.

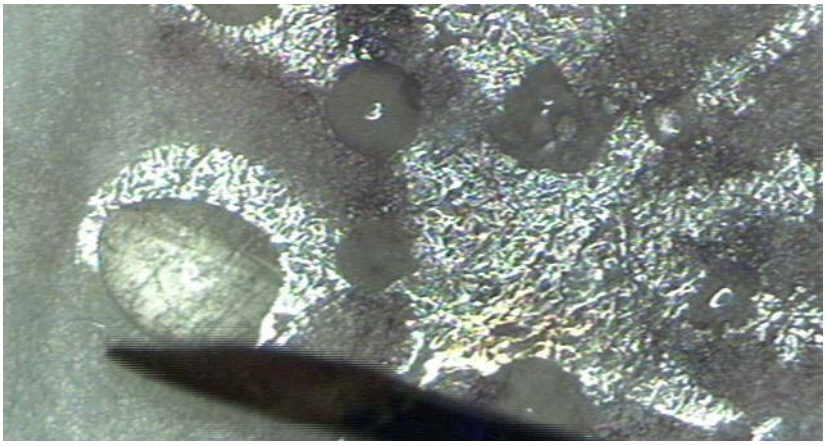

Fig. 104. Image showing the introduction of a drop of HEPES into a well.

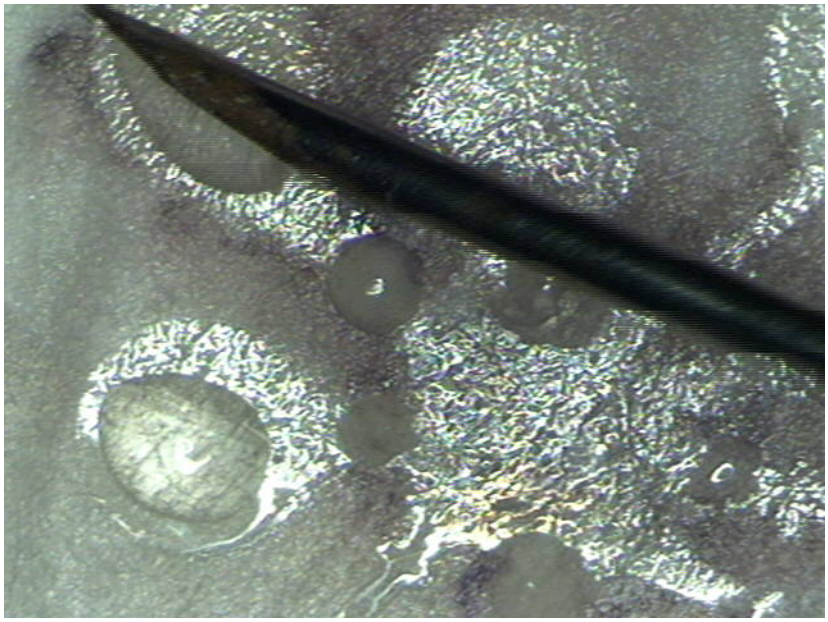

Fig. 105. Image showing the introduction of a drop of peptide solution (poly-tyrosine) introduced into another micro-chamber of the microfluidic substrate.

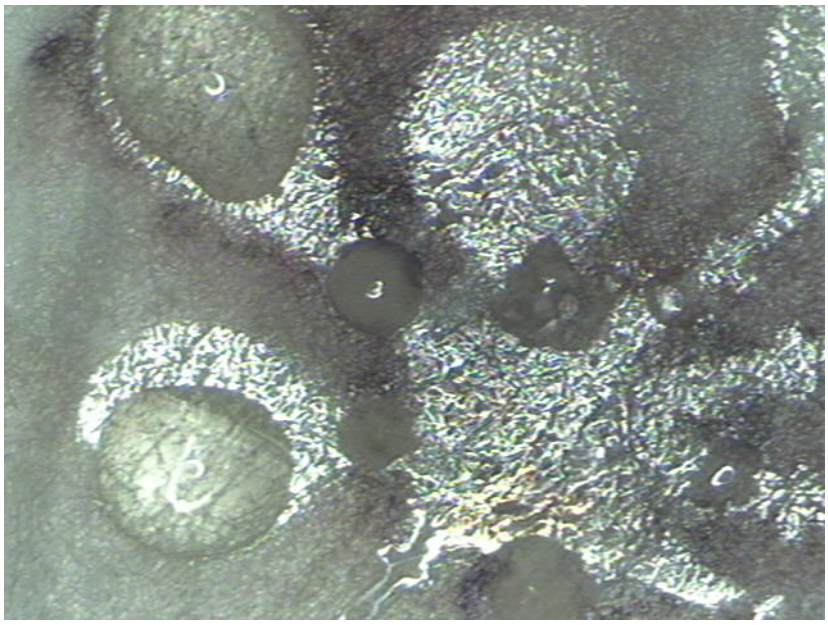

Fig. 106. Image showing the peptide and buffer solutions in their respective micro-chambers.

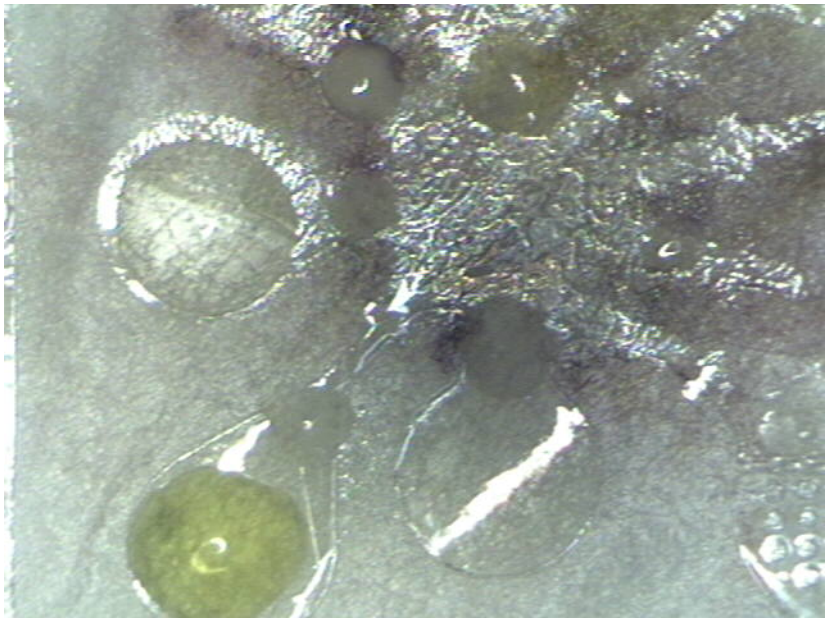

Fig. 107. Image showing the introduction of a drop of gold acid into another micro-chamber.

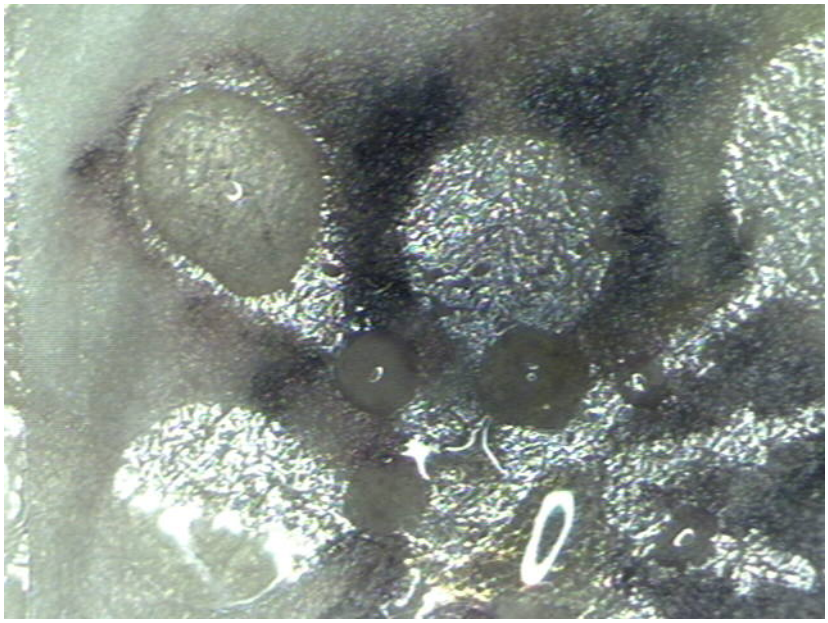

Fig. 108. Image showing that the HEPES has flown into the reaction chamber while the other two reagents are still in their micro-chambers.

Fig. 109. Image showing the HEPES and peptide inside the reaction chamber. The gold acid is about to flow into the reaction chamber at this time.

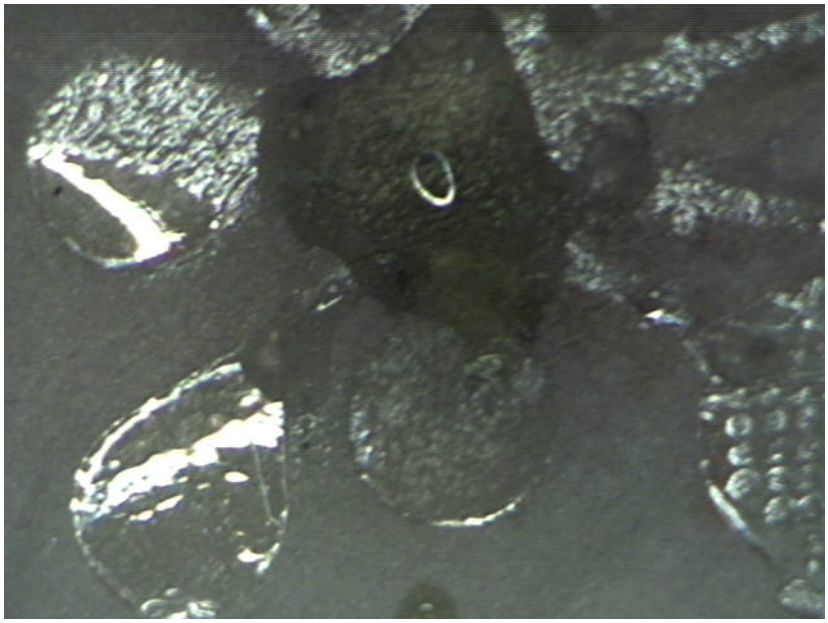

Fig. 110. Image showing the development of dark precipitate inside the reaction chamber confirming the presence of gold nano-particles.

6.5 Size Distribution of Gold Nano-Particles

The particle size distribution of gold nano-particles obtained by using the peptide based synthesis process was measured using scanning electron microscopy (SEM).

Fig. 111 shows the distribution of the nano-particles at 8,000x magnification while Fig. 112 and Fig. 113 show the same at magnifications of 18,000x and 45,000x respectively. A sample size of 20 nano-particles was used to analyze the size distribution. The average particle size was 193.5 nm with a standard deviation of 19.26 nm. The largest particle size found in the sample group was 220 nm and the smallest was 150 nm.

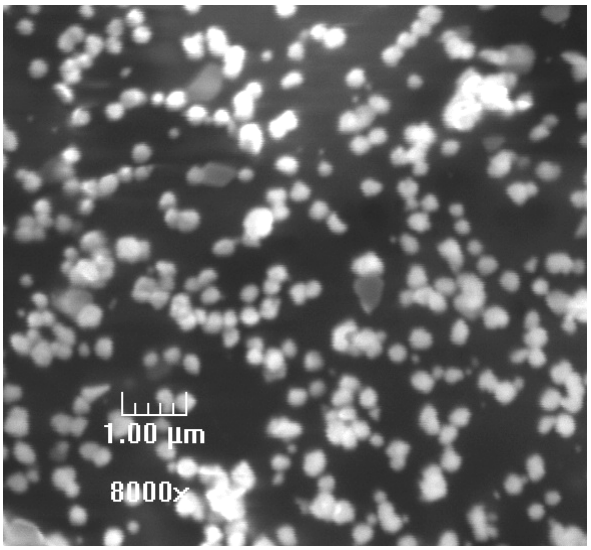

Fig. 111. SEM images of gold nano-particles at 8000x magnification.

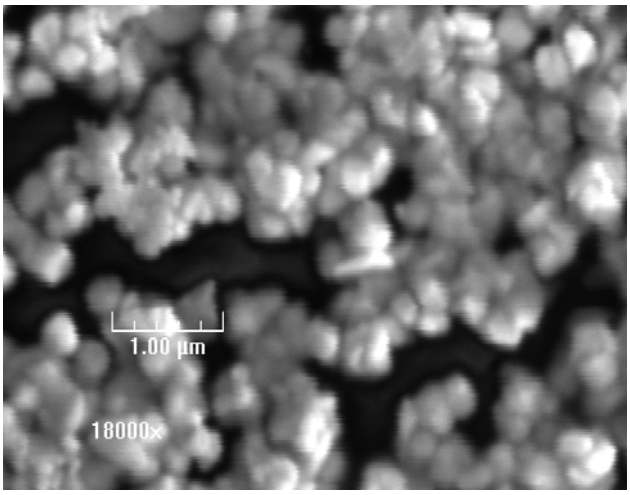

Fig. 112. SEM images of gold nano-particles at 18000x magnification.

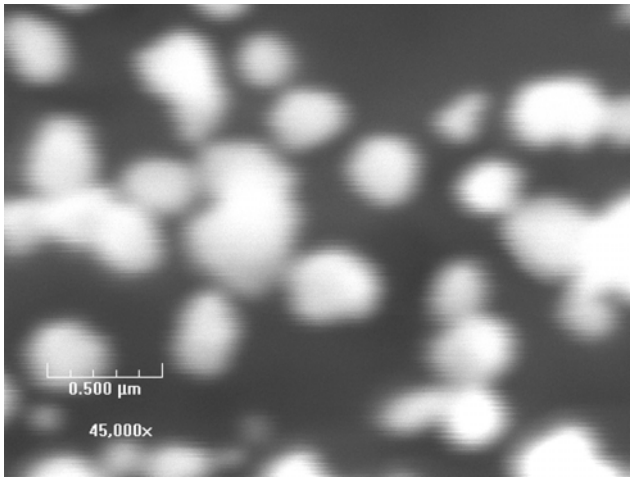

Fig. 113. Gold nano-particle distribution at 45000x magnification.

7. CONCLUSION AND FUTURE DIRECTIONS

7.1 Conclusions

The following steps were employed in this study:

1. Design, development, fabrication, testing and characterization of the microfluidic salt bridge valve were performed. Analytical models for valve performance were developed using one dimensional diffusion equations and compared with experimental data. The non-linear model (moving boundary model) was found to be more accurate than the linear model for predicting valve performance.

2. Several salt materials (polyethylene glycol, sodium chloride, and sodium acetate) were tested for micro-valve performance. Micro-valves fabricated using sodium acetate were found to provide the most reliable and consistent performance. Micro-valves fabricated using polyethylene glycol (PEG) were found to have inconsistent performance and not very reliable for valve actuation time. This is due to the “infinite” solubility of PEG in water.
3. Design, development, fabrication, testing, characterization and implementation of the Lab-On-Chip platform for synthesis of gold nano-particles using peptide assay (with and without the micro-valves) were performed. The LOC platform was realized using PDMS (single layer and bi-layer) as well as on paper substrates. The peptide assay for synthesis of gold nano-particles was

successfully implemented and tested on all three types of microfluidics substrates.

4. The synthesized gold nano-particles were characterized using Scanning Electron Microscopy (SEM). The SEM images showed that peptide assay yielded a narrow distribution for the diameter of the synthesized gold nano-particles.

7.2 Recommendations and Future Directions

The integrated microfluidic LOC device was designed to serve as a micro-TAS (Micro Total Analyses) platform for in-situ synthesis of gold nano-particles. This gold nano-particle synthesis technique serves as a feasibility demonstration module for future application in water quality monitoring – specifically for monitoring metal ion pollutants in water. The LOC was further realized and tested successfully on a paper microfluidics platform. This study proves the feasibility for developing a colorimetric assay for water quality monitoring using peptide based detection motifs and gold nano-particles. It is recommended that this lab-on-chip platform should be developed further and utilized as a water quality monitoring device to be tested on the field with water samples to determine the efficacy of the LOC platform. The device could be similar to a litmus paper where the paper (microfluidics device) turns red (or dark) in color in the presence of metal ion pollutants at a certain threshold concentration in a water sample. The device operation will be as simple as dipping the paper substrate in a water sample to observe color change. The color change can also be calibrated to the metal ion concentration in the water sample. Hence, the method developed in this study can be used to realize a

water quality monitoring platform that is portable, fast, easy to use, and does not require skilled users.

REFERENCES

[1] A. Baghel, B. Singh, P. Pandey, and K. Sekhar, "A rapid field detection method for arsenic in drinking water," *Anal. Sciences.,* vol. 23, pp. 135-137, 2007.

[2] Z. Jia, A. O. Simm, X. Dai, and R. G. Compton, "The electrochemical reaction mechanism of arsenic deposition on an Au(1 1 1) electrode," *Journal of Electroanalytical Chemistry*, vol. 587, pp. 247-253, 2006.

[3] E. J. King, *Qualitative Analysis and Electrolytic Solutions*, New York: Harcourt Brace and World, Inc.*,* p. 189, 1959.

[4] M. B. Sperling, and B. Welz, *Atomic Absorption Spectrometry*, Weinheim, Germany: Wiley-VCH*,* 1999.

[5] R. Klockenkamper, *Total Reflection X-Ray Fluorescence Spectroscopy*, New York: Wiley, 1997.

[6] Z. B. Alfassi, *Chemical Analysis by Nuclear Methods*, Chichester, United Kingdom: John Wiley and Sons, Inc., 1994.

[7] T. Mauro, G. Bench, E. S. Haddad, K. Feingold, P. Elias, and C. Cullander, "Acute barrier perturbation abolishes the Ca^{2+} and K^{+} gradients in murine epidermis: quantitative measurement using PIXE," *Journal of Investigative Dermatology,* vol. 111, pp. 1198-1201, 1998.

[8] S. Koponen, J. Pulliainen, K. Kallio, and M. Hallikainen, "Lake water quality classification with airborne hyperspectral spectrometer and simulated MERIS data," *Remote Sensing of Environment,* vol. 79, pp. 51-59, 2002.

[9] J. S. Lee, M. S. Han, and C. A. Mirkin, "Colorimetric detection of mercuric ion (Hg^{2+}) in aqueous media using DNA-functionalized gold nanoparticles," *Angew. Chem. Int. Ed.,* vol. 46, pp. 4093-4096, 2007.

[10] M. Sequeira, M. Bowden, E. Minogue, and D. Diamond, "Towards autonomous environmental monitoring systems," *Talanta*, vol. 56, pp. 355-363, 2002.

[11] J. S. Kilby, "The integrated circuit's early history," *Proc. IEEE* vol. 88, no. 1, pp. 109-111, 2000.

[12] K. E. Peterson, "Silicon as mechanical material," *Proc. IEEE* vol. 70, pp. 420-457, 1982.

[13] S. C. Terry, J. H. Jerman, and J. B. Angell, "A gas chromatographic air analyzer fabricated on a silicon wafer," *IEEE Trans. Electron Devices,* vol.26, pp. 1880-1886, 1979.

[14] A. Manz, N. Graber, and H. M. Widmer, "Miniaturized total analysis systems: a novel concept for chemical sensing," *Sensors Actuators B*, vol. 1, pp. 244-248, 1990.

[15] K. Oh, and C. H. Ahn, "A review of microvalves," *Journal of Micromechanics and Microengineering*, vol. 16, pp. 13-39, 2006.

[16] D. J. Sadler, K. W. Oh, C. H. Ahn, S. Bhansali, and H. T. Henderson, "A new magnetically actuator for microvalve for liquid and gas control applications," in *Proc. 10th Int. Conf. on Solid –State Sensors and Actuators (Transducers '99)*, Sendai, Japan, 1999, pp. 1812-1815.

[17] H. J. Cho, K. W. Oh, C. H. Ahn, P. Boolchand, and T. C. Nam, "Stress analysis of silicon membranes with electroplated permalloy films using Raman scattering," *IEEE Trans. Magn*., vol. 37, pp. 2749-2751, 2001.

[18] J. W. Choi, K. W. Oh, A. Han, C. A. Wijayawardhana, C. Lannes, S. Bhansali, K. T. Schlueter, W. R. Heineman, H. B. Halsall, J. H. Nevin, A. J. Helmicki, H. T. Henderson, and C. H. Ahn, "Development and characterization of microfluidics devices and systems for magnetic bead-based biochemical detection," *Biomed. Microdevices,* vol. 3, pp. 191-200, 2001.

[19] K. W. Oh, A. Han, S. Bhansali, and C. H. Ahn, " A low temp bonding technique using spin-on fluorocarbon polymers to assemble," *Microsystems J. Micromech. Microeng.*, vol. 12, pp. 187-191, 2002.

[20] K. Sato, and M. Shikida, "An electrostatically actuated gas valve with an S shaped film element," *Micromech Microengg.*, vol. 4, pp. 205-209, 1994.

[21] M. Shikida, K. Sato, S. Tanaka, Y. Kawamura, and Y. Fujisaki, "Electrostatically driven gas valve with high conductance," J *Microelectromech Syst.*, vol. 3, pp. 76-80, 1994.

[22] C. Goll, W. Bacher, B. Bustgens, D. Maas, R. Ruprecht, and W. K.Schomburg, "An electrostatically actuated polymer microvalve equipped with movable membrane electrode," *J. Micromech. Microeng.*, vol. 7, pp. 224-226, 1997.

[23] J. K. Robertson, and K. D. Wise, "A low pressure micromachined flow modulator," *Sensors Actuators A*, vol. 71, pp. 98-106, 1998.

[24] J. Schaible, "Electrostatic microvalves in silicon with two way function for industrial applications," *11th Int. Conf. on Solid-State Sensors and Actuators (Transducers '01)*, pp. 928-931, 2001.

[25] T. Rogge, Z. Rummler, and W. K. Schomburg, "Polymer micro-valve with a hydraulic piezo-drive fabricated by the AMANDA process," *Sensors and Actuators A*, vol. 110, pp. 206-212, 2004.

[26] P. Shao, Z. Rummler, and W. K. Schomburg, "Polymer micro piezo valve with small dead volume," *J Micromech Microeng.*, vol. 14, pp. 305-309, 2004.

[27] J. Peirs, D. Reynaert, and H. V. Brussel, "Design of miniature parallel manipulators for integration in a self propelling endoscope," *Sensors and Actuators A,* vol. 85, pp. 409-417, 2000 .

[28] H. Jerman, "Electrically activated, normally closed diaphragm valves," *J. Micromech. Microeng.*, vol. 4, pp. 210–216, 1994.

[29] C. A. Rich, and K. D. Wise, "A high-flow thermopneumatic microvalve with improved efficiency and integrated state sensing," *J. Microelectromech. Syst.*, vol. 12, pp. 201–218, 2003.

[30] A. Ruzzu, K. Bade, J. Fahrenberg, and D. Maas, "Positioning system for catheter tips based on an active microvalve system," *J. Micromech. Microeng.*, vol. 8, pp. 161–164, 1998.

[31] H. Takao, K. Miyamura, H. Ebi, M. Ashiki, K. Sawada, and K. Ishida, "A MEMS microvalve with PDMS diaphragm and two-chamber configuration of thermo-

pneumatic actuator for integrated blood test system on silicon," *Sensors Actuators A*, vol. 119, pp. 468–475, 2005.

[32] M. Kohl, K. D. Skrobanek, and S. Miyazaki, "Development of stress-optimised shape memory microvalves," *Sensors Actuators A*, vol. 72, pp. 243–250, 1999.

[33] C. Goll, W. Bacher, B. Bustgens, D. Maas, W. Menz, and W. K. Schomburg, "Microvalves with bistable buckled polymer diaphragms," *J. Micromech. Microeng.*, vol. 6, pp. 77–79, 1996.

[34] H. Ren, and E. Gerhard, "Design and fabrication of a current-pulse-excited bistable magnetic microactuator," *Sensors Actuators A*, vol. 58, pp. 259–264, 1997.

[35] C. R. Neagu, J. G. E. Gardeniers, M. Elwenspoek, and J. J. Kelly, "An electrochemical microactuator: principle and first results," *J. Microelectromech. Syst.*, vol. 5, pp. 2–9, 1996.

[36] K. Tashiro, S. Ikeda, T. Sekiguchi, S. Shoji, H. Makazu, T. Funatsu, and S. Tsukita, in *Proc. Micro Total Analysis Systems (MicroTAS 2001)*, Tokyo, 2001, pp. 471–473.

[37] L. Klintberg, M. Karlsson, L. Stenmark, J. A. Schweitz, and G. Thornell, "A large stroke, high force paraffin phase transition actuator," *Sensors Actuators A*, vol. 96, pp. 189–195, 2002.

[38] K. Yoshida, M. Kikuchi, J. H. Park, and S. Yokota, "Fabrication of micro electro-rheological valves (ER valves) by micromachining and experiments," *Sensors Actuators A*, vol. 95, pp. 227–233, 2002.

[39] H. Hartshorne, C. J. Backhouse, and W. E. Lee, "Ferrofluid-based microchip pump and valve," *Sensors Actuators B*, vol. 99, pp. 592–600, 2004.

[40] K. W. Oh, K. Namkoong, and P. Chinsung, "A phase change microvalve using a meltable magnetic material: ferro-wax," in *Proc. Micro Total Analysis Systems (MicroTAS 2005)*, Boston, pp. 554-556, 2005.

[41] Z. Yang, and R. Maeda, "A world-to-chip socket for microfluidic prototype development," *Electrophoresis*, vol. 23, pp. 3474–3478, 2002.

[42] T. Hasegawa, K. Ikuta, and K. Nakashima, "10-way micro switching valve chip for multi-directional flow control," in *Proc. Micro Total Analysis Systems (MicroTAS 2003),* California, pp. 215–218, 2003.

[43] R. Zengerle, and M. Richter, "Simulation of microfluid systems," *J. Micromech. Microeng.*, vol. 4, pp. 192–204, 1994.

[44] R. Zengerle, J. Ulrich, S. Kluge, M. Richter, and A. Richter, "A bidirectional silicon micropump," *Sensors Actuators A*, vol. 50, pp. 81–86, 1995.

[45] R. E. Oosterbroek, J. W. Berenschot, S. Schlautmann, G. J. M. Krijnen, T. S. J. Lammerink, M. C. Elwenspoek, and A. van den Berg, "Designing, simulation and realization of in-plane operating micro valves, using new etching techniques," J. *Micromech. Microeng.*, vol. 9, pp. 194–198, 1999.

[46] B. Li, Q. Chen, D. G. Lee, J. Woolman, and G. P. Carman, "Development of large flow rate, robust, passive micro check valves for compact piezoelectrically," *Sensors and Actuators A*, vol. 117, pp. 325-330, 2005.

[47] M. C. Carrozza, N. Croce, B. Magnani, and P. Dario, "A piezoelectric-driven stereolithography-fabricated micropump," *J. Micromech. Microeng.*, vol. 5, pp. 177–179, 1995.

[48] D. Accoto, M. C. Carrozza, and P. Dario, "Modelling of micropumps using unimorph piezoelectric actuator and ball valves," *J. Micromech. Microeng.*, vol. 10, pp. 277–281, 2000.

[49] E. F. Hasselbrink, T. J. Shepodd, and J. E. Rehm, "High-pressure microfluidic control in lab-on-a-chip devices using mobile polymer monoliths," *Anal. Chem.*, vol. 74, pp. 4913–4918, 2002.

[50] D. S. Reichmuth, T. J. Shepodd, and B. J. Kirby, "On-chip high-pressure picoliter injector for pressure-driven flow through porous media," *Anal. Chem.*, vol. 76, pp. 5063–5068, 2004.

[51] J. H. Tsai, and L. Lin, "A thermal-bubble-actuated micronozzle-diffuser pump," *J. Microelectromech. Syst.*, vol. 11, pp. 665–671, 2002.

[52] C. H. Ahn, J. W. Choi, G. Beaucage, J. H. Nevin, J. B. Lee, A. Puntambekar and J. Y. Lee, "Disposable smart lab on a chip for point-of-care clinical diagnostics," *Proc. IEEE*, vol. 92, pp. 154–173, 2004.

[53] J. Turkevich, "Colloidal gold Part II: Colour, coagulation, adhesion, alloying and catalytic Properties," *Gold Bulletin*, vol. 18, pp. 125-131, 1985.

[54] M. Brust, J. Fink, D. Bethell, D.J. Schiffrin, and C. Kiely, "Synthesis and reactions of functionalised gold nano-particles," *J. Chem. Soc., Chem. Commun.*, pp. 1655-1656, 1995.

[55] J. M. Slocik, M. O. Stone, R. R. Naik, "Synthesis of gold nano-particles using multifunctional peptides," *Small*, vol. 1, pp. 1048-1052, 2005.

[56] A. W. Martinez, S. T. Phillips, M. J. Butte, G. M. Whitesides, "Patterned paper as a platform for inexpensive, low-volume, portable bioassays," *Angew. Chem. Int. Ed.*, vol. 46, pp. 1318 –1320, 2007.

VITA

Sayak was born as the only child to Sumit & Sujata Datta in Calcutta, India. He pursued his primary education in La Martiniere, Calcutta, India followed by Bishop Cotton, Bangalore, India. He obtained his Bachelor of Engineering degree in mechanical engineering from R.V. College of Engineering, Bangalore, India with a first class and distinction, in the year 2006.

Sayak was admitted into the master's program in Fall 2006, with the Mechanical Engineering Department, Dwight Look College of Engineering at Texas A&M University. He joined the Multi Phase Flow and Heat Transfer Laboratory with Dr. Debjyoti Banerjee as his research advisor in that very semester. He joined the General Electric Company (GE- Energy) as a Gas Turbine Technical Specialist co-op in December 2007.

He pursued his research in the field of Microfluidics under the guidance of Dr. Debjyoti Banerjee and his committee members Dr. Jerald Caton and Dr. Kamran Entesari. He received his M.S. degree in Mechanical Engineering in December 2008.

Sayak Datta's permanent address and Email ID is:

3123 TAMU,

College Station, TX 77843- 3123, USA.

sayak636@yahoo.com